Oleg Todorov Radoslavov

Aquifer thermal energy storage (ATES) system application for district heating and cooling

Master's Thesis
Aalto University - School of Engineering
Advanced Energy Solutions
Major: Sustainable Energy in Buildings and Built Environment
Thesis submitted as a partial fulfillment of thExcel simplee requirements
for the degree of Master of Science in Technology
Espoo 27.8.2018
Supervisor: Professor Markku Virtanen
Advisor: D.Sc. Reijo Kohonen

Aalto University
School of Engineering

Aalto University, P.O. BOX 11000, 00076
AALTO
www.aalto.fi

Abstract of master's thesis

Author	Oleg Todorov Radoslavov
Title of thesis	Aquifer thermal energy storage (ATES) system application for district heating and cooling
Master programme	Advanced Energy Solutions **Code** ENG3068 Major: Sustainable Energy in Buildings and Built Environment
Thesis supervisor	Professor Markku Virtanen
Thesis advisor(s)	D.Sc. Reijo Kohonen
Date 27.8.2018	**Number of pages** 88+4 **Language** English

Abstract

Aquifer thermal energy storage (ATES) systems in combination with groundwater heat pumps (GWHP) are promising and effective alternatives for integrated heating and cooling energy supply in buildings and district networks. In the present Thesis ATES systems are presented and addressed from different perspectives, such as their technical rationale, economic feasibility and environmental impact.

Groundwater flow and thermal models are developed and calibrated, using a variety of available data sources (National Land Survey of Finland, Finnish Environment Institute) and tools (EXCEL, QGIS, MODFLOW, MT3DMS). Heat pump COP estimation analytical model is also implemented and coupled with the groundwater models. The purpose was to study different energy scenarios for ATES integration within the existing Pukkila's district heating network (Nivos Energia) as well as the long-term environmental flow and thermal impact generated to aquifer groundwater areas.

Among the different researched scenarios, the most feasible strategy is to introduce a roughly constant cooling demand (proceeding from e.g. data center or industrial waste heat) in combination with the existing local district heating demand. The introduction of variable cooling demand using standard office simulated data is also modeled, having shown promising results. On the other hand, the "only heating" integration scenario has poor economic results, at least for the assumed present level of boiler's fuel price, and is reasonably feasible only in the case when prices increase.

ATES systems are an efficient and a sustainable alternative for traditional fossil fuel boilers due to their capacity to annually store and recover cooling & heating energy from the subsurface. Significant technical and economical improvement could be achieved when simultaneous or seasonable cooling and heating loads are dispatched, within integrated district energy (heating & cooling) networks.

Keywords aquifer thermal energy storage, ATES, groundwater heat pump, GWHP, district heating and cooling network, Pukkila, Nivos Energia, hydrogeology, thermogeology, groundwater modeling, simulation, QGIS, MODFLOW, MT3DMS

Aquifer thermal energy storage (ATES) system application for district heating and cooling

Table of Contents

Figures

Tables

Preface

"If I have seen further it is by standing on the shoulders of Giants"

Isaac Newton (1643-1727)

When I started my work I didn't know too much about geology. To be honest, for me geology was a kind of "exotic" science dealing mostly with minerals classification. But, little by little, I understood that Earth is not only a big rock wandering in space, but it is more like a live organism where hydro- and thermo-regulation are key processes above and beneath its surface.

Now I know a little bit more about hydro- and thermo-geology, amazing branches of geology dealing with groundwater flow and solute & heat transport, as well as their practical application in water management, environmental protection and energy source & storage. This Thesis intends to deepen more in this direction, how subsurface can be utilized in order to generate and store useful energy. Perhaps the answer to our actual energy and climate crisis could be found beneath the surface?

I would like to thank Professor Risto Kosonen from Aalto University, who in the first place presented me the project and gave me the opportunity to participate in it.

Special thanks to the team of Global Eco Solutions - Kari Larjava, Reijo Kohonen and Jyrki Uurtio, who made this project possible. I also wish to thank Teppo Arola from GTK for his advice on hydrogeology, Markus Olin from VTT for his modeling and simulation expertise, Jarkko Okkonen from the University of Oulu for his guidance on groundwater modeling, as well as Heikki Hynynen from Nivos Energia who kindly sent me a copy of his recent Thesis. I am also grateful to my friend Tzvetalin Vassilev, professor at Nipissing University, for his style comments and suggestions.

I am extremely grateful to my supervisor, Professor Markku Virtanen from Aalto University, for his enormous patience and support. He encouraged me when I felt lost and always had time and good advice when I needed him.

Finally, I would like to express my gratitude to my wife Silja Siitonen for her sacrifice and patience during all these months. You believed in me and gave me strength and confidence when I was down. I love you.

Oleg Todorov
Helsinki, August 2018

Abbreviations

ATES	Aquifer Thermal Energy Storage
COP	Coefficient of Performance
DC	District Cooling
DH	District Heating
DHW	Domestic Hot Water
FDM	Finite Difference Method
FEM	Finite Element Method
FVM	Finite Volume Method
GIS	Geographic Information System
GRD	Surfer grid file extension
GTK	Geological Survey of Finland
GWHP	Ground Water Heat Pump
HP	Heat Pump
HVAC	Heat, Ventilation, Air Conditioning
LGR	Local Grid Refinement
NLSF	National Land Survey of Finland
RMSE	Root Mean Squared Error
SYKE	Suomen Ympäristö Keskus
TIFF	Tagged Image File Format
USGS	United States Geological Survey

Nomenclature

α	[m]	Longitudinal dispersivity
A	[m^2]	Area
a	[m]	Cell size of square discretization grid
b	[m]	Aquifer thickness
c_m	[J/kgK]	Aquifer material heat capacity
c_s	[J/kgK]	Solid material heat capacity
c_w	[J/kgK]	Water heat capacity
D_m	[m^3/kg]	Molecular diffusion coefficient
h	[m]	Head
K	[m/s]	Hydraulic conductivity
K_h	[m/s]	Horizontal hydraulic conductivity
K_v	[m/s]	Vertical hydraulic conductivity
K_d	[m^2/s]	Distribution coefficient
λ_m	[W/mK]	Aquifer material thermal conductivity
λ_s	[W/mK]	Solid material thermal conductivity
λ_w	[W/mK]	Water thermal conductivity
n	[%]	Aquifer porosity
q	[m/s]	Flux, specific discharge
Q	[m^3/s]	Flow rate of source/sink
Q_H	[W]	Heat pump condenser heating output
Q_L	[W]	Heat pump evaporator heating input
R	[m/s]	Recharge
ρ_b	[kg/ m^3]	Dry bulk density
ρ_m	[kg/ m^3]	Aquifer material density
ρ_s	[kg/ m^3]	Solid material density
ρ_w	[kg/ m^3]	Water material density
s	[m]	Drawdown
S	-	Storativity
S_s	[1/m]	Specific storage
S_y	[%]	Specific yield
$S_{VC,aq}$	[J/m^3K]	Aquifer volumetric heat capacity
$S_{VC,wat}$	[J/m^3K]	Water volumetric heat capacity
t	[s]	Time
T	[m^2/s]	Transmissivity
T_H	[K]	Heat pump condensation temperature
T_L	[K]	Heat pump evaporation temperature
W(u)	-	Theis well function
W	[W]	Heat pump compressor input

1. Introduction

This chapter introduces the research area, scope and structure of the present thesis. Also the general approach and methodology of the applied engineering process, separating the different phases of project implementation, is described.

This thesis is a part and an important starting point of the GESATES project, an innovative initiative for groundwater heat pump (GWHP) application with aquifer thermal energy storage (ATES). It was kicked-off in March 2018 and is promoted and funded by Business Finland and different participating companies (HELEN, Turku Energia, Nastolan Energiasäätiö, Nivos Energia). It also includes different research locations in Helsinki, Turku, Nastola and Pukkila-Mäntsälä region. The aim of this Thesis is to demonstrate the potential benefits of GWHP and ATES integration using a real case of Pukkila district heating network.

1.1. Background

Heat pump (HP) is an extremely interesting engineering device capable to transfer heat in the direction opposite to the natural flow. During the short but intensive heat pump history of roughly 150 years, starting in 1852 when Lord Kelvin described it theoretically and in 1855-57 Peter von Rittinger built the first prototype, heat pumps have demonstrated their ability for heat generation from low enthalpy sources. They have also revealed their enormous potential to become an alternative substitute of traditional fossil fuels heating systems.

Surprisingly, modern hydrogeology had similar history, starting in 1855, when Henry Darcy as a municipal engineer of Dijon, conducted a series of experiments aimed to understand the rates of water flow through sand layers, and their relationship to pressure loss along the flow paths during the process of water filtration. His discovery was fundamental to the understanding of subsurface processes and a cornerstone of groundwater flow knowledge.

Furthermore, groundwater heat pumps (GWHP) take advantage of stable subsurface temperatures and the ability of groundwater areas to store the excess energy in order to use it when necessary (seasonal shifting of energy demand). This long-term energy storage minimizes the apparent energy paradox, eliminating the need to separate heat generation during the winter (burning fossil fuels), while during the summer heat recovered from buildings (cooling) is typically wasted.

Moreover, the availability in Finland of numerous groundwater resources (known as aquifers) is an important additional advantage for GWHP introduction and deployment, taking into account the variety of GWHP+ATES projects implemented during the last decades in countries like the Netherlands and Sweden.

1.2. Aim and scope of the thesis

The present thesis will explore the benefits and advantages of introducing a groundwater heat pump (GWHP) coupled with aquifer thermal energy storage (ATES) in order to satisfy efficiently an important part of (or the entire) annual energy demand of existing district heating network.

Different heating and cooling energy demands are considered, as well as several possible energy scenarios are simulated and evaluated in terms of technical adequacy, economic feasibility, energy efficiency and underground environmental impact.

The relevant concepts and phases of the engineering process are summarized and presented in the following Figure 1-1, where the area and scope of the present Thesis are delimited mostly within the Prefeasibility phase.

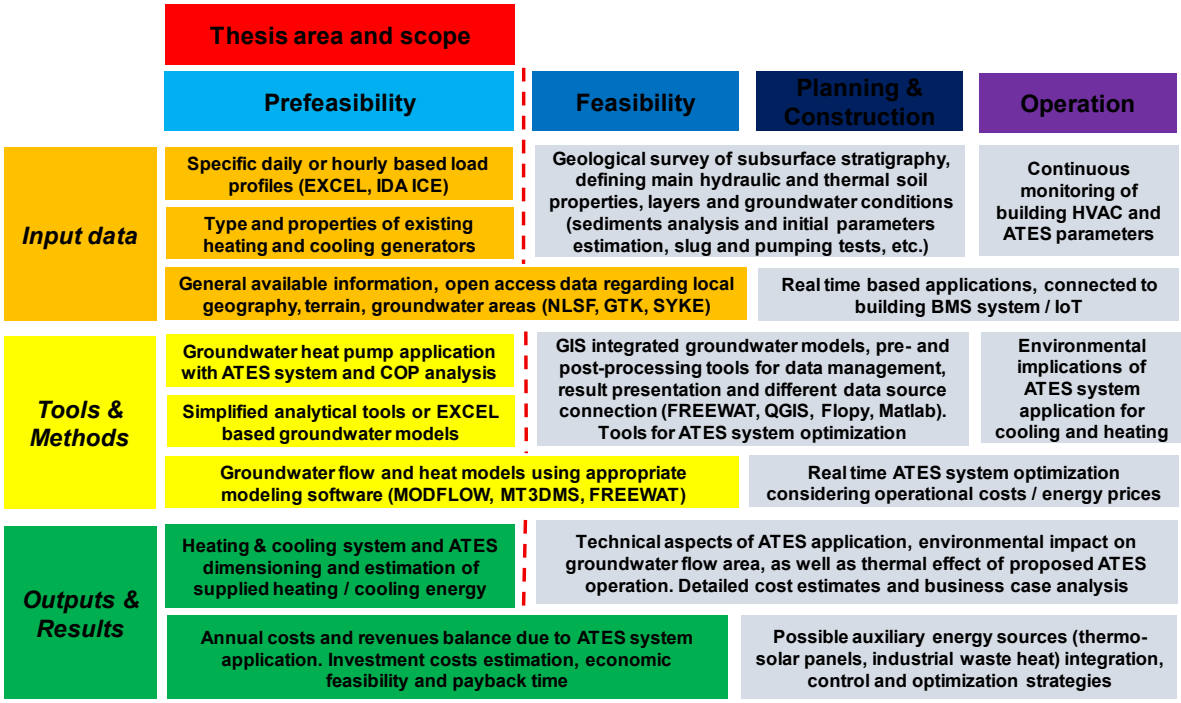

Figure 1-1: Engineering process summary and Thesis area and scope

1.3. Research questions and methods

In the present Thesis the research questions are the following:

- Is the ATES system application for heating and cooling technically reasonable, environmentally sustainable and economically feasible?
- What are the short- and long-term implications and impacts of ATES operation on the affected groundwater areas?

- What are the relevant phases, methods and tools for efficient data management and results presentation?

These are the typical questions motivating our research and its engineering process, as well as presented and addressed from different angles in this Thesis.

Generally speaking, depending on the initial data uncertainty and complexity level of the generated results, there are four grossly differentiated phases: prefeasibility, feasibility, planning & construction and operation (see Figure 1-2, source Reijo Kohonen, Global Eco Solutions).

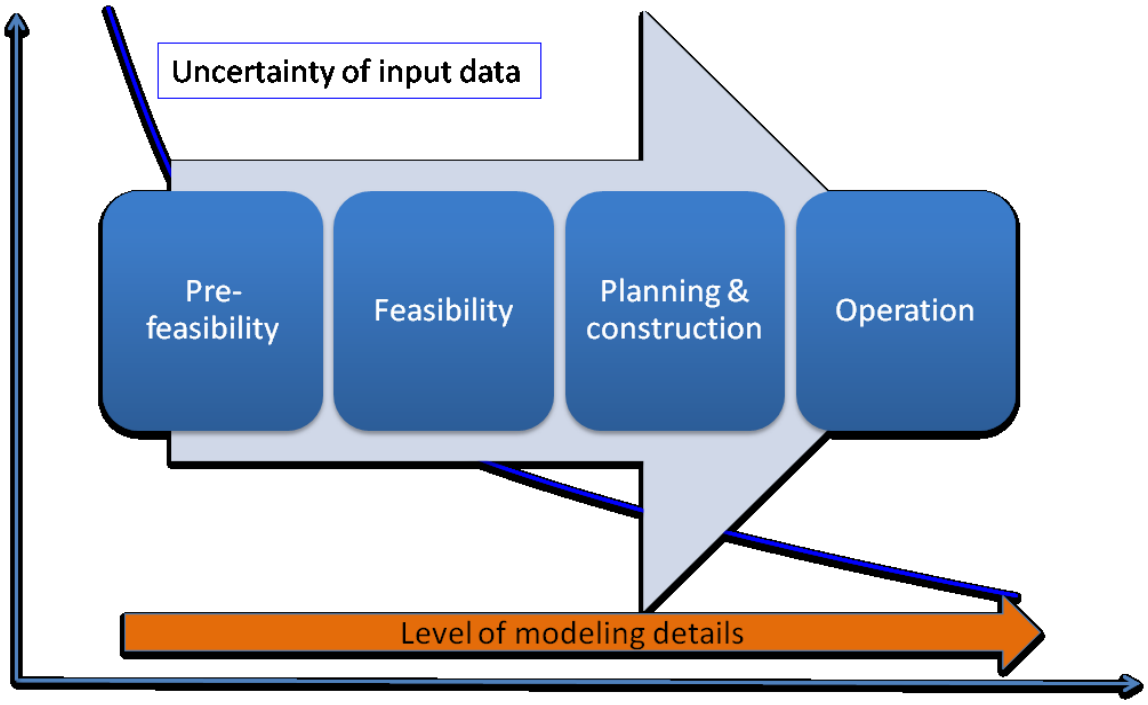

Figure 1-2: Engineering process - main phases
Each phase decreases the uncertainty level of input data, at the same time increasing modeling accuracy and the level of details

All project phases are articulated around several chronologically linked concepts like initial input data, tools & methods used for pre-/post-processing and outputs & results.

1.3.1. Input data

Among the initial data input it is possible to establish the following classification:

- Specific daily or hourly based load profiles, including heating and cooling energy demands for at least one complete year

- Data concerning the type (base / peak load), energy used, efficiency or COP, etc. of all existing heating and cooling generators
- General geographical and geological information in order to select the appropriate possible area for ATES application (initial prefeasibility phase)
- Geological survey of subsurface stratigraphy, defining main hydraulic and thermal soil properties, layers and groundwater conditions (sediments analysis and initial parameters estimation, slug and pumping tests, etc.). All this information would be later used for accurate groundwater model set up and calibration.

1.3.2. Tools and methods

The available tools and methods are classified with increasing level of complexity as follows:

- Available open access data regarding local geography, terrain, groundwater areas, observation wells with information of groundwater capacity, levels, composition and quality
- Simplified analytical tools or Excel based groundwater models
- Heating and cooling loads analysis tools
- Groundwater heat pump application with ATES system and COP analysis depending on different heating and cooling scenarios
- Environmental implications of ATES system application for cooling and heating
- Groundwater flow and heat models using appropriate modeling software with accurate simulation of all proposed ATES scenarios
- Pre- and post-processing tools for data management, result presentation and different data source connection

1.3.3. Output and results

Important information regarding technical aspects of ATES system and its feasibility is included in the final proposals and results, classified from low to high degree of complexity:

- Heating & cooling system and ATES dimensioning and optimization
- Annual estimation of ATES system supplied heating / cooling energy
- Annual cost and revenue balance due to ATES system application
- Investment cost estimation, economic feasibility and payback time
- Technical aspects of ATES application, environmental impact on groundwater flow area, as well as thermal effect of proposed ATES operation
- Detailed cost estimates and business case analysis
- Possible auxiliary energy sources (thermo-solar, industrial waste heat) integration, control and optimization strategies within ATES system
- Optimized ATES system operation considering operational costs and energy prices
- Real time optimization strategies

1.4. Modeling structure of ATES system

As mentioned previously, the modeling structure is developed through the following general steps - pre-processing of input data, data processing using different tools & methods, as well as post-processing with results presentation and analysis. In order to adequately model an ATES system, it is fundamental to develop and calibrate a specific groundwater model. Basically, both ATES and groundwater models should be connected and linked together using different tools for data interaction (see Figure 1-3).

Depending on the adopted numerical solution for spatial discretization, groundwater numerical models could be based on the finite difference method (FDM), finite element method (FEM) or finite volume method (FVM). Finite difference method based groundwater flow (MODFLOW, Harbaugh et al. 2005) and solute (MT3DMS, Zheng et al. 1999) models are adopted and developed in the present Thesis.

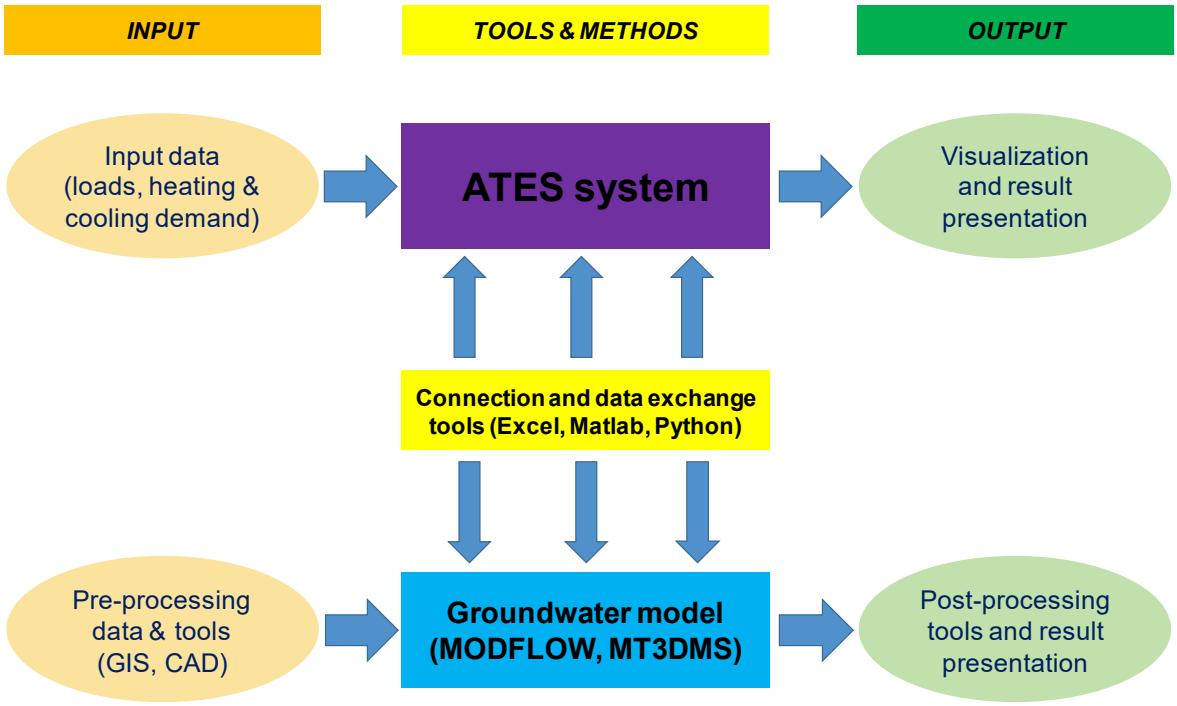

Figure 1-3: Modeling structure of ATES system

1.5. Structure of the Thesis

The present Thesis is carried out and developed using the following structural scheme:

- Chapter 2 introduces the general concepts of heat pump, its performance and applications, as well as develops a concrete model to calculate heat pump performance applied lately in energy simulations. Also the general ATES system application using GWHP and well doublet is presented in this chapter

- Chapter 3 presents a theoretical overview of groundwater hydro-geological processes and describes main aquifer parameters to be considered. Also the relevant analytical solutions and concepts applied to ATES well doublets are explained. In addition, the most relevant software for groundwater flow and solute/heat transport modeling, their structure, main characteristics and packages are introduced

- Chapter 4 presents a real case study and introduces an existing district heating network of Pukkila area, as well as all initial data used for subsequent energy simulations

- Chapter 5 presents all tools & methods used for Pukkila's groundwater areas characterization, using available open access sources regarding local topography, aquifer areas, observation wells, etc.

- Chapter 6 describes the development of different groundwater flow / heat transport models, their setup, calibration and result comparison

- In Chapter 7 different energy scenarios of ATES application for district heating and cooling are developed and studied

- Chapter 8 is dedicated to the economic evaluation of all presented scenarios, where additional sensitivity analysis is performed

- Chapter 9 explores the possibilities for further work implementing additional geological survey, pumping and slug tests

2. Groundwater heat pumps and ATES systems

2.1. General overview of heat pumps

2.1.1. Background

Naturally, heat flows from warmer (high enthalpy) to colder (low enthalpy) objects. Heat pumps utilize low enthalpy sources, and using mechanical work (compressor), transfer it to high enthalpy sources, using a special closed loop fluid, known as refrigerant. The ideal thermodynamic process begins with an isentropic compression, where fluid's (gas) pressure and temperature are increased (point 1).

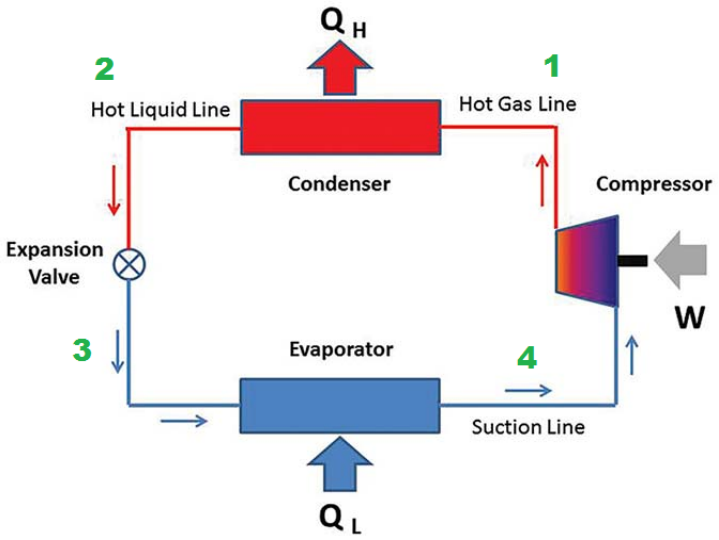

Figure 2-1: Heat pump general thermodynamic cycle

Upper chart: Carnot cycle process; Lower chart: Pressure-Enthalpy diagram

In real compressors, temperature increase is higher due to so called compressor's isentropic efficiency, which requires more work input into the system (W). After the condenser, heat (Q_H) is ceded to the warm source, extracting it from the refrigerant under a constant temperature (T_H) phase change process from gas to liquid (condensation process 1-2).

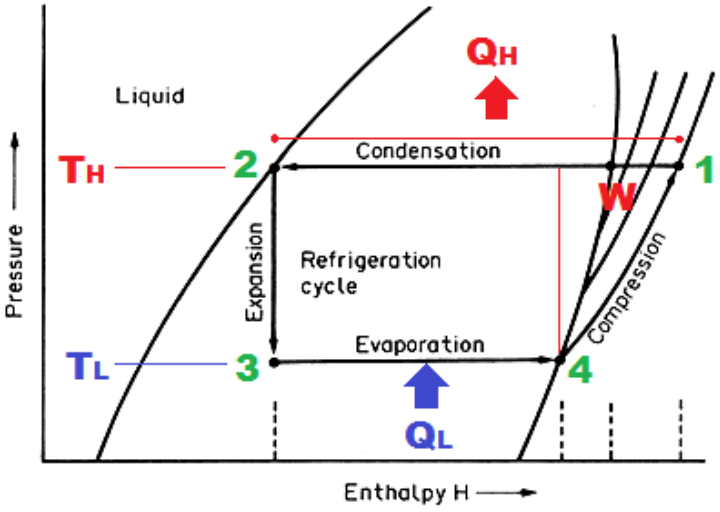

After that, the expansion valve releases adiabatically fluid pressure (at constant enthalpy), and therefore temperature decreases abruptly, even below cold source temperature (point 3).

Finally, cold liquid evaporates (refrigerant phase change in the evaporator, process 3-4) at constant temperature (T_L), absorbing heat (Q_L) from low enthalpy source, before starting another thermodynamic cycle as cold gas entering the compressor (point 4).

From system's heat balance (see Figure 2-1), $\Rightarrow Q_H = Q_L + W$ ***(2-A)***

2.1.2. Heat pump efficiency

Heat pump efficiency, also known as coefficient of performance (COP) is defined in heating (H) and cooling (C) mode respectively as:

$$COP_H = \frac{Q_H}{W}; COP_C = \frac{Q_L}{W} \Rightarrow COP_C = \frac{Q_H - W}{W} = COP_H - 1 \quad \textbf{(2-B)}$$

For ideal thermodynamic cycle, the maximum theoretical heating and cooling efficiencies depend only on condensing and evaporating temperatures (expressed in Kelvin):

$$COP_{H,\max} = \frac{T_H}{T_H - T_C}; COP_{C,\max} = \frac{T_L}{T_H - T_C} \quad \textbf{(2-C)}$$

From equation (2-B), it is clear that the maximum possible theoretical COP (also known as Carnot efficiency) is higher when temperatures T_H and T_L are higher, as well as temperature difference T_H - T_L is lower (COP is much more sensitive to the latter condition).

2.1.3. Efficiency illustration example

In order to practically demonstrate the previously exposed ideas on heat pump efficiency, it is being studied on a real R134a refrigerant chart, for two different thermodynamic processes. The first process (red curve) operates between evaporation temperature T_L=0ºC and condensation temperature T_H=80ºC, while in the second process (blue curve) these temperatures are T_L=20ºC / T_H=60ºC respectively.

In both processes isentropic compressor efficiency is assumed to be 1 (compression is following the pink lines of equal entropy). Compressor mechanical input W (enthalpy change during compression) and the total enthalpy change during condensation (rejected heat Q_H) are estimated in both cases. Heating mode COP can be calculated according to equation (2-A) and estimated graphically from p-h diagram as Q_H/W ratio. Maximum theoretical COP can also be calculated from equation (2-B).

The results presented in Figure 2-2 confirm that when temperature difference T_H - T_L is restricted, heat pump COP can be potentially improved significantly. When heat pump is operating in heating mode, this goal could be achieved increasing source temperature (evaporator side) and decreasing heat pump production temperature (condenser side).

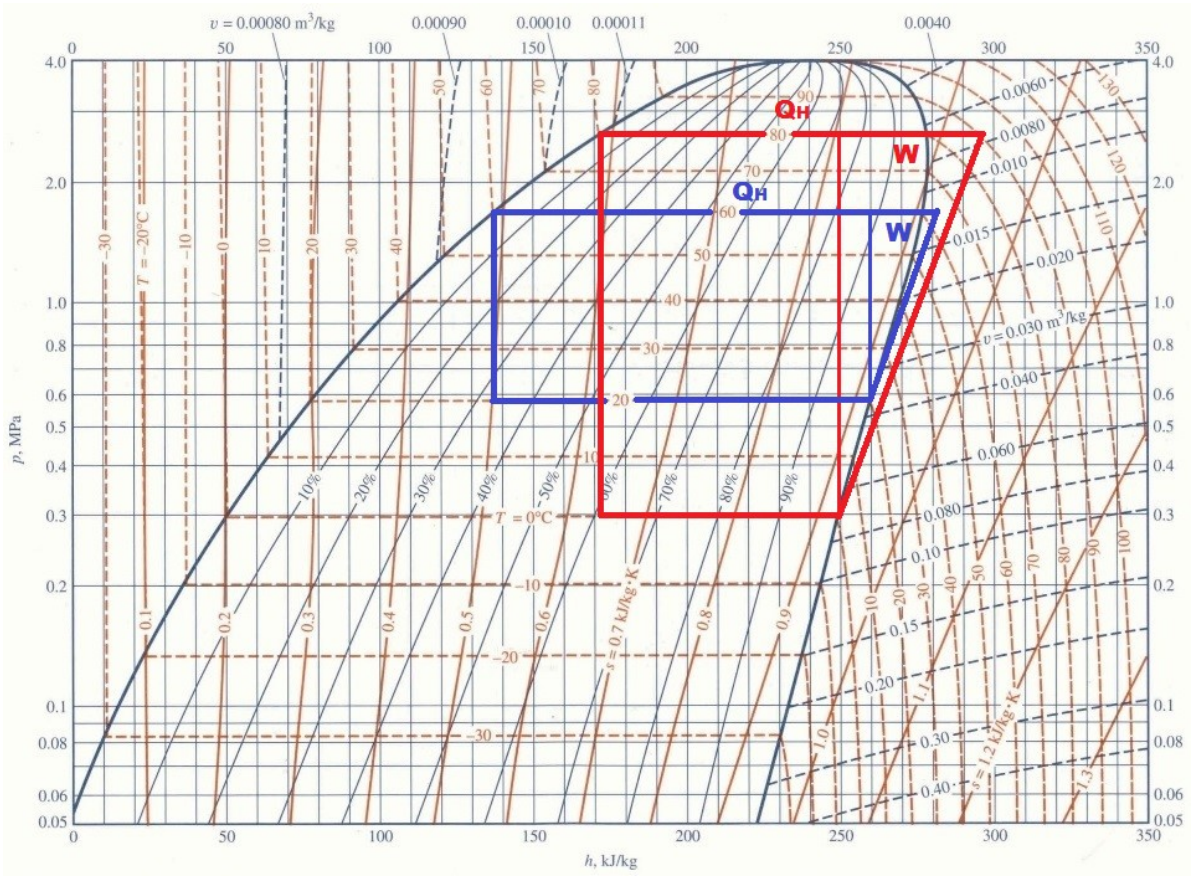

Figure 2-2: Heat pump heating mode efficiency illustration (R134a)

Process 1(red curve): max. theoretical COP: 4.4, isentropic compression COP: 2.6
Process 2(blue curve): max. theoretical COP: 8.3, isentropic compression COP: 6.4
In Process 2, significantly less mechanical work (W) is needed to supply more thermal energy (Q_H), therefore heat pump efficiency is more than doubled

2.1.4. COP_H estimation model

In order to evaluate how both source temperature (direct aquifer water or after intercalated waste heat exchanger) and HP production temperature affect GWHP efficiency, a simple model based on GWHP producer's data is developed (Pero, 2016 and Hynynen, 2018). Available data is used for four source temperatures T_1 (0º, 10º, 20º and 30º) and for five HP production temperatures T_2 (40º, 50º, 60º, 70º and 80º). In addition, data was linearly fitted in order to obtain analytical equations for each match line.

These analytical equations are used in further simulations, interpolating for any value of source temperatures T_1 in order to estimate heat pump COP_H as a function of T_1 and T_2 .

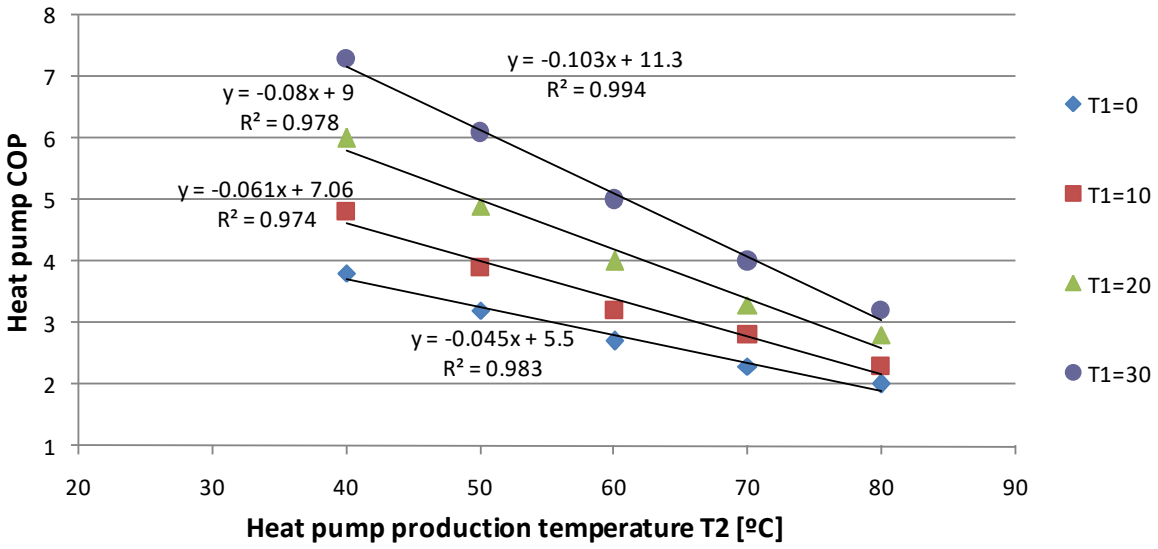

Figure 2-3: COP_H dependence on source (T_1) / production (T_2) temperatures

Heat pump COP_H model - analytical fit of real HP producer's data (source Pemco Oy)
Linear equation is fitted to real data for each source temperature (T_1) with high order of confidence (R^2=0.974÷0.994)

2.2. ATES principles and applications

Aquifer thermal energy storage (ATES) systems store and recover thermal energy using groundwater subsurface structure. Storage and recovery of thermal energy is achieved by abstraction and injection of groundwater from aquifers using groundwater wells. Systems normally operate in a seasonal mode (summer and winter periods). The groundwater extracted during summer, is used for cooling. Depending on the available groundwater temperature this process is direct known as "free cooling" (through heat exchanger) or indirect using an additional chiller (GWHP in cooling mode). Subsequently, the heated groundwater is injected back into the aquifer, which creates a storage of heated groundwater near the warm well.

Normally, an ATES system consists of two wells (called a doublet). One well is used for heat storage, and the other for cold storage. During the winter period, groundwater is abstracted from the warm well and injected into the cold storage well. During summer, the flow direction is reversed such that groundwater is abstracted from the cold storage well and injected into the heat storage well. Because each well serves both as an abstraction and injection well, these systems are called bi-directional. There are also one-way directional systems. These systems do not switch pumping direction, and groundwater is always abstracted at the natural aquifer temperature.

Therefore, ATES system operation utilizes the subsurface as a temporal storage to buffer seasonal variations in heating and cooling demand. When replacing traditional fossil fuel dependent heating and cooling systems, ATES systems in combination with groundwater

heat pumps can serve as a cost-effective technology to reduce the primary energy consumption and the associated CO_2 emissions. Taking into account that groundwater temperature is annually stable and normally, in Northern climate, several degrees above the average air temperature, heating mode operation of GWHP is much more efficient compared to traditionally used air-to-air heat pumps or conventional fossil fuel boilers. This has been pointed out by Arola et al. 2014, and in urban areas it could be even 3-4º higher due to the heat island effect.

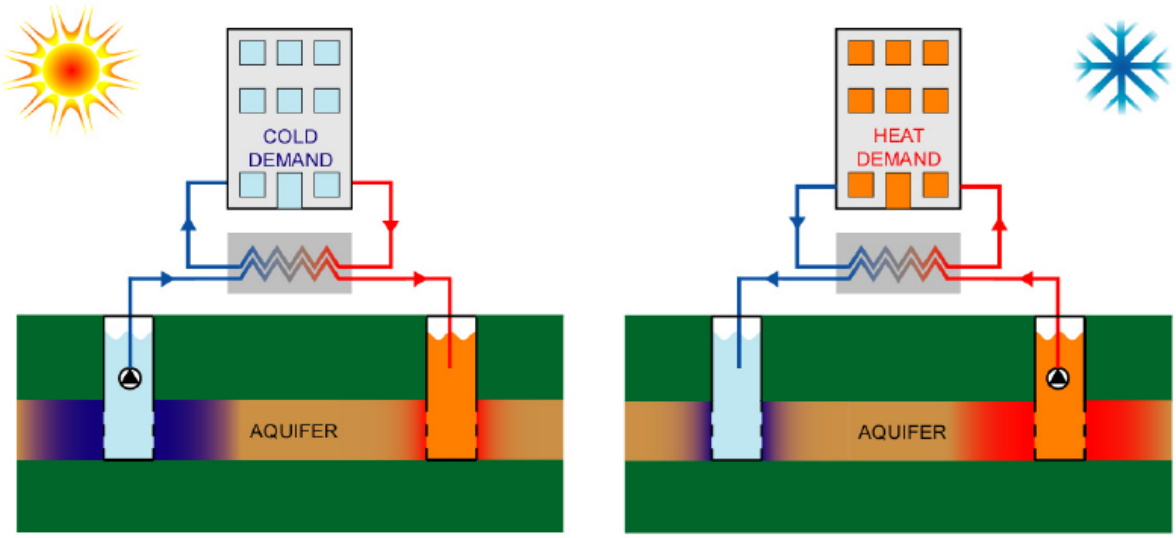

Figure 2-4: Open loop ATES system principles

Abstraction / injection well doublet scheme with seasonable reversible operation. In summer, aquifer water is abstracted is from the cold well (left)and injected into the warm well (right). Free cooling (through heat exchanger) or additional GWHP (cooling mode) is used for cooling. During the winter period, the operation is reversed using GWHP for heating (image source Drijvert et al., 2001)

The legislation of shallow geothermal installations (depth less than 400 m) is diverse among countries (Haehnlein et al. 2010). Regulations for installations of wells concern the use of hazardous materials and proper backfilling of the drilling hole to avoid hydraulic short circuiting between aquifers. Other legislation concerns protection of groundwater areas for drinking water supply. Some countries adopt limits for minimum and maximum storage temperatures, like Austria (5–20°C), Denmark (2–25°C) and the Netherlands (5–25 °C) - while others adopt a maximum change in groundwater temperature, for example Switzerland (3 °C) and France (11 °C).

In Finnish legislation, there is no explicit reference to groundwater use for energy generation and storage, the only generally related laws are the Water Act (1961) and the Environmental Protection Act (2000).

3. Groundwater modeling tools

Groundwater models describe the groundwater flow and solute / heat transport processes using mathematical equations based on some reasonable simplifications and assumptions. These assumptions typically involve groundwater flow direction, aquifer geometry, the heterogeneity or anisotropy of sediments or bedrock within the aquifer, the solute / heat transport mechanisms and chemical reactions.

Due to the simplifying assumptions embedded in mathematical equations and parameter uncertainties in the values of model input data, a model must be viewed as a reasonably accurate approximation and not as an exact representation of reality. Even as approximations, groundwater models are a extremely useful tools in order to correctly represent current groundwater conditions, as well as to be able to predict groundwater flow and thermal behavior of the subsurface for different future scenarios.

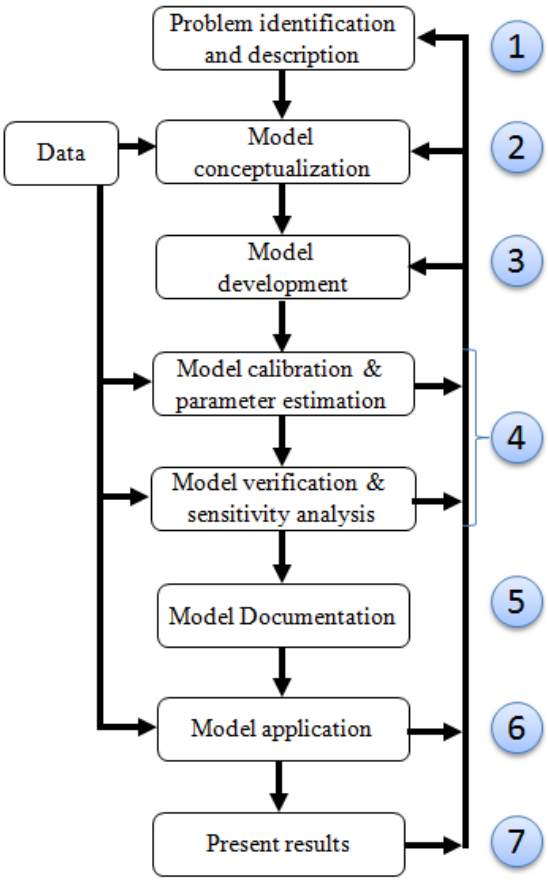

Figure 3-1: Modeling process and steps

Although not all studied hydrogeologic problems require a model, most of them would definitely benefit from it in order to "provide a quantitative framework for synthesizing field information and for conceptualizing hydrogeologic processes" (Anderson et al. 2015). As pointed out by Anderson "If not a model, what else?" The whole modeling process with its main steps and flows is presented in Figure 3-1.

3.1. Theoretical background of groundwater flow

We are living on a planet where as much as 97.2% of total reserves are concentrated in oceans as saline water (Fetter 2001). Fresh water is distributed as follows:

- Ice caps and glaciers 2.14%
- Groundwater 0.61%
- Surface water 0.009%
- Soil moisture 0.005%
- Atmosphere 0.001%

It is important to acknowledge that groundwater reserves represent 98% of the available fresh water reserves. Therefore, the understanding and management of groundwater flow is essential in hydrology and hydrogeology.

3.1.1. Hydrologic cycle

The hydrologic cycle of our planet (Fetter 2001) comprises the following processes (shown graphically in Figure 3-2):

- Evaporation
- Transpiration
- Evapotranspiration
- Condensation
- Precipitation and snow
- Groundwater recharge

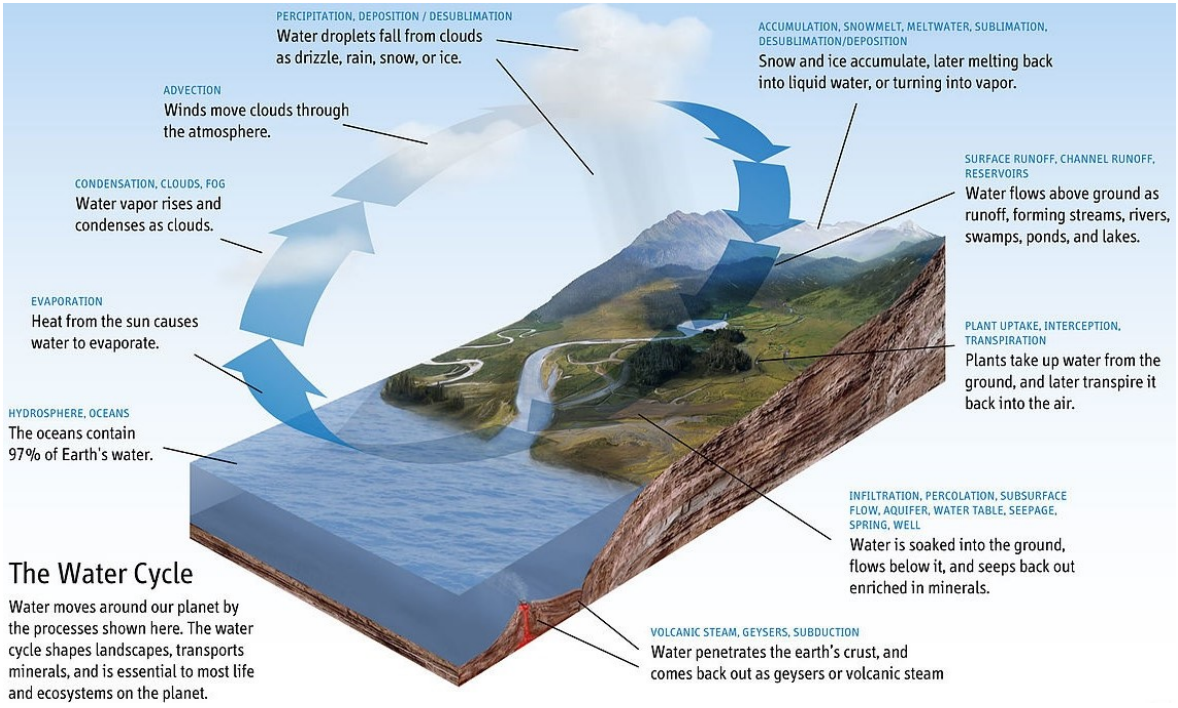

Figure 3-2: The hydrologic cycle

All hydrologic processes are interconnected and in strict balance

3.1.2. Aquifers main properties

According to aquifer's definition given by Fetter, "An aquifer is a geologic unit that can store and transmit water at rates fast enough to supply reasonable amounts to wells". Aquifer's ability to transmit water is defined by its hydraulic conductivity. Normally aquifers (high hydraulic conductivity) are comprised between confining layers (low hydraulic conductivity) or rock basin (very low hydraulic conductivity, almost impermeable).

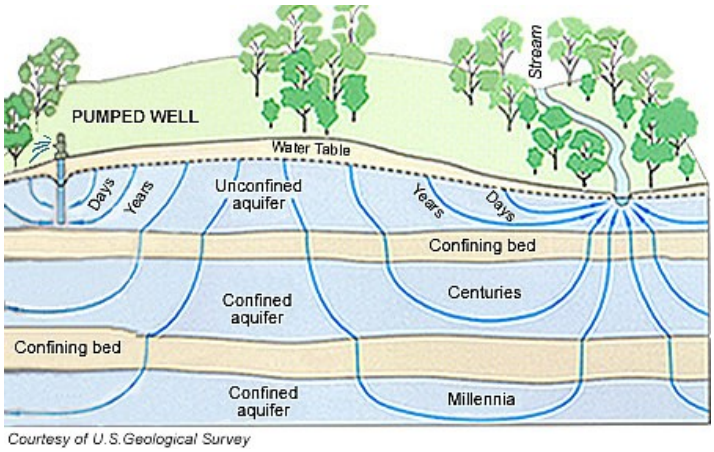

Figure 3-3: Aquifers structure and flows
Source: U. S. Geological Survey

Aquifer's relevant parameters are summarized as follows:

- Porosity, **n** [dimensionless] - defined as the ratio of volume of voids to the total volume of porous medium
- Specific yield, $\mathbf{S_y}$ [dimensionless] - the amount of water that can be extracted from the unit volume of aquifer by pumping or under the action of gravity is called as specific yield, the fraction of water held back in the aquifer is known as specific retention, therefore porosity is the sum of specific yield and specific retention
- Hydraulic conductivity, **K** [m/s] - describes the ease with which a fluid (usually water) can move through pore spaces or fractures. It is a basic parameter related to Darcy's law and defines the relation between flux (Q/A) and head drop per unit length of formation ($\Delta h/\Delta L$)
- Transmissivity, **T** [m^2/s] - in confined aquifers is the product of hydraulic conductivity K and aquifer thickness b
- Specific storage, $\mathbf{S_s}$ [m^{-1}] - the amount of water per unit volume of formation that can be stored or expelled from storage due to the compressibility of the mineral skeleton
- Storativity, **S** [dimensionless] - in confined aquifers, defined as the product of the specific storage and the aquifer thickness b
- Homogeneity and isotropy - unit with the same properties in all locations, e.g. same hydraulic conductivity → isotropic medium
- Hydraulic gradient, **i** [dimensionless] - a slope of the potentiometric surface, a head drop per unit length of formation ($\Delta h/\Delta L$) in a direction perpendicular to equal-potentiometric curves

3.1.3. Groundwater and wells

Wells are important elements of groundwater flow, since they alter and modify the natural steady state potentiometric surface, as well as create the so called cone of depression. It is important to know the water drawdown (head change as a consequence of pumping), because depending on the pumping rate it can affect important groundwater areas.

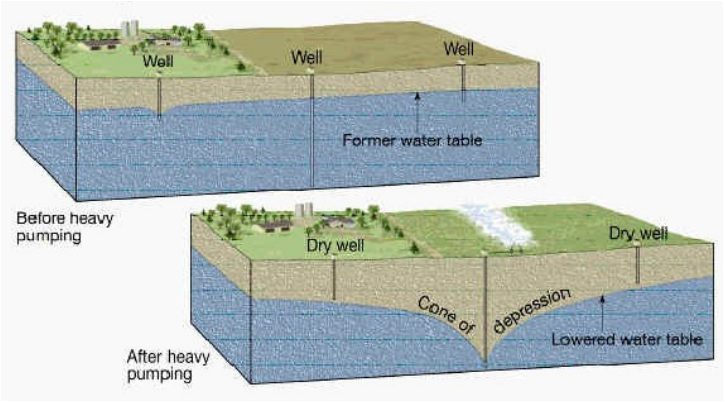

Figure 3-4: Pumping well and cone of depression

The drawdown **s** in confined isotropic aquifer can be estimated using Theis equation:

$$s = h_0 - h = \frac{Q}{4\pi T} W(u) \quad \textit{(3-A)}$$

where

- s [m] is the drawdown, difference between the initial head h0 and the head h after pumping
- Q [m^3/s] is well pumping rate
- T [m^2/s] is aquifer transmissivity
- S is aquifer storativity
- r [m] is the radial distance from the pumping well
- t [s] is time after starting pumping
- the argument u is defined as: $u = \frac{r^2 S}{4Tt}$
- W(u) is Theis well function defined as:

$$W(u) = \int_u^\infty \frac{e^{-y}}{y} dy = -0.5772 - \ln u + \sum_{i=1}^{\infty} \frac{(-1)^{i-1} u^i}{i \cdot i!} \quad \textit{(3-A1)}$$

For small values of u (less than 0.05), all polynomial terms of Theis function could be neglected, and equation 3-A could be simplified as follows:

$$s = h_0 - h = \frac{Q}{4\pi T}\left[-0.5772 - \ln\left(\frac{r^2 S}{4Tt}\right)\right] = \frac{2.3Q}{4\pi T} \log\left(\frac{2.25Tt}{r^2 S}\right) \quad \textit{(3-A2)}$$

3.1.4. Well doublet drawdown

In the case of well doublet with abstraction and injection well, the steady state drawdown at any point separated a distance $\mathbf{r_{abs}}$ from abstraction well and $\mathbf{r_{inj}}$ from injection well can be calculated using Thiem equation as follows:

$$s = h_0 - h = \frac{Q}{2\pi T} \ln\left(\frac{r_{inj}}{r_{abs}}\right) \quad \textbf{(3-B)}$$

Since cones of depression or ascension could be superposed independently, in order to compute the drawdown of any aquifer point, the previous equation could be extended for general well doublet field (well doublets i=1.. n, each with pumping rate Q_i):

$$s = h_0 - h = \sum_{i=1}^{n} \frac{Q_i}{2\pi T} \ln\left(\frac{r_{inj,i}}{r_{abs,i}}\right) \quad \textbf{(3-C)}$$

3.1.5. Hydraulic feedback of well doublet

Hydraulic breakthrough time $\mathbf{t_{hyd}}$ is the time it takes for groundwater to travel between injection and abstraction well (Banks, 2008) and neglecting a steady state hydraulic gradient **i**, hydraulic breakthrough time $\mathbf{t_{hyd}}$ can be calculated as follows:

$$t_{hyd} = \pi n b \frac{L^2}{3Q} \quad \textbf{(3-D)}$$

where

- n is aquifer porosity
- b [m] is aquifer thickness
- L [m] is the distance between abstraction/injection wells
- Q [m^3/s] is the pumping rate

In the case of negative natural hydraulic gradient **i** between the abstraction and the injection well, the hydraulic breakthrough time is estimated as (Banks, 2008):

$$t_{hyd} = \frac{Ln}{Ki}\left[1 + \frac{4\alpha}{\sqrt{-1-4\alpha}} \tan^{-1}\left(\frac{1}{\sqrt{-1-4\alpha}}\right)\right] \quad \textbf{(3-E)}$$

where

- K [m/s] is aquifer hydraulic conductivity
- $\alpha = \frac{Q}{2\pi KbiL} = \frac{Q}{2\pi TiL}$
- T [m^2/s] is aquifer transmissivity

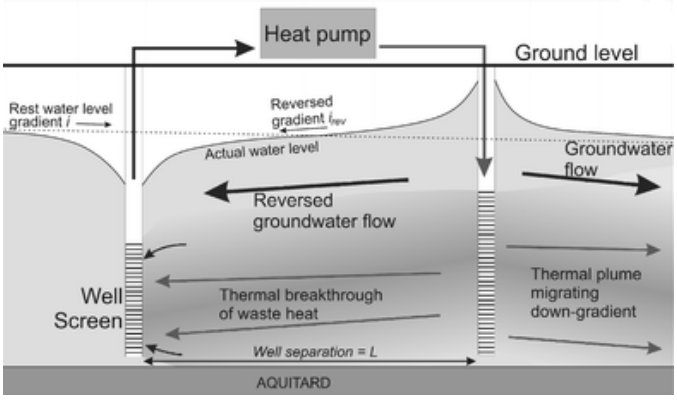

Figure 3-5: Hydraulic / thermal feedback of well doublet

With negative natural hydraulic gradient i, depending on pumping intensity, gradient could be reversed and abstraction well receives feedback from injection well (source Banks, 2008)

3.1.6. Thermal feedback of well doublet

Similarly, the thermal breakthrough time $\mathbf{t_{the}}$ can be defined as the time it takes for thermal front to travel between injection and abstraction well (Banks, 2008), and with zero steady state hydraulic gradient **i**, the thermal breakthrough time $\mathbf{t_{the}}$ can be calculated as follows:

$$t_{the} = \pi b \frac{S_{VC,aq} L^2}{3 S_{VC,wat} Q} \quad \textbf{(3-F)}$$

where

- $S_{VC,aq}$ [J/m^{3}K] is aquifer volumetric heat capacity
- $S_{VC,wat}$ [J/m^{3}K] is water volumetric heat capacity
- b [m] is aquifer thickness
- L [m] is the distance between abstraction/injection wells
- Q [m^3/s] is the pumping rate

In the case of negative natural hydraulic gradient **i** between the abstraction and the injection well, the hydraulic breakthrough time is estimated as (Banks, 2008):

$$t_{the} = \frac{S_{VC,aq} L}{S_{VC,wat} K i} \left[1 + \frac{4\alpha}{\sqrt{-1-4\alpha}} \tan^{-1}\left(\frac{1}{\sqrt{-1-4\alpha}} \right) \right] \quad \textbf{(3-G)}$$

It is possible also to estimate how temperature in the abstraction well $\mathbf{T_{abs}}$ would be affected after time $\mathbf{t>t_{the}}$ ($\mathbf{T_0}$ is initial aquifer temperature and $\mathbf{T_{inj}}$ is the injection temperature), using the following relation (Banks, 2008):

$$\frac{T_{abs} - T_{inj}}{T_0 - T_{inj}} = 0.34 \cdot \exp\left(-0.0023 \frac{t}{t_{the}} \right) + 0.34 \cdot \exp\left(-0.109 \frac{t}{t_{the}} \right) + 1.37 \cdot \exp\left(-1.33 \frac{t}{t_{the}} \right) \quad \textbf{(3-H)}$$

The estimated distance **L** in order to avoid the risk of thermal feedback (Banks, 2008) between pumping wells in well-doublet scheme (abstraction-injection) is:

$$L = \frac{2Q}{\pi T i} \quad \textbf{(3-I)} \text{ , where}$$

- Q [m^3/s] is pumping flow rate
- T [m^2/s] is aquifer transmissivity
- i [m/m] is hydraulic gradient

3.1.7. Retardation factor

According to Banks, the retardation factor **R** is the fraction between thermal and hydraulic breakthrough times, and defines how thermal front is retarded relative to hydraulic groundwater velocity:

$$R = \frac{t_{the}}{t_{hyd}} = \frac{S_{VC,aq}}{nS_{VC,wat}} \quad \textbf{(3-J)}$$

3.1.8. Thermal radius

According to Drijver et al. 2001, the thermal radius around the injection well $\mathbf{r_{th}}$ is defined as follows:

$$r_{th} = \sqrt{\frac{c_w Q}{c_m \pi b}} \quad \textbf{(3-K)}$$

where

- c_w [J/kg.K] is water heat capacity
- c_m [J/kg.K] is aquifer heat capacity
- b [m] is aquifer thickness
- Q [m^3] is total pumped water in the considered period

In order to avoid thermal feedback, Drijver recommends the following minimum distance between wells for seasonably reversible well doublet ATES system (heating and cooling period): $\mathbf{L=3r_{th}}$

3.1.9. Heat recovery factor

When ATES system is functioning in reversible operation, the heat recovery factor (HRF) for heating / cooling stored energy is defined as a ratio between the annually discharged and charged energy (Kranz et al. 2010). Bloemendal et al. (2018), also utilizes a term of recovery efficiency, referred to a warm or cold stored energy over the whole charge/discharge cycle (normally one year), defined as follows:

$$HRF = \frac{E_{out}}{E_{in}} = \frac{\int_{t,out} \left[Q_{out}(t) \rho_w c_w \left(T_{warm,out}(t) - T_{cold,out}(t) \right) \right] dt}{\int_{t,in} \left[Q_{in}(t) \rho_w c_w \left(T_{warm,in}(t) - T_{cold,in}(t) \right) \right] dt} \quad \textbf{(3-L)}$$

where

- indices *out* / *in* stand for discharge / charge cycles
- indices *warm* / *cold* stand for warm / cold wells
- c_w [J/kg.K] is water heat capacity
- ρ_w [kg/m^3] is water density
- Q [m^3/s] is the pumping rate in the considered cycle
- E [J] is the stored aquifer energy

3.2. MODFLOW for groundwater flow modeling

MODFLOW (Harbaugh et al. 2005) is a modular and versatile block centered FDM (finite difference method) code developed by USGS (United States Geological Survey) with several decades of continues development and debugging. It is also much used and highly accepted among groundwater and hydro-geological scientific community.

3.2.1. MODFLOW general overview

The general governing differential equation solved in MODFLOW for confined aquifer is:

$$S_s \frac{\partial h}{\partial t} = \frac{\partial}{\partial x}(K_x \frac{\partial h}{\partial x}) + \frac{\partial}{\partial y}(K_y \frac{\partial h}{\partial y}) + \frac{\partial}{\partial z}(K_z \frac{\partial h}{\partial z}) + W \qquad \textit{(3-M)}$$

where

- K_x, K_y and K_z [m/s] are the values of hydraulic conductivity along the x, y, and z coordinate axes
- h [m] is the potentiometric head
- W [s^{-1}] is a volumetric flux per unit volume representing sources and/or sinks of water, where negative values are extractions, and positive values are injections
- S_s [m^{-1}] is the specific storage of the porous material
- t [s] is time

Spatially, the modeled groundwater domain is discretized in blocks or cells distributed in rows (i-index), columns (j-index), and layers (k-index). Active and inactive cells can also be assigned in order to establish model boundaries (see Figure 3-6).

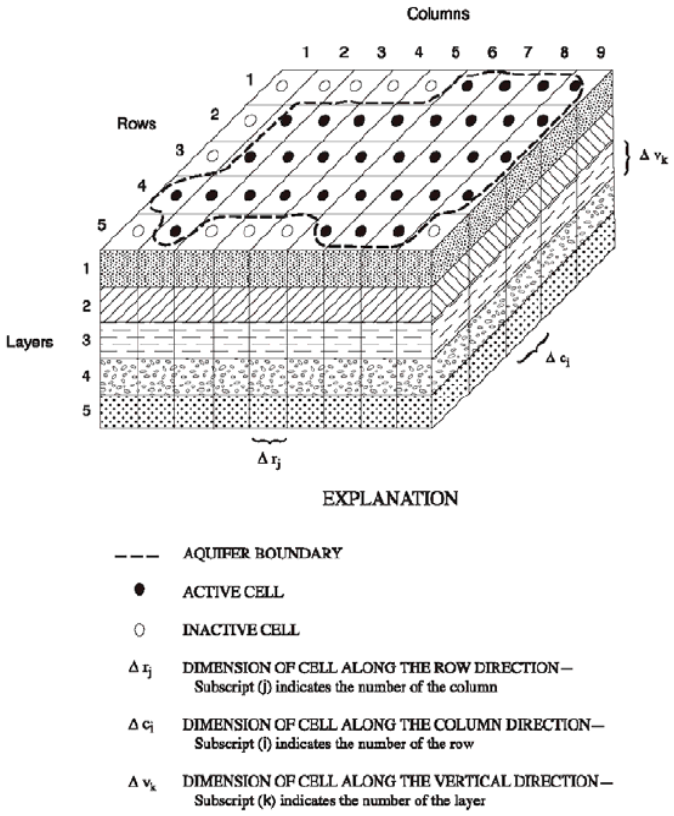

Figure 3-6: MODFLOW model spatial domain distribution

3.2.2. Groundwater flow process

MODFLOW design is based on program modularity, therefore different packages can be loaded on-demand when needed. In ModelMuse, MODFLOW graphical user interface, the Groundwater Flow process is required for all MODFLOW models and includes the Basic package (BAS6), the groundwater flow packages, the boundary conditions packages and solvers. Additionally, different packages groups are available, such as subsidence, observation, output and post-processors.

3.2.3. Groundwater flow packages

The groundwater flow packages are used to define the aquifer properties such as hydraulic conductivity or transmissivity. There are three groundwater flow packages in MODFLOW:

- In the Block-Centered Flow package (BCF6), the user defines all the aquifer properties for all cells directly; parameters are not used
- In the Layer Property Flow package (LPF), the user defines aquifer properties for all cells either directly or through the use of parameters
- In the Hydrogeologic Unit Flow package (HUF2), the user defines the properties of hydrogeologic units exclusively through the use of parameters. The hydrogeologic units do not correspond directly to model layers. Instead, the user defines the top and the thickness of each hydrogeologic unit and MODFLOW combines data from multiple hydrogeologic units to determine the appropriate values for the aquifer properties at each cell

Two additional packages provide additional options related to groundwater flow:

- The Horizontal Flow Barrier package (HFB6) can be used to reduce the conductances between horizontally adjacent cells
- In the Unsaturated-Zone Flow (UZF) package, water is routed from the land surface, through the unsaturated zone to the water table. Evapotranspiration (ET) can be simulated in the UZF package and whatever is not removed by ET becomes recharge to the saturated zone. Infiltration excess, can be routed to streams (SFR) or lakes (LAK)
- The Seawater Intrusion Package (SWI2) simulates variable density flow with a sharp interface approximation

3.2.4. Boundary conditions packages

There are three types of boundary conditions in the Groundwater Flow process - specified head boundaries, specified flux boundaries and head-dependent flux.

Specified Head boundaries (which are examples of Dirichlet or first-type boundary conditions) can be defined using the following packages:

- In the Basic package (BAS6), IBOUND is used to identify specified head boundaries and STRT gives the head at those boundaries
- The Time-Variant Specified-Head package (CHD) can be used
- The Flow and Head Boundary package (FHB) can be used

Specified Flux boundaries (which are examples of Neumann or second-type boundary conditions) can be specified with:

- Flow and Head Boundary package (FHB) is used to introduce a series of times and corresponding flux rates at specific cells. Linear interpolation is used to determine the flux rates at intervening times. The times do not need to be a the beginnings or ends of stress periods.
- Recharge Package (RCH) - the user enters an array of flux values covering the entire upper surface of the model. The rates can be positive, negative or zero. There are several options for determining to which layer the recharge will be applied
- Well Package (WEL) - the user defines a flux rate for particular cells in particular stress periods

Head-Dependent Flux boundaries (which are examples of Robin or mixed boundary conditions). There are a large number of head-dependent flux boundary packages, including the following:

- General-Head Boundary (GHB) package
- Drain (DRN) package
- Drain-Return (DRT) package
- River (RIV) package
- Reservoir (RES) package
- Evapotranspiration (EVT) package
- Evapotranspiration Segments (ETS) package

3.2.5. Solvers packages

Every MODFLOW model must include one and only one of the solver packages. Six different solvers have been incorporated into MODFLOW-2000:

- DE4 - Direct Solver Package
- GMG - Geometric Multigrid Solver
- LMG - Link-AMG Package
- PCG - Preconditioned Conjugate-Gradient Package
- PCGN - Preconditioned Conjugate Gradient Solver with Improved Nonlinear Control
- SIP - Strongly Implicit Procedure Package

3.2.6. Subsidence packages

MODFLOW has several packages that can be used to simulate subsidence due to groundwater withdrawal. The ones supported in ModelMuse are the SUB and SWT packages:

- The Subsidence and Aquifer-System Compaction (SUB) package is used for simulating the drainage, changes in groundwater storage, and compaction of aquifers, interbeds and confining units that constitute an aquifer system

- The Subsidence and Aquifer-System Compaction Package for Water-Table Aquifers (SWT) package simulates vertical compaction in models of regional ground-water flow

3.2.7. Observation packages

The various observation packages are used to compare observed values with simulated values. Such comparisons are useful in model calibration. The available observation packages are listed as follows:

- HOB: Head Observation Package Pane - head observations are compared with simulated heads interpolated to the location of the head observations. If the observed head represents more than one layer, a weighted average of the heads in the various layers is calculated

- CHOB: Specified-Head Flow Observation Package Pane - specified-head flow observations are compared with simulated flows at a group of specified head cells

- DROB: Drain Observation Package Pane - rain observations are compared with simulated flows at a group of drain cells

- GBOB: General-Head-Boundary Observation Package Pane - general-head boundary observations are compared with simulated flows at a group of general-head boundary cells.

- RVOB: River Observation Package Pane - river observations are compared with simulated flows at a group of river cells

- STOB: Stream Observation Package Pane - stream observations are compared with simulated flows at a group of stream cells

3.2.8. Output packages

Only one package related to output is the HYD: HYDMOD package. The HYDMOD package is used to define specified locations at which data will be written to a binary file at every time step of a simulation.

3.2.9. Post processors

ModelMuse supports two post processors: MODPATH and ZONEBUDGET.

- MODPATH is used for particle tracking. The user assigns starting locations for particles and MODPATH will track the advective transport of those particles either forward or backwards

- ZONEBUDGET is used for constructing subregional water budgets. The user assigns cells to zones and ZONEBUDGET constructs a water budget for all the cells in each zone

ModelMuse is not capable to post-process the head results in order to generate the flow field (groundwater velocity vectors). That's why MODPATH is an available option for spatially / temporally particles flow field representation, but also the external post-processors Model Viewer and GW Chart could be used for flow and thermal results analysis and presentations.

3.2.10. Convergence and stability criteria

A summary of all inflows (sources) and outflows (sinks) of water to a region is generally called a water budget. The model program calculates a water budget for the overall model as a check on the acceptability of the solution, and to provide a summary of the sources and sinks of water to the flow system. Numerical solution techniques for simultaneous equations do not always result in a correct answer; in particular, iterative solvers may stop iterating before a sufficiently close approximation to the solution is attained. A water budget provides an indication of the overall acceptability of the solution.

Stability criteria approach used by MODFLOW and MT3DMS is that simulations are divided into stress periods and transport time steps. The concept of a MODFLOW time step is known as flow time step. The lengths of transport time steps are determined by stability criteria (e.g. Courant / Pèclet numbers) automatically by MT3DMS, but may be specified by the user if the implicit finite difference option is used to solve the solute-transport equation.

3.3. Solute and heat transport modeling

MT3DMS (Zheng et al. 1999) is a finite difference code for solute transport simulation. Its almost 20 years of development and improvement, as well as its intrinsic data integration with MODFLOW makes MT3DMS a perfect match for integral groundwater flow/transport modeling.

3.3.1. General overview

The solute transport model MT3DMS is used to simulate heat transport in shallow confined aquifers due to similarities between mathematical description of solute and heat transport equations (Méndez et al. 2010). The following equations represent respectively solute and heat transport in porous media:

Solute transport:

$$\left(1+\frac{\rho_b K_d}{n}\right)\frac{\partial C}{\partial t} = div\left[\left(D_m+\alpha v_a\right)gradC\right]-div\left(v_a C\right)+\frac{q_k C}{n} \quad \textbf{(3-N)}$$

concentration change *hydrodynamic dispersion* *solute advection* *source/sinks mass*

Heat transport:

$$\left(\frac{\rho_m c_m}{n\rho_w c_w}\right)\frac{\partial T}{\partial t} = div\left[\left(\frac{\lambda_m}{n\rho_w c_w}+\alpha v_a\right)gradT\right]-div\left(v_a T\right)+\frac{q_h}{n\rho_w c_w} \quad \textbf{(3-O)}$$

temperature change *thermal diffusion + dispersion* *thermal convection* *source/sinks energy*

In both equations:

- indices **w**, **m** and **b** stand for water, porous media and dry bulk material respectively
- ***C*** and ***T*** are solute concentration and temperature respectively
- ρ, c, n and λ are density, heat capacity, porosity and thermal conductivity respectively
- K_d is the distribution coefficient (solute equation)
- D_m is the molecular diffusion coefficient (solute equation), $D_h=\lambda_m/(n\rho_w c_w)$ is the thermal diffusion coefficient (heat equation)
- αv_a is the mechanical dispersion term, where v_a is groundwater velocity and α is longitudinal dispersivity

The following coefficient correlation should be done in order to utilize MT3DMS for heat transport simulation. Solute coefficients reformulation in terms of heat transport parameters, as well as MT3DMS corresponding packages are listed below:

- Chemical reaction package: $K_d = \frac{c_s}{\rho_w c_w}\left[\frac{m^3}{kg}\right]$
- Dispersion package: $D_m = \frac{\lambda_m}{n\rho_w c_w}\left[\frac{m^2}{s}\right]$
- Dispersion package: $\alpha = \alpha[m]$
- Sink and source mixing package: instead of concentration *C [kg/m³]* should be specified temperature *T [K]*

In the following table are summarized the main parameters and correlation coefficients used in MT3DMS for heat transport simulation:

Table 3-I: MT3DMS parameters and correlation coefficients

Parameter	Notation	Units	Value
Solid material density	ρ_s	kg/m^3	2670
Dry bulk density	ρ_b	kg/m^3	2000
Water density	ρ_w	kg/m^3	1000
Water heat capacity	c_w	J/(kg.K)	4190
Solid material heat capacity	c_s	J/(kg.K)	860
Porous thermal conductivity	λ_m	W/(m.K)	2
Aquifer porosity	n	%	25
Distribution coefficient	K_d	m^3/kg	2.1E-04
Diffusion coefficient	D_m	m^2/s	1.9E-06
Longitudinal dispersivity	α	m	0.5

3.3.2. Software packages

The available MT3DMS packages which are directly linked and can be selected in the MODFLOW Packages and Programs dialog box are the following:

- Basic Transport Package (BTN)
- Advection Package (ADV)
- Dispersion Package (DSP)
- Sink & Source Mixing Package (SSM)
- Chemical Reactions Package (RCT)
- Generalized Conjugate Gradient Solver (GCG)
- Transport Observation Package (TOB)

The BTN and GCG packages are always used in MT3DMS.

3.3.3. Solvers and stability

In addition to the explicit formulation of the original MT3D code, MT3DMS includes an implicit formulation that is solved with an efficient and versatile solver. The iterative solver is based on generalized conjugate gradient (GCG) methods with three preconditioning options and the Lanczos/ORTHOMIN acceleration scheme for nonsymmetrical matrices.

If the GCG solver is selected, dispersion, sink/source, and reaction terms are solved implicitly without any stability constraints. For the advection term, the user has the option to select any of the solution schemes available, including the standard finite-difference method, the particle-tracking-based Eulerian-Lagrangian methods, and the third order TVD method.

The finite-difference method can be fully implicit without any stability constraint to limit transport step sizes, but the particle-trackingbased Eulerian-Lagrangian methods and the third-order TVD method still have time-step constraints associated with particle tracking and TVD methodology.

If the GCG solver is not selected, the explicit formulation is automatically used in MT3DMS with the usual stability constraints. The explicit formulation is efficient for solving advection-dominated problems in which the transport step sizes are restricted by accuracy considerations. It is also useful when the implicit solver requires a large number of iterations to converge or when the computer system does not have enough memory to use the implicit solver.

4. Case study: Pukkila's district heating network

4.1. General overview

Pukkila is a Finnish municipality, located in the Uusimaa region in the southern part of Finland. The municipality has a population of 1,939 (Statistics Finland, October 2017) and covers an area of roughly 146 square kilometers of which 0.6% is water.

Figure 4-1: Location of Pukkila

(geographical coordinates 60°38.7'N 025°35'E) →

4.2. Existing district heating network

Pukkila's district heating network is part of Nivos Energia Oy (until 2017, Mäntsälän Sähkö). It is located in the village of Pukkila and its heat is mainly produced by chips in a 1.5MW nominal boiler. In addition to the base load chips boiler, the heating plant has two peak load oil boilers (2MW), which have been used very sporadically.

Figure 4-2: Pukkila's district heating network

The approximate Pukkila's heat plant location is in the northern part of the village. Porvoonjoki river is an important natural boundary, limiting the village from south-east

The total district heat generation in Pukkila was 4407 MWh in 2017. Base load boiler (chips fuel) efficiency is estimated to be about 80%. The Pukkila heating plant is located at the northern end of the village and the network comprises roughly 40 connection points (Figure 4-2, source Heikki Hynynen, Nivos Energia Oy).

4.3. Heating energy demand

The power of Pukkila's DH network ranges from roughly 0.3-1MW. The following *Figure 8.3* presents the annual heating energy demand (real data for 2017) of Pukkila's district heating network. The curve plateau during the summer period is an indicator of domestic hot water share (more or less constant during the year), roughly estimated in 0.3MW.

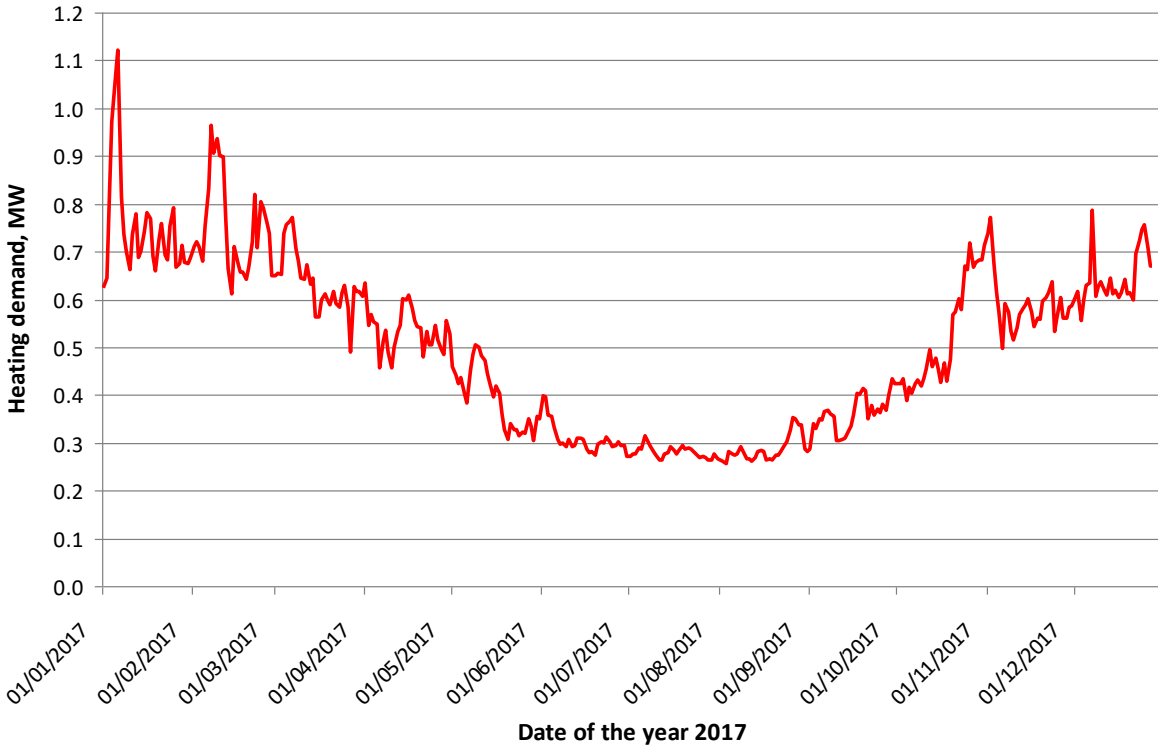

Figure 4-3: Pukkila's annual heating demand (2017)

4.4. Annual heating duration curve

Real annual heating energy demand data for 2017 is used in order to prepare the annual heating durability curve (see Figure 4-4). Heating peak load is very steep, as only during 12 days per year the needed heating power is over 0.8MW. On the other hand, the introduction of groundwater source heat pump (GWHP) for base load heating demand could be in the range of 0.3-0.6MW, using chips boiler only for peak loads. The other possibility is to completely substitute the boiler by GWHP and this option is also studied among the available scenarios.

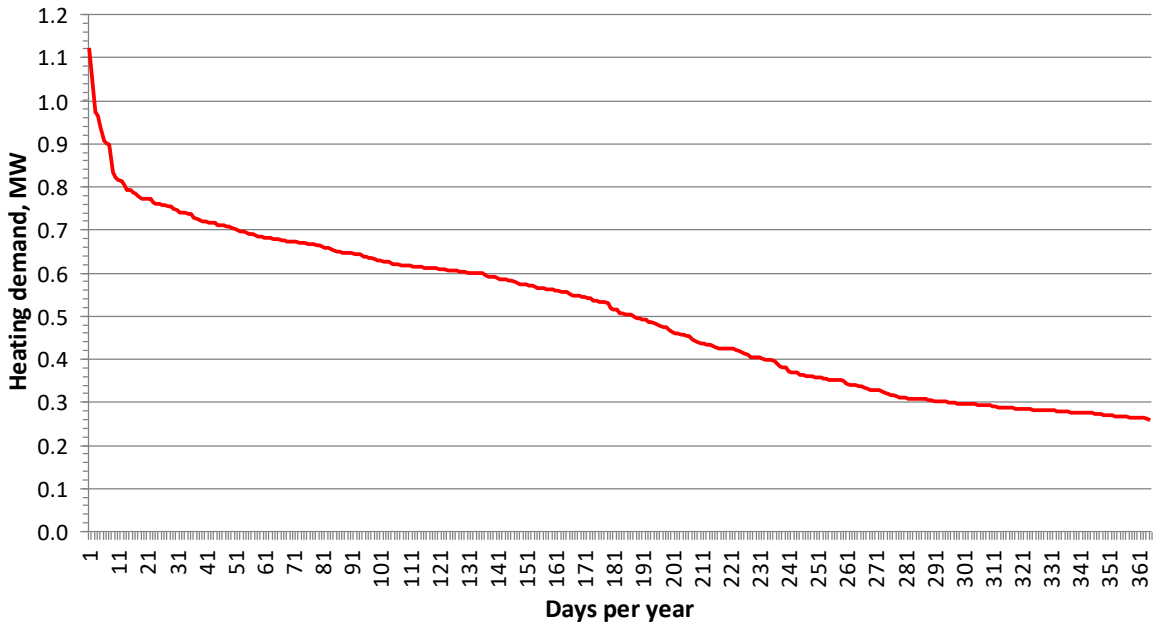

Figure 4-4: Pukkila's annual heating duration curve (2017)

5. Pukkila's aquifer area

In order to retrieve available open data of Pukkila's aquifer area, Finnish Environment Institute (Suomen Ympäristökeskus, SYKE) website is used, and particularly Hertta 5.7 application regarding underground water areas, as well as monitoring stations and observation wells (https://wwwp2.ymparisto.fi/scripts/hearts/welcome.asp).

5.1. Groundwater areas

Pukkila's groundwater area is composed of three different aquifer zones, of which two (Vanhalanmäki-161602 and Pukkilan kk-161601) are close to Pukkila village and its district heating plant. Porvoonjoki river is a natural border of the south-eastern part of the village and separates zone 161601 in two parts, being also a specified head boundary for the studied area. Similarly, small streams of Porvoonjoki, Virenoja and Kuutinoja, limit the Vanhalanmäki-161602 area from the north, as well as separate 161602 and 161601 areas (see Figure 5-1 and Figure 5-2).

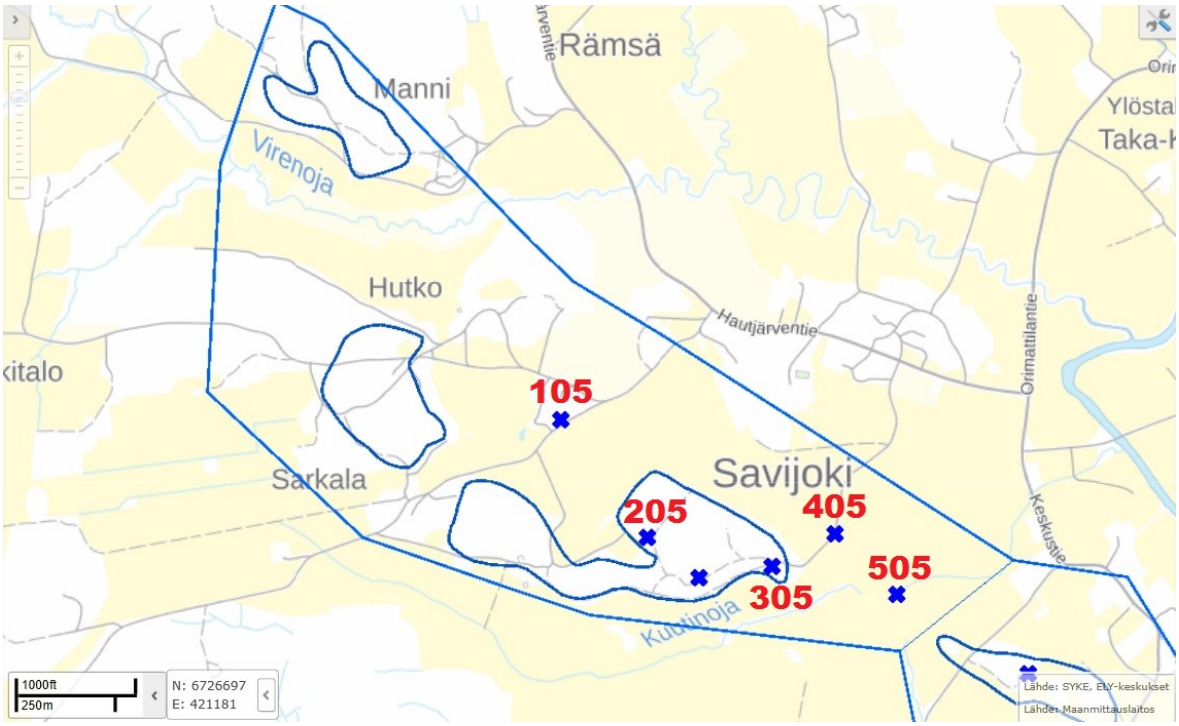

Figure 5-1: Pukkila's groundwater area #161602

Blue crosses with red numbers are observation wells (#105, 205, 305, 405 and 505)
Natural boundaries are streams Virenoja from north and Kuutinoja (middle)

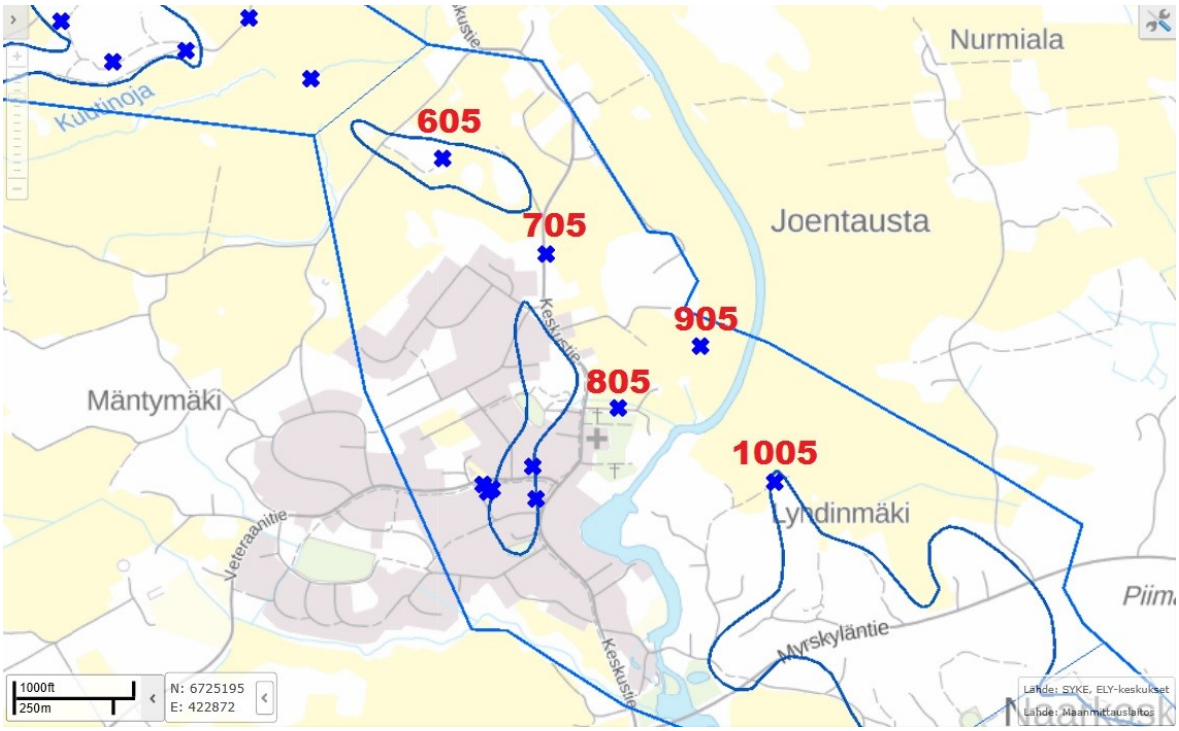

Figure 5-2: Pukkila's groundwater area #161601

Blue crosses with red numbers are observation wells (#605, 705, 805, 905 and 1005)
Important natural boundary is Porvoonjoki river limiting the village from south-east

Table 5-I: Pukkila's groundwater areas (summary)

Number	**161602**	**161601**
Name	Vanhalanmäki	Pukkilan kk
Area class	I	II
Location of the municipality	Pukkila	Pukkila
Total Area, km^2	1.87	2.39
Area of formation, km^2	0.33	0.51

5.2. Observation wells

There is available information for 5 observation wells in area 161602 (# 105, 205, 305, 405 and 505) and 5 observation wells in area 161601 (# 605, 705, 805, 905 and 1005). The water level variation of each well has been recorded during the last 10 years and the results are summarized in the following Figure 5-3 and Figure 5-4. The average water level (piezometric head) during the period 2006-2016, as well as its standard deviation for each well are estimated from the available data. Recently carried out observations revealed an average aquifer temperature of 6.5-7ºC. Since level data standard deviation is less than 1m, average water level values would be used in order to calibrate the groundwater flow model. All available information for observation wells in areas 161602 and 161601 are summarized in Table 5-II and Table 5-III respectively.

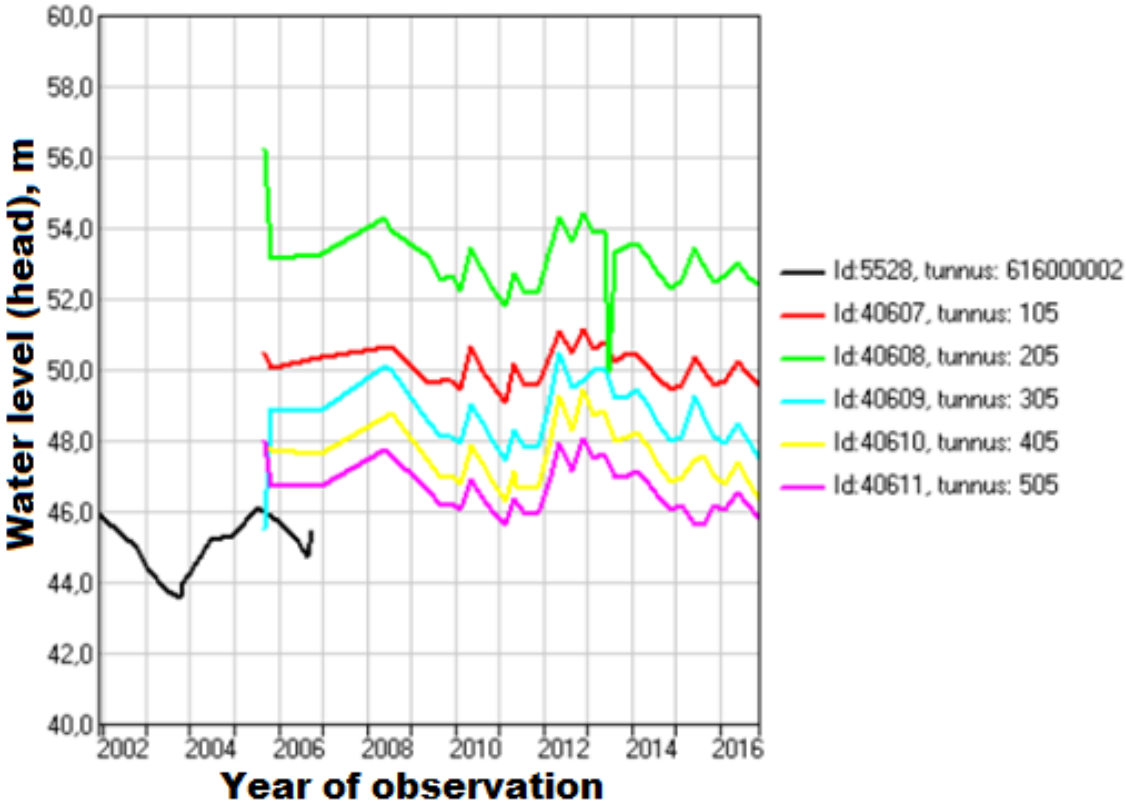

Figure 5-3: Water level variation in observation wells (area 161602)

Observation wells #105, 205, 305, 405 and 505 between 2006 and 2016. Relatively stable levels among the years, in the range between roughly 46.6±0.7m and 53.1±1m (Hertta 5.7 application, SYKE).

Table 5-II: Observation wells area 161602 (summary)

Observation well number	**105**	**205**	**305**	**405**	**505**
ETRS-TM35FIN (North), m	6725806	6725475	6725394	6725484	6725314
ETRS-TM35FIN (East), m	420877	421119	421468	421645	421820
EUREF-FIN/WGS84 (decimal degrees North - East)	60.66015 - 25.55245	60.65723 - 25.55701	60.65657 - 25.56342	60.65741 - 25.56662	60.65592 - 25.56989
Top of the pipe, m	61.46	70.77	59.51	51.83	49.38
Elevation (terrain), m	61.03	69.92	58.33	51.13	48.7
Bottom of the pipe, m	42.33	39.92	42.33	25.63	31.2
Impermeable rock elev., m	42.33	39.92	42.33	25.63	31.2
Average water level, m estimation (2006-2016)	50.1	53.1	48.7	47.6	46.6
Standard deviation, m	±0.5	±1	±1	±0.8	±0.7
Actual water level, m *measured level 17.5.2018	49.55	52.45	47.49 (50.57*)	46.37 (49.33*)	45.81

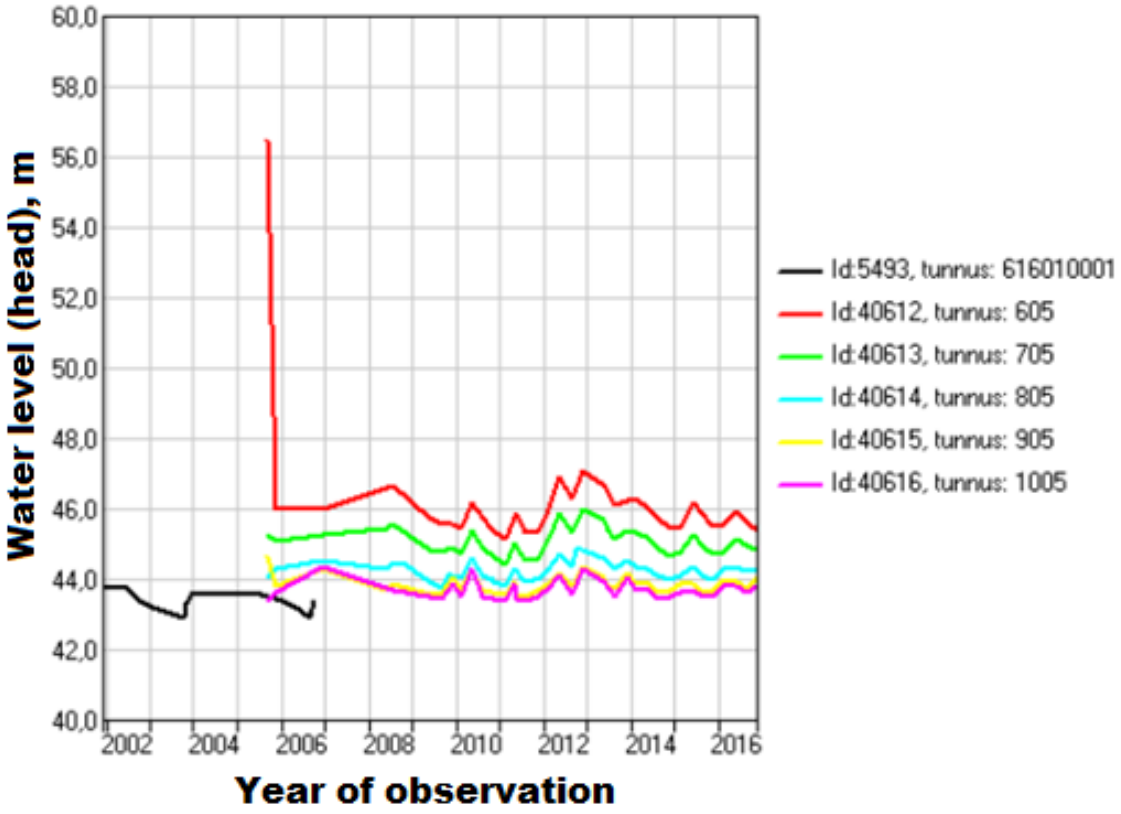

Figure 5-4: Water level variation in observation wells (area 161601)

Observation wells #605, 705, 805, 905 and 1005 between 2006 and 2016. Relatively stable levels among the years, in the range between roughly 43.7±0.3m and 45.9±0.5m (Hertta 5.7 application, SYKE).

Table 5-III: Observation wells area 161601 (summary)

Observation well number	**605**	**705**	**805**	**905**	**1005**
ETRS-TM35FIN (North), m	6725091	6724823	6724390	6724564	6724181
ETRS-TM35FIN (East), m	422189	422479	422682	422914	423121
EUREF-FIN/WGS84 (decimal degrees North - East)	60.65399 - 25.57672	60.65164 - 25.58213	60.64780 - 25.58601	60.64940 - 25.59018	60.64601 - 25.59411
Top of the pipe, m	57.86	51.3	46.73	47.66	51.57
Elevation (terrain), m	57.06	50.65	46.25	46.88	50.96
Bottom of the pipe, m	39.56	16.65	34.55	40.28	28.46
Impermeable rock elev., m	39.56	16.65	34.55	40.28	28.46
Average water level, m estimation (2006-2016)	45.9	45.1	44.3	43.9	43.7
Standard deviation, m	±0.5	±0.4	±0.3	±0.3	±0.3
Actual water level, m *measured level 17.5.2018	45.37	44.83	44.26 (44.8*)	44.05	43.82

5.3. Geographical data

In order to assess and model appropriately the groundwater flow, it is important to start with reliable terrain model. For this purpose the open data of the National Land Survey of Finland (https://tiedostopalvelu.maanmittauslaitos.fi/tp/kartta?lang=en), specifically its "10m elevation model" is used. This elevation model divides all Finnish topography into separated sheets and square grid of 10x10m where elevation is provided for each grid vertex (since TM35FIN coordinate system is used, all coordinates are expressed in meters).

Figure 5-5: Elevation model(general map)

Elevation model data extracted from Geological Survey of Finland. Green zones are aquifers formation areas (http://en.gtk.fi/informationservices/map_services/)

The elevation model was downloaded as Geo-TIFF raster file in two separate cadastral sheets, L4111 and L4112, as well as converted into Surfer Grid file (GRD) using QGIS (geographic information system) software. After that, the surfer grid file was imported into MODFLOW, assigning it to "Model_Top" parameter with "point average" interpolation.

The extracted area of roughly 5.2km in length and 1.3km in width contains a dynamic terrain with elevations between roughly 35 and 95m above sea level, as seen in Figure 5-6. Porvoonjoki river and its effluents Virenoja and Kuutinoja determine the hydrogeological contours and will play a key role as natural boundaries of our groundwater model (see Figure 5-6).

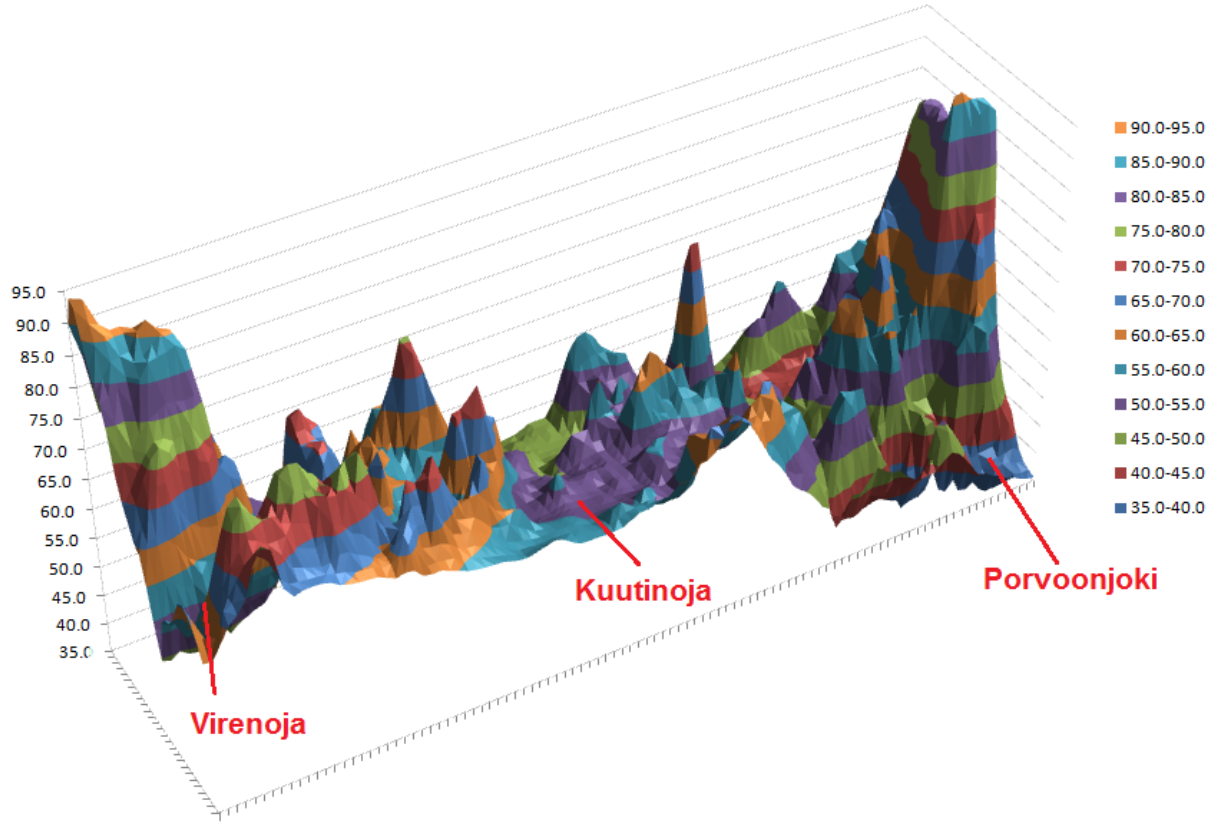

Figure 5-6: Pukkila's area elevation model (3D representation)

3D view of Pukkila's area seen from west (elevation highly exaggerated). Elevation model data extracted from National Land Survey of Finland. Main river Porvoonjoki, as well as streams Virenoja and Kuutinoja are presented since their elevations would be used as specified head boundaries in groundwater flow model

6. Groundwater flow model

Groundwater model is a simplified quantitative tool developed in order to synthesize and represent the actual hydrological processes as accurate as possible, as well as to be able to describe and predict their future development and trends.

In order to study both steady state and transient behavior (due to additional stresses like artificial pumping), the groundwater model was developed using the finite difference code MODFLOW-2005 (Harbaugh et al. 2005) under ModelMuse as graphical user interface. Alternatively, a simple steady state model was created with Microsoft Excel in order to compare the simulated results.

6.1. Boundary conditions

As mentioned previously, the studied aquifer area has natural boundaries with "specified head boundary" (Dirichlet condition). Porvoonjoki river limits the area from south-east, Virenoja stream from north and Kuutinoja stream crosses the area in the middle.

Aquifer north-east and south-west limits would be considered as "no flow" boundaries, special cases of "specified flow boundary" (Neumann condition) applied with zero flow. Abstraction and injection wells would be represented as point sources and modeled with "specified flow boundary". Similarly, the recharge rate is represented by a "specified flow boundary" distributed evenly over the total model area.

6.1.1. Specified head boundaries

Specified head boundaries are designated for Porvoonjoki river between 43.5m (north) and 40.5m (south), Virenoja stream between 48m (east) and 48.8m (west) and Kuutinoja stream from 46-47m (east part) to 53m (west part).

In MODFLOW, the specified head boundaries are introduced using CHD: Time-Variant Specified-Head package.

6.1.2. Specified flow boundaries

In MODFLOW specified flow boundaries are implemented using WEL: Well package, for point source pumping or injecting wells. On the other hand, it is not needed to specify no flow boundaries, they are the default option for all MODFLOW boundaries.

Recharge is defined in MODFLOW using RCH: Recharge package. Initially, a typical value for recharge rate of 5E-9 m/s is used (Arola et al. 2016), and after model's calibration, adjusted to 6E-9 m/s .

6.2. Numerical model in MODFLOW

Aquifer area is discretized using 100x100m square cell and grid of 40 columns (designated in MODFLOW by "j"-index) by 13 rows ("i"-index), covering a physical area of roughly 3km^2, comprised between the aquifer north-west border and the natural boundary, Porvoonjoki river, from the east.

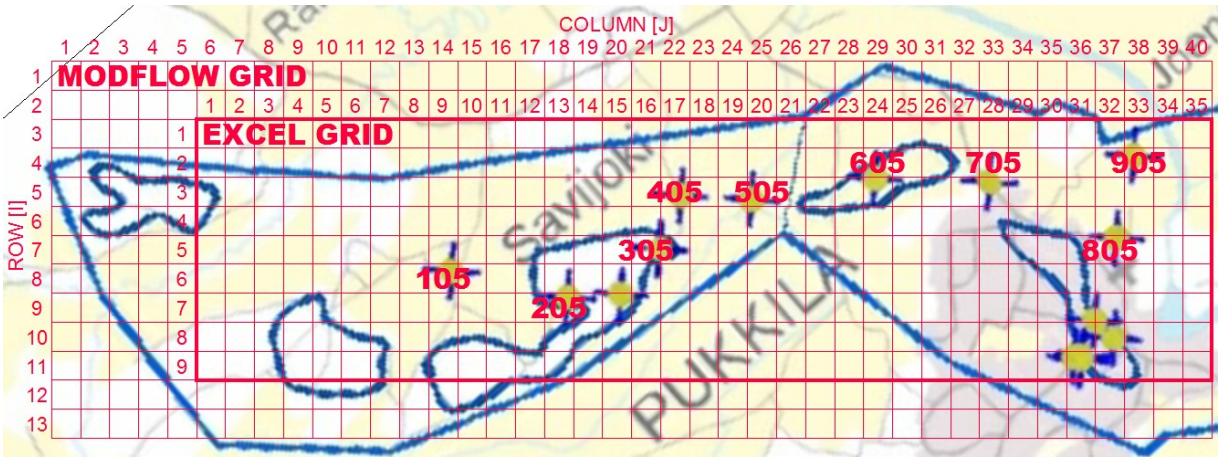

Figure 6-1: Numerical models - discretization grids

MODFLOW model contains 40 columns by 13 rows (outer rectangle), while a simple Excel model is a smaller sub-domain of 35 columns by 9 rows (inner bold rectangle). Yellow points designate the observation wells locations and their numbers in red.

The model is divided in 2 layers ("k"-index in MODFLOW).The terrain topography is introduced as "point average interpolation" for "Model_Top" parameter of the upper layer (#1), using National Land Survey of Finland "10m elevation model". The lower layer (#2) is a confined aquifer between elevations 20 and 40m (assuming average aquifer thickness of 20m).

A standard value for horizontal hydraulic conductivity is chosen (sand/gravel aquifer) K_x= K_y=1E-4 m/s (Arola et al. 2016). Vertical hydraulic conductivity is set as K_z= 0.1K_x. Standard values are also used for porosity (n=0.25) and storativity (S=1E-5).

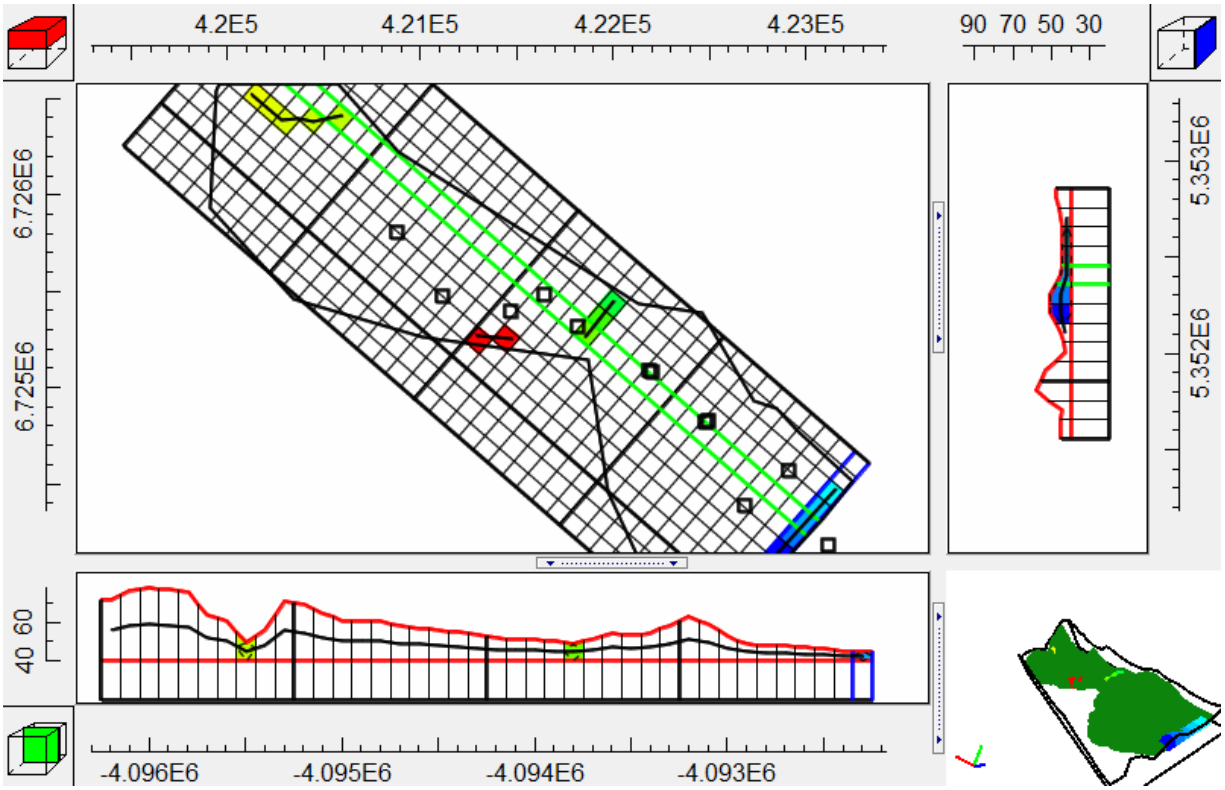

Figure 6-2: Numerical models - MODFLOW environment

Discretization grid implementation in ModelMuse (MODFLOW). Terrain elevation information is assigned to the upper layer, as well as are assigned the specified head boundaries (color cells). Square points designate the observation wells locations, all coordinates are set using TM35FIN coordinate system (in meters) as seen in primary x-axis (up) and y-axis (left)

6.3. Setting up a simple groundwater model

A simple steady state model is implemented and calibrated using Microsoft Excel. For confined isotropic aquifer with recharge, two dimensional steady state groundwater flow is governed by the following equation, known as Poisson equation, a simplified 2D form of the general equation for flow in porous media (3-L):

$$\frac{\partial^2 h}{\partial x^2} + \frac{\partial^2 h}{\partial y^2} = -\frac{R}{T} \qquad \textbf{(6-A)}$$

where

- h [m] represents the water head,
- R [m/s] is the recharge rate,
- T=Kb [m^2/s] is aquifer transmissivity (K [m^2/s] and b [m] are hydraulic conductivity and confined aquifer thickness respectively).

6.3.1. Discretization equations

Substituting the discretization of second derivative terms (left side of equation 6-A) and assuming square grid cell (Δx=Δy=a), the discretization equation for cell (i,j) is:

$$\frac{h_{i-1,j} - 2h_{i,j} + h_{i+1,j}}{\Delta x^2} + \frac{h_{i,j-1} - 2h_{i,j} + h_{i,j+1}}{\Delta y^2} = -\frac{R}{T}$$

$$\Rightarrow h_{i,j} = \frac{1}{4}\left(h_{i-1,j} + h_{i+1,j} + h_{i,j-1} + h_{i,j+1} + a^2 \frac{R}{T} \right) \quad \textbf{(6-B)}$$

Without recharge (R=0), equation (6-B) reduces to the solution of Laplace equation, where the head of each cell is the average of its four neighbors. On the other hand, it is clear that steady state solution depends on *R/T* ratio, therefore in order to calibrate the model according to observation wells measured values, *R/T* ratio would be an important sensitive parameter to vary. In case of injection or abstraction well with pumping flow rate Q [m^3/s] (positive for injection and negative for abstraction), the discretization equation of the cell containing the well is:

$$h_{i,j} = \frac{1}{4}\left(h_{i-1,j} + h_{i+1,j} + h_{i,j-1} + h_{i,j+1} + a^2 \frac{R}{T} + \frac{Q}{T} \right) \quad \textbf{(6-C)}$$

The pumping flow is assumed to be evenly distributed within the whole pumping cell, therefore the computed head (or alternatively, the drawdown) is a cell value average. The real head within the pumping well can be computed additionally, applying Thiem equation:

$$h_w = h_{i,j} - \frac{Q}{2\pi T} \ln \frac{r_e}{r_w} \quad \textbf{(6-D)}\text{ , where}$$

- Q [m^3/s] is pumping flow rate
- T [m^2/s] is aquifer transmissivity
- r_w [m] is well radius
- r_e [m] is the distance from well center where the head equals the average value of the cell. According to Anderson et al. (2015), for square grid cell with side a[m], $\Rightarrow r_e = 0.208a$

6.3.2. Implementation in Excel

The previously described numerical model with irregular aquifer shape would be approximated to rectangular shape area of 3500m long and 900m width (the area comprised between the effluents Virenoja and Kuutinoja of roughly $3km^2$), using the same cell size of 100x100m (35x9 cells grid).

First of all, it's important to disable Excel's formulas automatic calculation option and set it to manual, enabling iterative calculation (e.g. maximum number of iterations 10-50, maximum change 0.0001). This step is crucial in order to avoid the cross-reference formulas introduced by equation (6-B).

Specified head boundary conditions values are introduced as constant values in column 1 and 35, as well as in the middle cells (red border). No flow boundaries are specified as "ghost cells" (yellow) outside the model and each yellow cell is equal to its corresponding model cell neighbor. All inner cells are defined according to equation (6-B).

A special flag is established in order to initialize the model (assigning to all model cells the initial head value of 46m if the flag is "on", otherwise setting the formula corresponding to equation 6-B, see Figure 6-3). This is important, since the number of iterations needed and the potential convergence of the model depends on the cells' initial values.

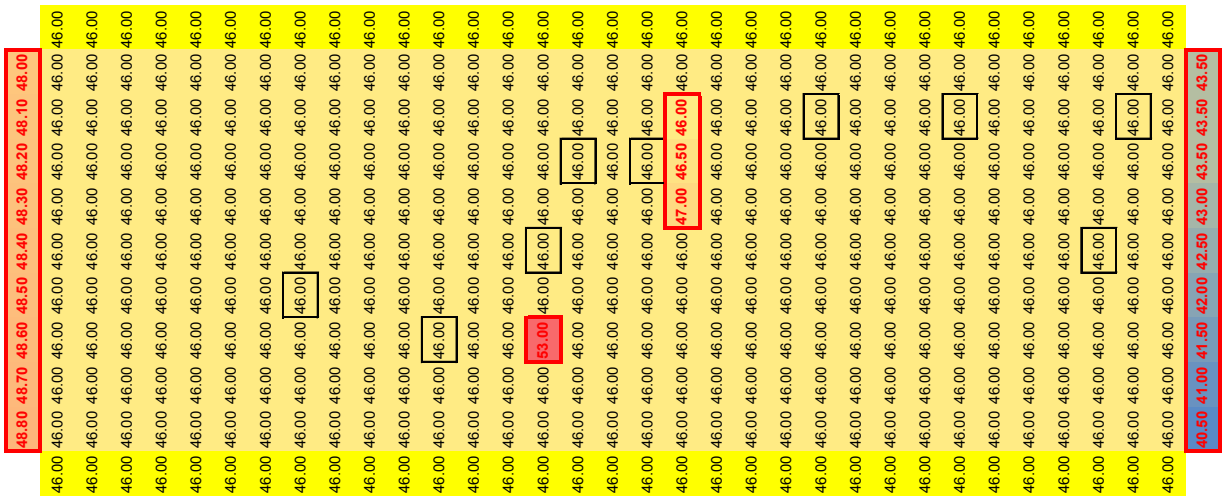

Figure 6-3: Simple Excel model - boundary conditions

Simple Excel model with boundary conditions and initial head values (46m). Red border cells are specified head cells (first column - Virenoja, mid cells - Kuutinoja and 35th-column - Porvoonjoki). Yellow cells are the "ghost cells" outside the model representing a "no flow" boundary. All intermediate cells are set according to equation (6-B). Black border cells represent the observation wells (from left to right - #105, 205, ... , 905)

6.3.3. Groundwater model convergence criteria

MODFLOW principle for convergence criteria and its concept of water budget is applied in the simple steady state Excel model. According to water budget principles, system's inflow is calculated, like recharge from precipitation or snowmelt, injection wells, inflow from specified head boundaries, etc. After that system's outflows are computed, such as drains, sinks, pumping / abstraction wells and outflow from specified head boundaries. Finally, water budget and water budget error are calculated according to the following expressions:

$$WaterBudget = Inflow - Outflow, \left[\frac{m^3}{s}\right]$$

$$WaterBudget\_error = \frac{WaterBudget}{0.5 \cdot (Inflow + Outflow)} 100\%$$

The convergence criteria are met when water budget error is below some established value (e.g. less than 0.2-1%, although even higher value is acceptable, depending on model complexity). In the particular groundwater model, the water budget is computed as follows:

- Inflow from recharge - computed as recharge rate *R* times model surface area, excluding specified head cells
- Inflow / outflow from injection / abstraction wells *Q*
- Inflow / outflow from storage is neglected (for steady state or quasi steady state model)
- Inflow / outflow from specified head boundaries Q_s, applying Darcy's equation:

$$\frac{Q_s}{ab} = -K\frac{h_{i,j} - h_s}{a}, \Rightarrow Q_s = -Kb(h_{i,j} - h_s) = -T(h_{i,j} - h_s) \quad \textbf{(6-E)}$$

  where
  - h_s is boundary specified head cell
  - $h_{i,j}$ is the adjacent inner model cell head

  If the resulted flow value is positive, then it is computed as inflow, if negative - the absolute result value is accounted as outflow.

For our model, inflow and outflow from specified head boundaries are calculated separately for left and right model boundaries (columns 1 and 35 respectively in Figure 6-4). Up and down boundaries have no inflow neither outflow since they are assumed as no-flow boundaries.

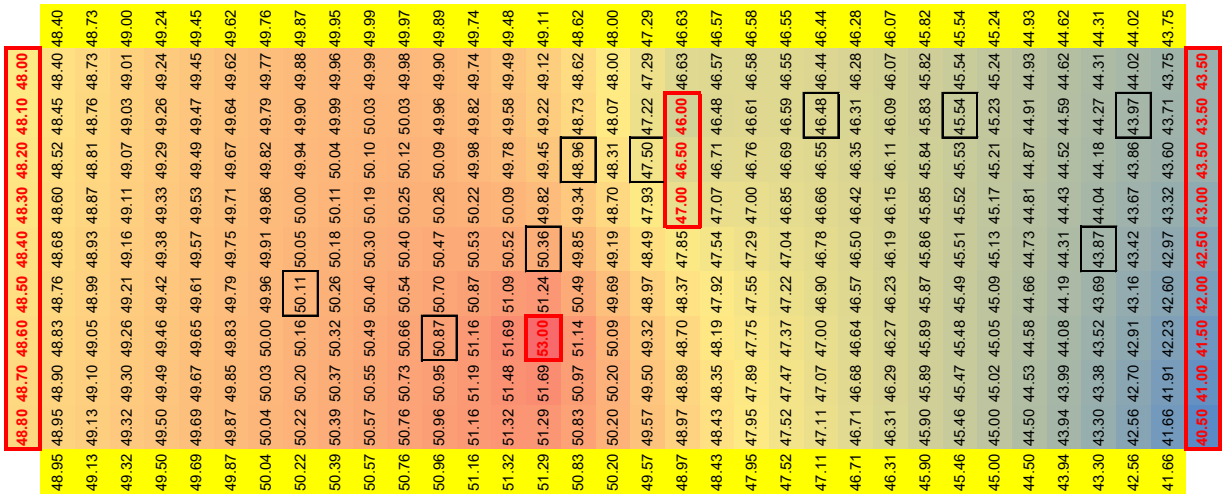

Figure 6-4: Simple Excel model steady state solution

Upper chart: Steady state solution (heads in meters) with recharge R=5E-9 m/s and transmissivity T=2E-3 m^2/s. Total system inflow / outflow are respectively 1.45E-2 m^3/s and 1.446E-2 m^3/s. Water budget error is 0.4%

Lower chart: Steady state 3D view chart (heads in meters) seen from the east

6.4. Steady state model calibration

Groundwater flow model needs to be calibrated against the measured head values of the observation wells. Since there is no active pumping wells and measured water levels are stable (maximum variation ±1m), for steady state model calibration would be used the estimated average heads between 2006 and 2016 (Anderson et al. 2015).

Trial-and-error matching was applied varying the sensitive parameter *R/T* using both Excel and MODFLOW groundwater models. Hydraulic transmissivity was left constant (T=2E-3 m^2/s), only varying the recharge rate R from 4E-9 to 7E-9 m/s in order to generate comparable results for sensitivity analysis.

Near-field target heads values (observation wells 605, 705, 805 and 905 in area 161601) would have higher matching ranking than far-field target heads values (Anderson et al. 2015). Root mean squared error (RMSE) would be used as more robust indicator than a simple average (when positive and negative residuals potentially could cancel out), calculated as:

$$RMSE = \left[\frac{1}{n} \sum_{i=1}^{n} \left(h_m - h_s \right)_i^2 \right]^{\frac{1}{2}} \quad \textbf{(6-F)}$$

where n is the number of target values, as well as h_m and h_s are respectively target measured heads and simulated head values.

RMSE has been computed for all residual well head values, but also separately for near-field (#161601) and far-field (#161602) areas. The results are summarized in the following tables (Table 6-I, Table 6-II, Table 6-III, Table 6-IV).

Table 6-I: Steady state model calibration with ratio R/T=2E-6

In dark cyan is highlighted the best RMSE result for Excel near-field simulation

Observation well # [1]	Measured average head, m (2006-2016) [2]	Simulated head, m Excel [3]	Residual [4]=[2]-[3] m	Simulated head, m Modflow [5]	Residual [6]=[2]-[5] m
105	50.10	49.54	0.56	49.87	0.23
205	53.10	50.44	2.66	50.39	2.71
305	48.70	50.11	-1.41	50.16	-1.46
405	47.60	48.71	-1.11	48.88	-1.28
505	46.60	46.50	0.10	47.72	-1.12
605	45.90	46.41	-0.51	45.75	0.15
705	45.10	45.38	-0.28	44.80	0.30
805	44.30	43.78	0.52	43.49	0.81
905	43.90	43.91	-0.01	43.53	0.37
Root mean squared error (RMSE) area 161602:			**1.46**	-	**1.58**
Root mean squared error (RMSE) area 161601:			**0.39**	-	**0.48**
Root mean squared error (RMSE) both areas:			**1.12**	-	**1.22**

Table 6-II: Steady state model calibration with ratio R/T=2.5E-6

In dark pink is highlighted the best RMSE result for Excel far-field simulation and in yellow the best Excel overall RMSE result

Observation well # [1]	Measured average head, m (2006-2016) [2]	Simulated head, m Excel [3]	Residual [4]=[2]-[3] m	Simulated head, m Modflow [5]	Residual [6]=[2]-[5] m
105	50.10	50.11	-0.01	50.04	0.06
205	53.10	50.87	2.23	50.53	2.57
305	48.70	50.36	-1.66	50.26	-1.56
405	47.60	48.96	-1.36	48.98	-1.38
505	46.60	46.50	0.10	47.78	-1.18
605	45.90	46.55	-0.65	45.90	0.00
705	45.10	45.53	-0.43	44.99	0.11
805	44.30	43.87	0.43	43.63	0.67
905	43.90	43.97	-0.07	43.45	0.45
Root mean squared error (RMSE) area 161602:			**1.39**	-	**1.57**
Root mean squared error (RMSE) area 161601:			**0.45**	-	**0.41**
Root mean squared error (RMSE) both areas:			**1.07**	-	**1.20**

Table 6-III: Steady state model calibration with ratio R/T=3E-6

In dark pink and dark cyan are highlighted the best RMSE results for MODFLOW far-field and near-field simulations respectively, and in yellow the best MODFLOW overall result

Observation well # [1]	Measured average head, m (2006-2016) [2]	Simulated head, m Excel [3]	Residual [4]=[2]-[3] m	Simulated head, m Modflow [5]	Residual [6]=[2]-[5] m
105	50.10	50.56	-0.46	50.24	-0.14
205	53.10	51.21	1.89	50.77	2.33
305	48.70	50.57	-1.87	50.35	-1.65
405	47.60	49.17	-1.57	49.07	-1.47
505	46.60	46.50	0.10	47.83	-1.23
605	45.90	46.72	-0.82	46.06	-0.16
705	45.10	45.72	-0.62	45.18	-0.08
805	44.30	43.99	0.31	43.77	0.53
905	43.90	44.05	-0.15	43.73	0.17
Root mean squared error (RMSE) area 161602:			**1.40**	-	**1.54**
Root mean squared error (RMSE) area 161601:			**0.54**	-	**0.29**
Root mean squared error (RMSE) both areas:			**1.10**	-	**1.16**

Table 6-IV: Steady state model calibration with ratio R/T=3.5E-6

In dark cyan is highlighted the best RMSE result for MODFLOW near-field simulation

Observation well # [1]	Measured average head, m (2006-2016) [2]	Simulated head, m Excel [3]	Residual [4]=[2]-[3] m	Simulated head, m Modflow [5]	Residual [6]=[2]-[5] m
105	50.10	50.74	-0.64	50.40	-0.30
205	53.10	51.37	1.73	50.91	2.19
305	48.70	50.67	-1.97	50.45	-1.75
405	47.60	49.28	-1.68	49.16	-1.56
505	46.60	46.50	0.10	47.89	-1.29
605	45.90	46.87	-0.97	46.22	-0.32
705	45.10	45.89	-0.79	45.36	-0.26
805	44.30	44.09	0.21	43.91	0.39
905	43.90	44.13	-0.23	43.82	0.08
Root mean squared error (RMSE) area 161602:			**1.42**	-	**1.55**
Root mean squared error (RMSE) area 161601:			**0.64**	-	**0.29**
Root mean squared error (RMSE) both areas:			**1.14**	-	**1.17**

Based on the sensitivity analysis, it can be concluded that near-field target values are much more accurately matched than far-field targets. Ratios for *R/T* in the range from 2.5E-6 to 3E-6 produce best target heads match, the former value for Excel and the latter for MODFLOW. In order to unify both Excel and MODFLOW input parameters, we'll adopt values of R=6E-9 m/s and T=2E-3 m^2/s for both models.

6.5. Transient mode and quasi steady state validation

In this case a MODFLOW model is set up with functioning both abstraction and injection wells in order to evaluate its transient response after some period of time. If simulation period is long enough, e.g. one year, changes in head distribution become so small that one can speak of a quasi steady state mode. Similar simulation are reproduced and performed in Excel (quasi steady state mode) in order to compare the results.

Assuming the locations of pumping wells (observation well #605 as abstraction well and observation well #705 as injection well), and a constant pumping rate of 0.01 m^3/s (864 m^3/d), MODFLOW steady state results (before pumping) are presented in Figure 6-5 and Figure 6-6. The results after 1 year of pumping, as well as a hydrograph for all observation wells are shown in Figure 6-7. The quasi steady state solution of the simple Excel model is presented in Figure 6-8.

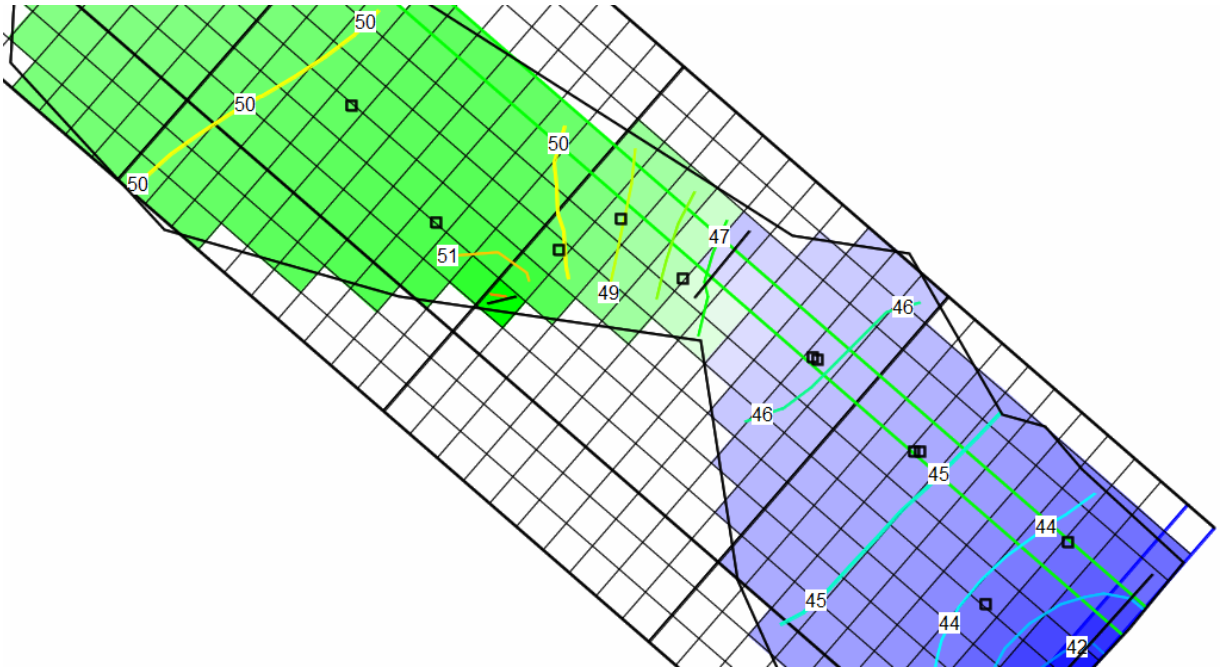

Figure 6-5: MODFLOW steady state simulation results

Isosurfaces represent aquifer piezometric heads in meters, color code - from blue (lower) to green (higher). Parameters: recharge R=6E-9 m/s and transmissivity T=2E-3 m^2/s

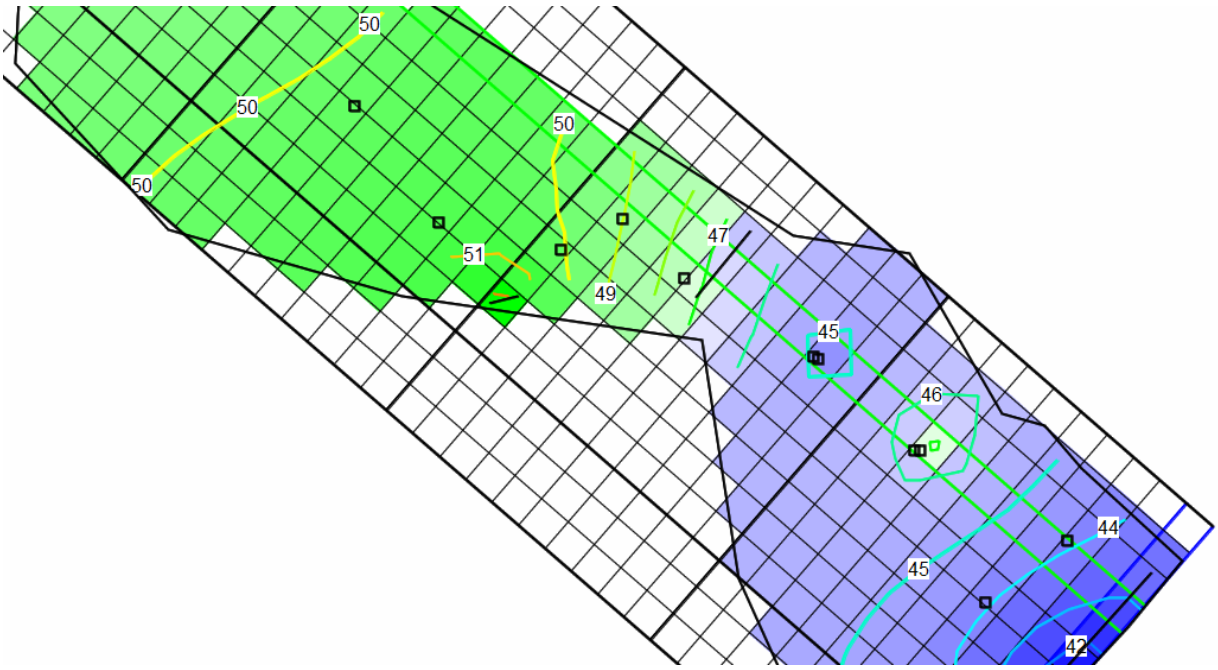

Figure 6-6: MODFLOW simulation results after one year of pumping

*Isosurfaces represent aquifer piezometric heads in meters, color code - from blue (lower) to green (higher). Parameters: recharge R=6E-9 m/s, transmissivity T=2E-3 m^2/s, storage coefficient S=1E-5. As shown also in the hydrograph (*Figure 6-7*), aquifer area near the pumping wells (#161601) is more dynamically affected by pumping*

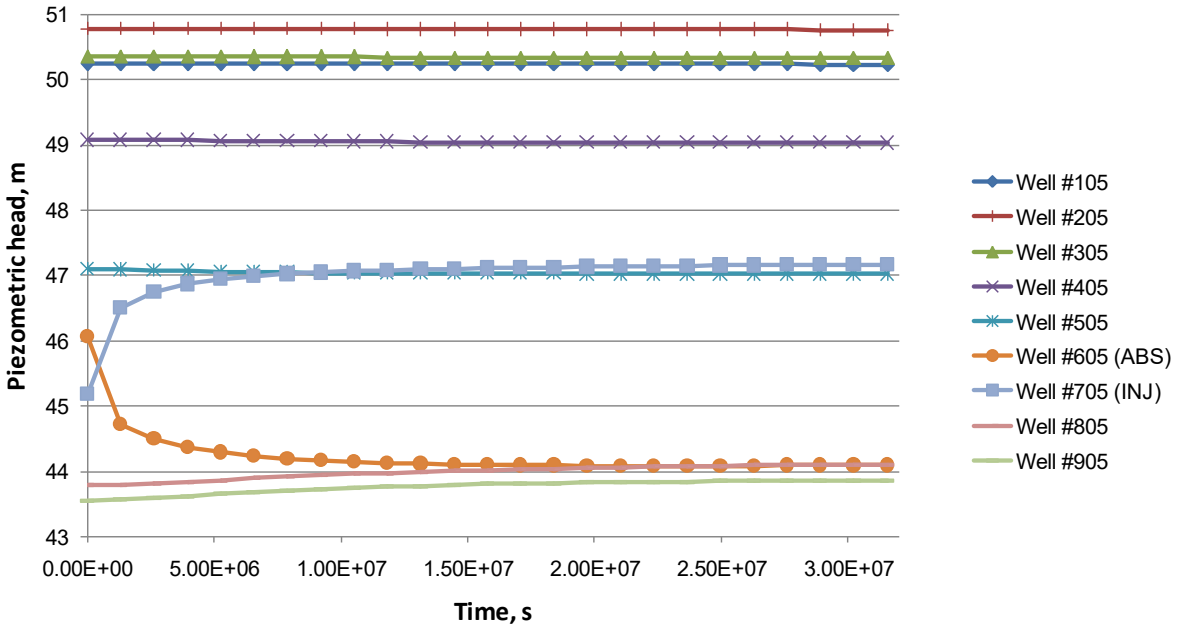

Figure 6-7: MODFLOW hydrograph (observation wells)

Hydrograph showing piezometric heads of all observation wells after one year of pumping. Quasi steady state mode can be observed at the end of the period

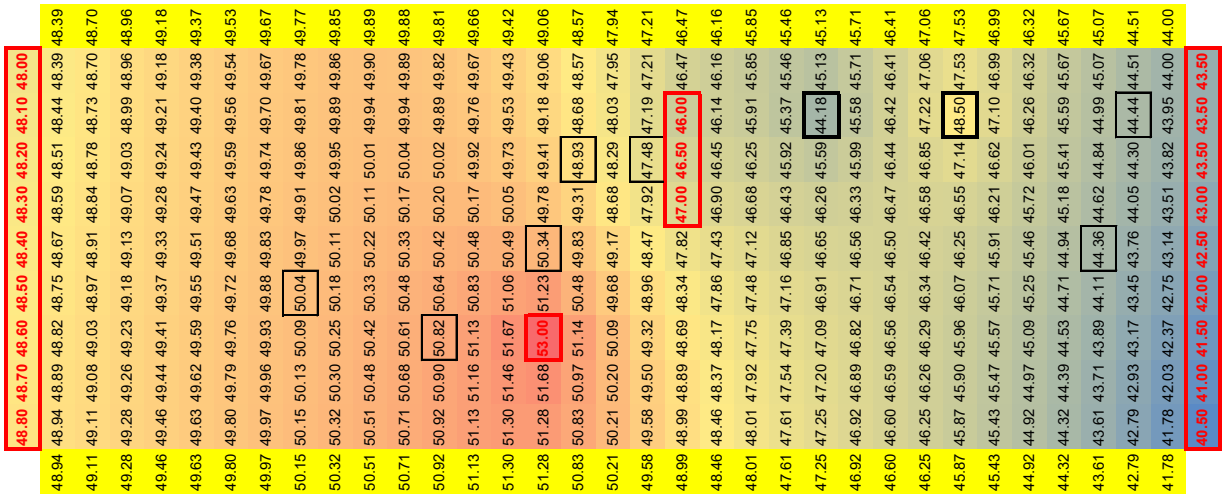

Figure 6-8: Quasi steady state solution of simple Excel model

Upper chart: Quasi steady state solution (heads in meters) of simple model with the same parameters as in MODFLOW (recharge R=6E-9 m/s and transmissivity T=2E-3 m^2/s). Total system inflow and outflow are respectively 2.746E-2 m^3/s and 2.737E-2 m^3/s. Water budget error is 0.4%. It can be acknowledged also a good correlation with MODFLOW quasi steady state solution results.

Lower chart (next page): Results 3D view chart (heads in meters) seen from the east, abstraction and injection wells are in columns 24 and 28 respectively (x-axis)

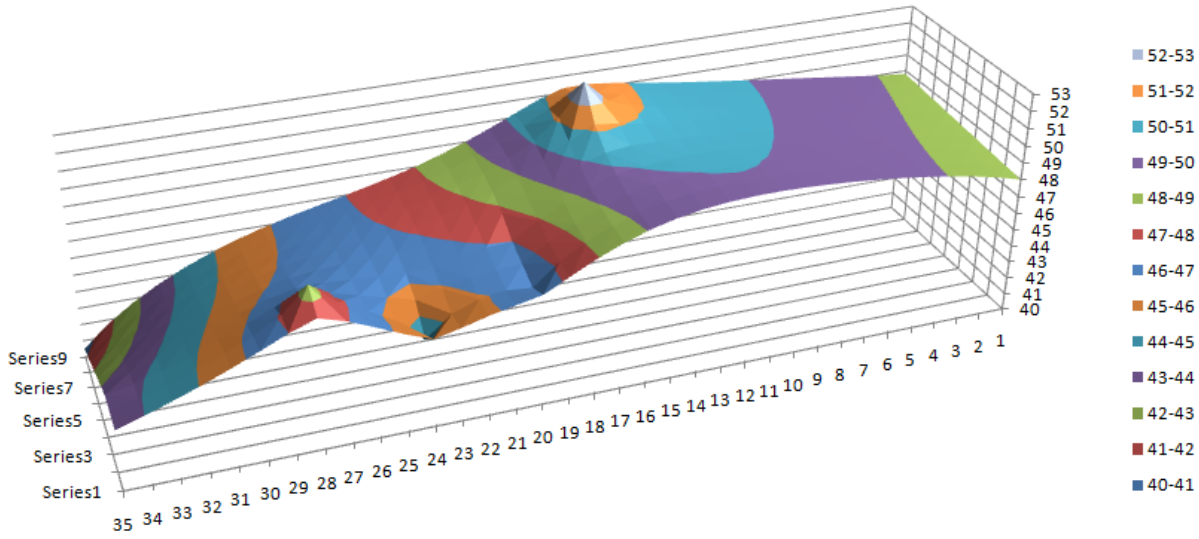

As seen from the previous figures (Figure 6-4, Figure 6-5, Figure 6-6 and Figure 6-8), both Excel and MODFLOW models present a good correlation in steady state (also calibrated against the measured observation data) and transient simulation results. In transient mode, nearby area (#160161) is mostly affected by the pumping abstraction/injection well doublet (observation wells #605/#705 respectively).

6.6. Groundwater heat transport model

The solute transport numerical code MT3DMS as part of ModelMuse (MODFLOW) environment is used to simulate the heat transport, taking into account the similarities between solute and heat transport in porous media with several coefficients reformulation. ModelMuse is a modular environment when different packages are loaded on demand depending on concrete project needs. In order to link MODFLOW and MT3DMS, the following MT3DMS packages are needed:

- BTN: Basic transport package
- ADV: Advection package
- DSP: Dispersion package
- SSM: Sink and Source Mixing package
- RCT: Chemical reaction package

The equivalent coefficient settings for heat transport simulation are:

- Diffusion coefficient D_m=1.9E-6 m^2/s
- Sorption coefficient K_d=2.1E-4 m^3/kg
- Longitudinal dispersivity α=0.5m
- Transverse horizontal/vertical dispersivity α_T=0.05m
- Porosity n=0.25
- Dry bulk density ρ_b=2000 kg/m^3

The initial values for aquifer layer are set to 280K (roughly 7ºC) with specified temperature boundary of 280K for all transient stress periods assigned to the top layer.

7. Scenarios for Pukkila's DH network update

Groundwater source heat pump (GWHP), operating with injection and abstraction well (so called well doublet) is considered. For this purpose, both #605 and #705 observation wells are considered, since they are located close to the actual district heat production plant. According to the steady state head distribution and gradient (supported by observation wells measurements and simulations), the dominant underground flow is from the north (higher head values) to the south reaching Porvoonjoki river as lowest head boundary.

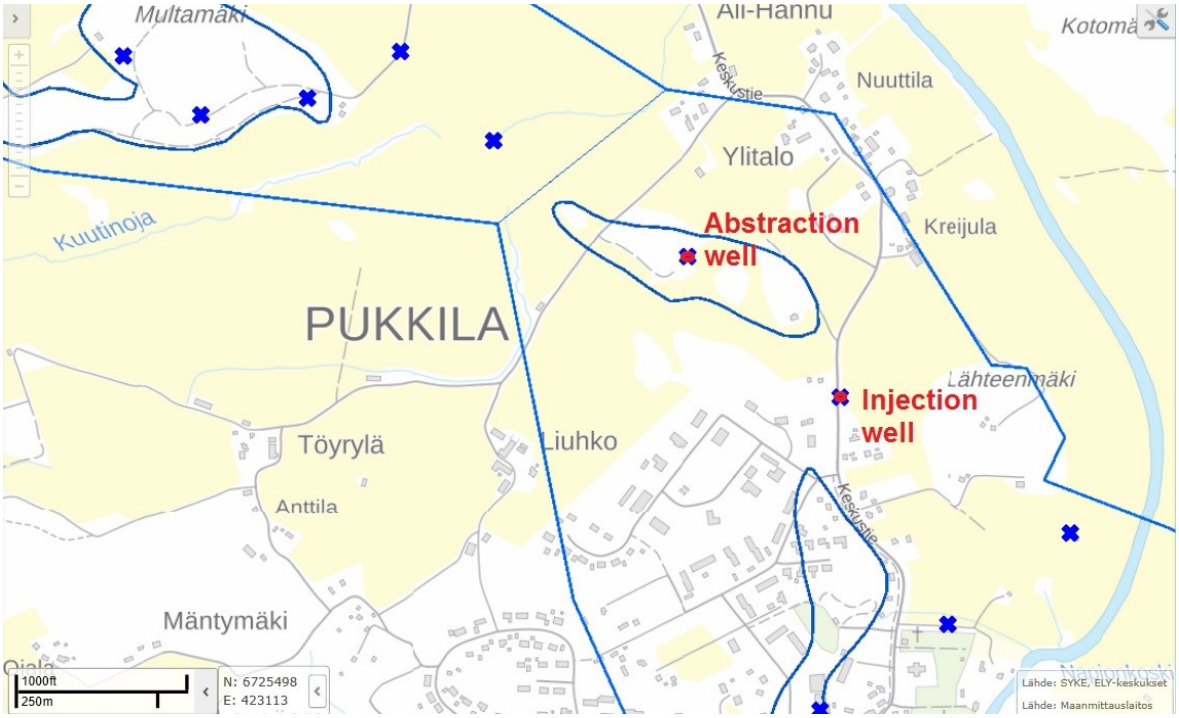

Figure 7-1: Location of injection and abstraction wells

Location of injection and abstraction wells near the actual DH plant (for only heating and constant cooling scenarios, ATES one-way operation with abstraction warm well and injection cold well; for dynamic cooling scenario wells' operation is seasonably reversed). The location of observation well #605 is assumed as warm well and #705 as cold well respectively (estimated distance between wells: 395m)

The first possible scenario is the utilization of GWHP in order to satisfy partially the present heating demand (base load), using the existing chips boiler for peak loads. If boiler is needed, GWHP would be used first to increase DH network temperature from 40º (assumed return temperature) to some intermediate value, and after that, the final DH flow temperature would be reached by the boiler. This would improve HP efficiency in partial load mode, since COP_H is better with lower HP production temperature.

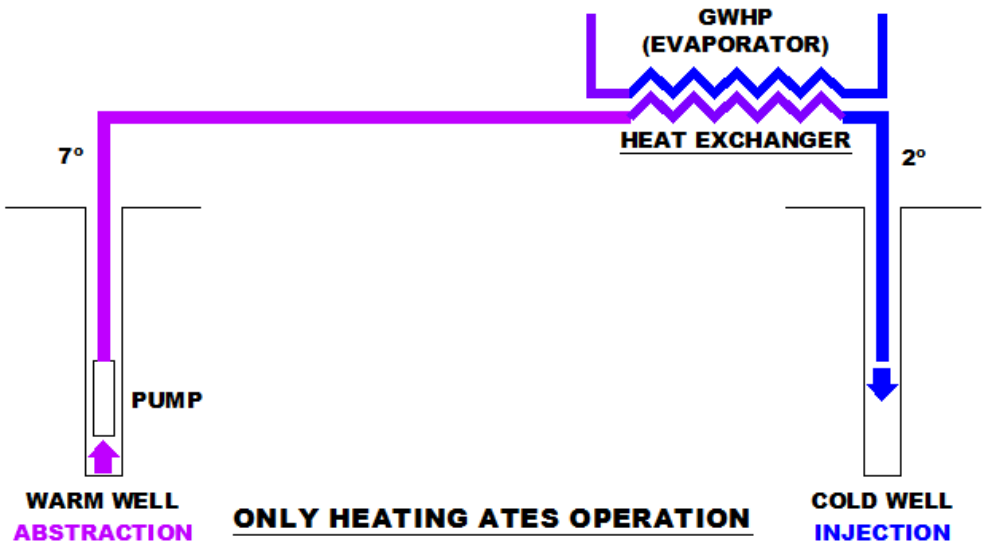

Figure 7-2: Only heating ATES operation scheme (scenario 1)

One-way ATES operation is used to drive GWHP for district heating base load generation

In the second scenario an additional roughly constant cooling demand is introduced (e.g. data center, industrial waste heat) and the following processes are combined sequentially: pumping from aquifer via the abstraction well, free cooling using cooling exchanger (1), GWHP operation covering base load district heating (or total coverage, eliminating the additional peak boiler) and finally injection into the aquifer.

With this configuration GWHP efficiency is significantly increased, due to the higher temperature after exchanger 1 (assumed 25ºC), as shown in Figure 7-3.

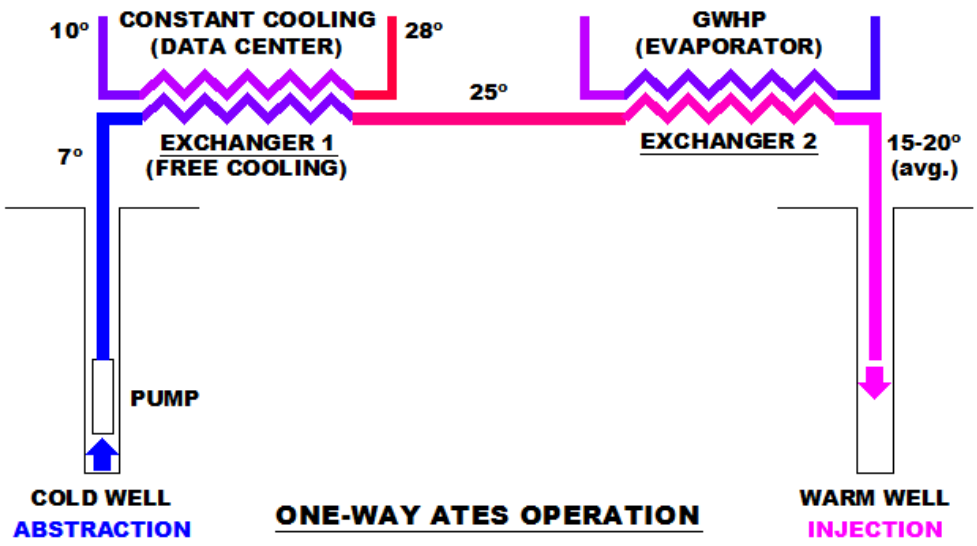

Figure 7-3: ATES operation with waste heat utilization scheme (scenario 2)

One-way ATES operation introducing a constant waste heat (cooling load from data center, industrial waste heat, etc.) before GWHP operation for partial or total district heating demand. Since HP source temperature is higher (25°), COP_H is significantly improved

The third scenario is similar to the second one, substituting constant cooling demand of data center by more dynamic heating and cooling demand (e.g. office buildings). This additional dynamic energy demand (necessary for office cooling), especially concentrated during the summer period, could be assimilated to dynamically generated heat from e.g. thermal-solar panels field (another source of heat potentially beneficial for ATES system efficiency).

ATES reversible operation during summer and winter period is presented in Figure 7-4. It should be noted that main streams are not mixed within the central flow commutation during the winter operation.

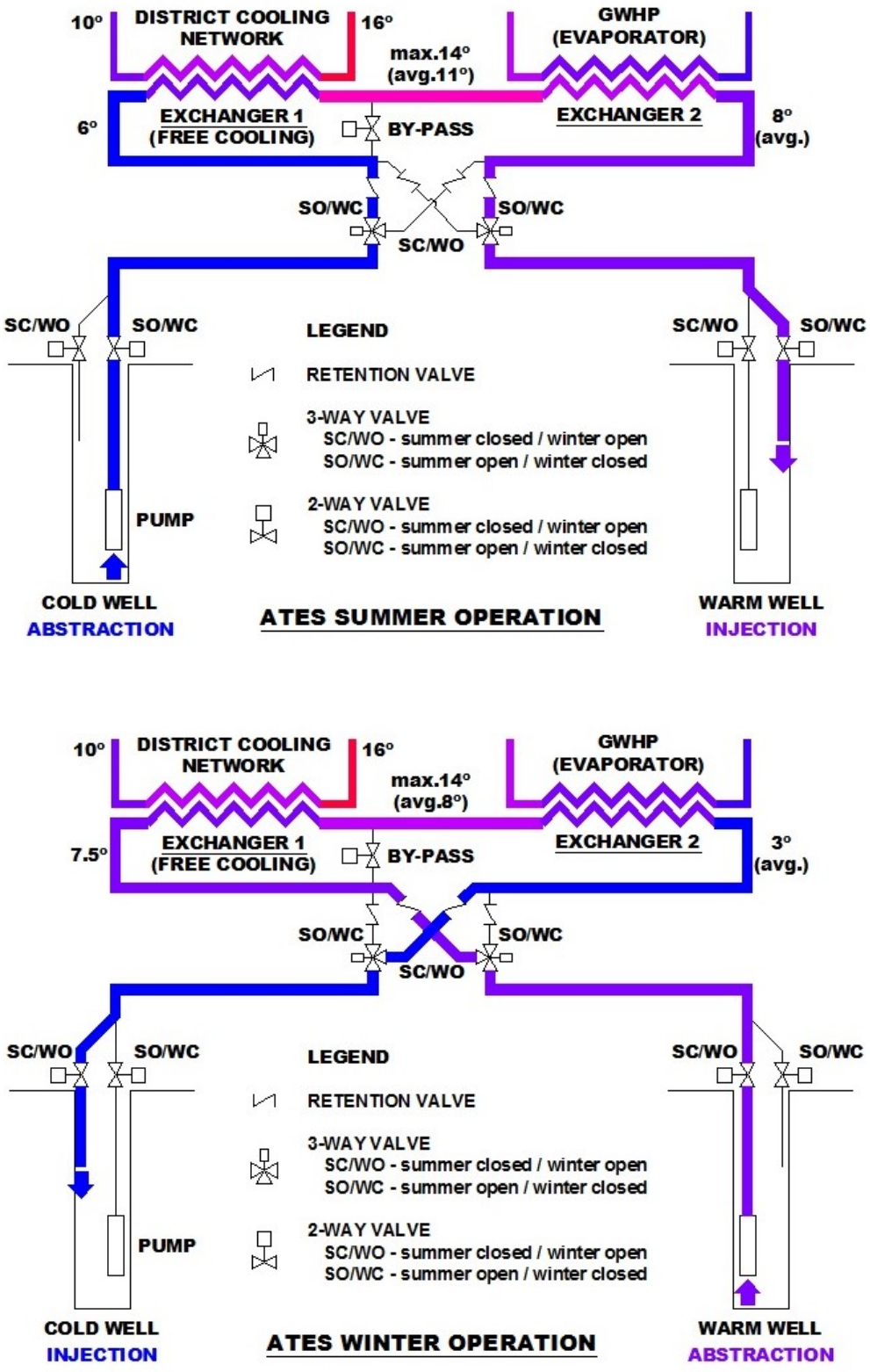

Figure 7-4: Seasonably reversed ATES operation scheme (scenario 3)

With different configurations of 2/3-way controlled valves, it is possible to reverse ATES operation for summer period (up figure) and winter period (down figure). Cooling exchanger (1) could be additionally by-passed when cooling is not needed (for the studied case, mostly during the winter period) in order to reduce the pumping energy demand

7.1. ATES system for heating

In this first scenario is explored the possibility of base load heat production using groundwater source heat pump coupled with aquifer injection-abstraction well doublet. The initial dimensioning of the heat pump capacity is the estimated domestic hot water demand of roughly 0.35MW.

In principle, it would be beneficial to limit DH network flow temperature to a maximum value of 80ºC (Hynynen, 2018) and reduce it according to the annual heating demand to limit network losses and improve the overall efficiency. The minimum temperature of domestic hot water is recommended to be in the range 55-60º (in order to prevent the risk for *Legionella* formation, Banks 2008), and therefore, the minimum recommended DH flow temperature could be established in 70º (Finnish Energy, 2013).

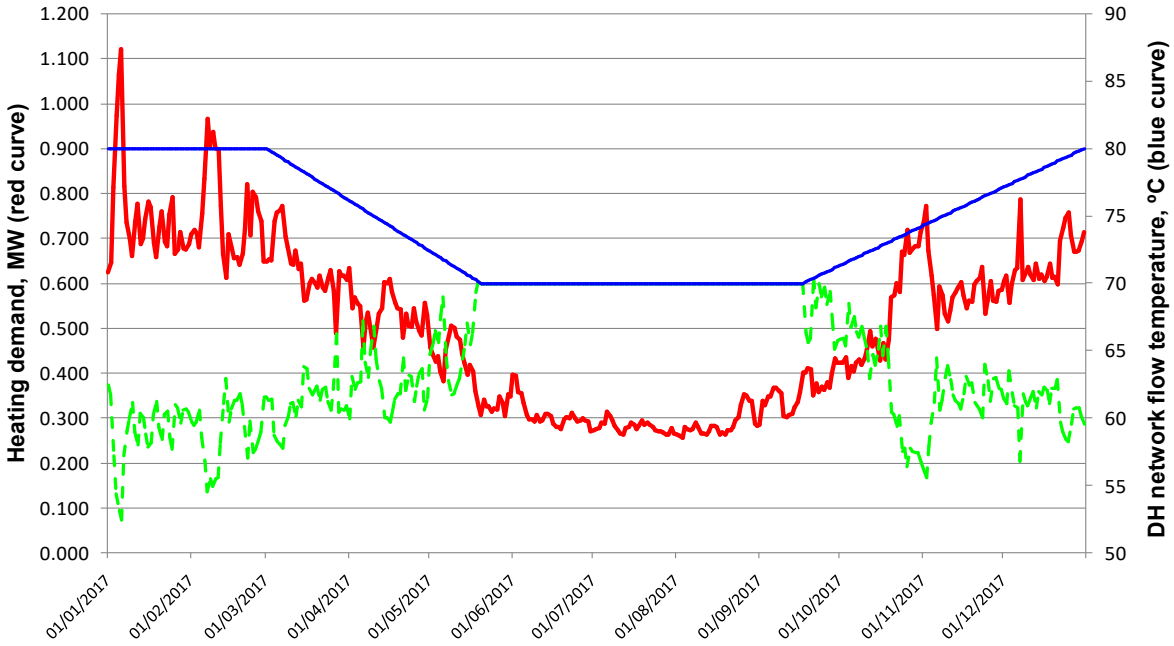

Figure 7-5: Only heating scenario (heat pump 0.35MW)

Annual heating demand(red curve, left axis) and district heating network flow temperature (blue curve, right axis). With green dashed line is represented the heat pump production temperature T_2. ATES abstraction and injection temperatures are 7ºC and 2ºC respectively. Pumping flow rate is almost constant between 0.008 and 0.012 m^3/s (average 0.0105) and heat pump COP varies from 2.6 to 3.6 (average 3)

With these assumptions, during the summer period (between mid-May and mid-September) it is possible to use GWHP exclusively (without boiler). On the other hand, during the rest of the year, the heat pump would be used in the first place. This would increase DH network temperature from 40º (assumed DH network return temperature) to

some intermediate value T_2 (calculated on a daily based DH flow temperature and taking into account the ratio between the maximum heat pump power and the demanded power). After that the chips boiler would be utilized as an additional peak load generator.

Assuming aquifer abstraction temperature of T_1=7ºC and calculating the GWHP production temperature T_2 it is possible to estimate heat pump COP_H (according to our adopted and described in Chapter 2 COP_H model) and finally calculate the needed average daily water flow (assuming aquifer injection temperature of T_3=2ºC):

$$Q_i = \frac{\Phi_i \left(1 - \frac{1}{COP_H{}^i}\right)}{\rho c_p \Delta T} \quad \textbf{(7-A)}\text{, where}$$

- Q_i [m^3/s] is the average water flow for a day i=1...365
- Φ_i [W] is the heat demand for a day i=1...365
- $COP_H{}^i$ is the heat pump coefficient of performance (in heating mode, computed for a day i=1...365)
- ρ [kg/m^3] is the water density for an average value of operation temperature range
- c_p [J/kgK] is the water heat capacity for an average value of operation temperature range
- ΔT [K] is water temperature drop in heat pump evaporator side (water temperature drop between abstraction and injection wells)

The electric energy demand for pumping is estimated on a daily-based average pumping rate, according to the following equation:

$$E_i = \frac{Q_i p}{\eta} \quad \textbf{(7-B)}\text{, where}$$

- E_i [kW] is the average pumping power for a day i=1...365
- Q_i [m^3/s] is the average water flow for a day i=1...365
- p [kPa] is the pump pressure needed (assumed constant, estimated in 600kPa)
- η is pump efficiency (based on producers' data for submersible pumps Grundfos SP, estimated between 0.5 and 0.6 depending on pump's size)

In order to study the long-term influence of the described operational scenario, a local grid refinement (LGR) is performed in MODFLOW near the wells (gradual refinement from 100m to 20m) in order to improve model accuracy. Monthly average of injection / abstraction flows is computed and introduced as 300 different stress periods and aquifer's temperature field after 25 years is presented in Figure 7-6.

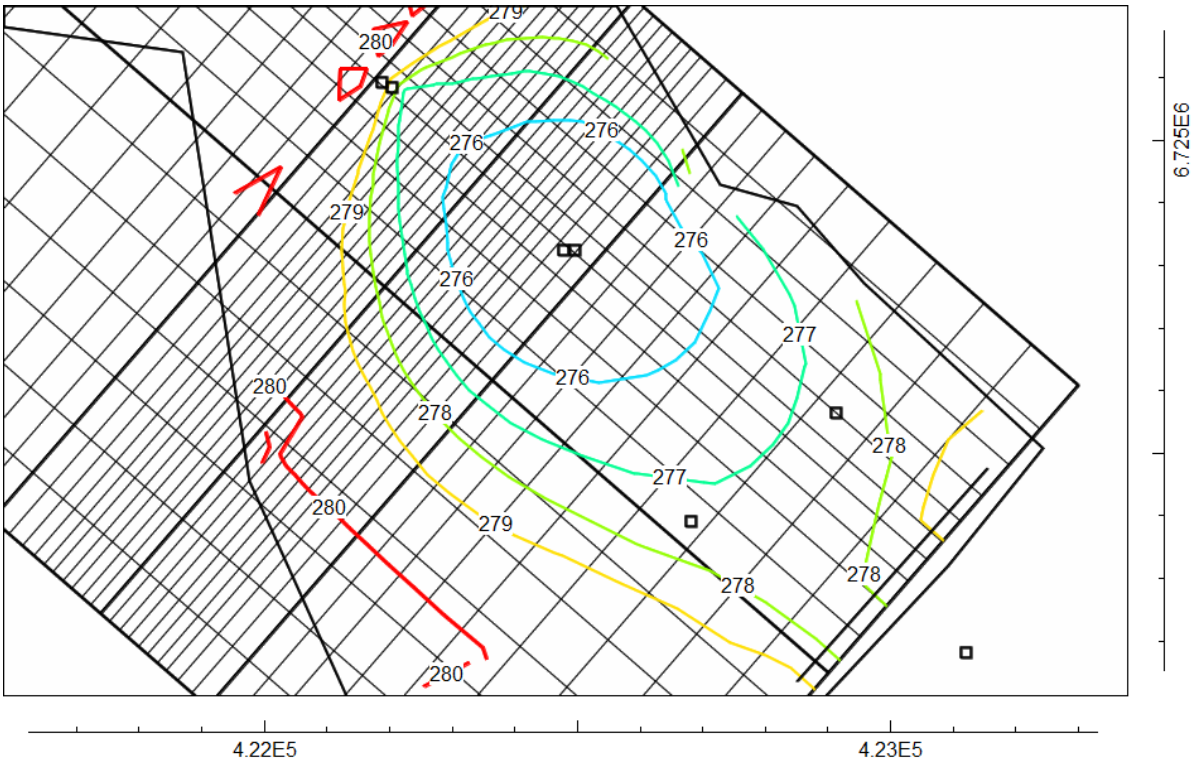

Figure 7-6: Scenario 1 - aquifer temperature after 25 years of operation

Aquifer temperature distribution after 25 years of operation (iso-lines in Kelvin)

As acknowledged from the previously conducted simulations, flow (and heat front) displacement is mostly in south-east direction (towards Porvoonjoki river acting as a cooling sink). After 25 years of operation, abstraction well temperature is only 1ºC lower than the average aquifer temperature (7ºC). The distance between wells in order to avoid the risk of thermal feedback is analytically estimated in 1337m (equation 3-I).

7.2. ATES system for constant cooling and waste heat utilization

In the second scenario a constant cooling demand is introduced between aquifer abstraction well and GWHP heat exchanger. An additional cooling exchanger utilizes directly aquifer abstraction water flow at 7ºC increasing its temperature to 25ºC (free cooling, absorbing e.g. data center heat, industrial waste heat, etc.) and after that enters the heat pump exchanger. In this configuration GWHP achieves much higher COP_H compared to the previous case. The pumping flow rate is calculated as follows:

$$Q = \frac{\Phi}{\rho c_p \Delta T} \quad \textbf{(7-C)}\text{, where}$$

- Q [m^3/s] is the pumping flow rate
- Φ [W] is the constant cooling demand
- ρ [kg/m^3] is water density for an average value of operation temperature range

- c_p [J/kgK] is water heat capacity for an average value of operation temperature range
- ΔT [K] is water temperature drop in the cooling exchanger (25º-7º=18º)

Heat pump COP is estimated for each day according to our adopted and previously described COP_H model (Chapter 2). The injection temperature (after GWHP) is calculated using equation (7-A) and solving for temperature drop ΔT, equal to the difference between 25ºC and aquifer injection temperature. Electric energy demand for pumping is estimated according to equation (7-B).

7.2.1. Partial heating power design of heat pump (scenario 2a)

In scenario 2a, a base load heat pump of 0.5MW is considered (using chips boiler as peak load generator) in combination with constant cooling load of 0.6MW of data center. Since cooling load is constant during the course of the year and annual cooling demand is higher than annual heat pump demand, all rejected heat needs to be injected and stored in one way ATES operation.

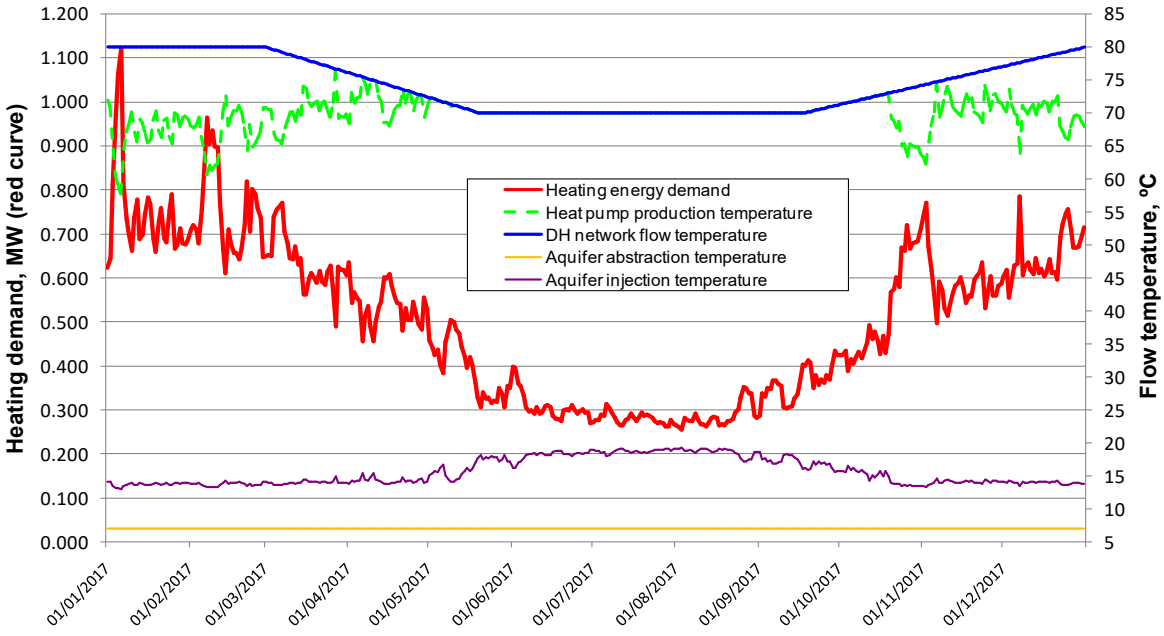

Figure 7-7: Scenario 2a (data center 0.6MW / heat pump 0.5MW)

Annual heating demand (red curve, left axis), district heating network flow temperature (blue), heat pump production temperature (dashed green). Heat pump COP varies from 3.1 to 4.9 (annual weighted average 3.8). One way operation with aquifer abstraction temperature 7ºC and injection temperature between 13.1º and 19.4ºC (average 15.7ºC), constant pumping rate 0.008m³/s

In this case, ATES system is used for one way operation (without seasonal inversion of the well doublet), therefore heat rejected by the data center, after its utilization for Pukkila's DH network, would be injected and stored into the aquifer.

The long-term effect of this operation was studied simulating the process in MODFLOW over a 25-year period, making local grid refinement (LGR) near the wells (gradual refinement from 100m to 20m) in order to improve model accuracy. For this purpose monthly average of injection temperature is computed and introduced as 300 different stress periods and aquifer's temperature field after 25 years is presented in Figure 7-8.

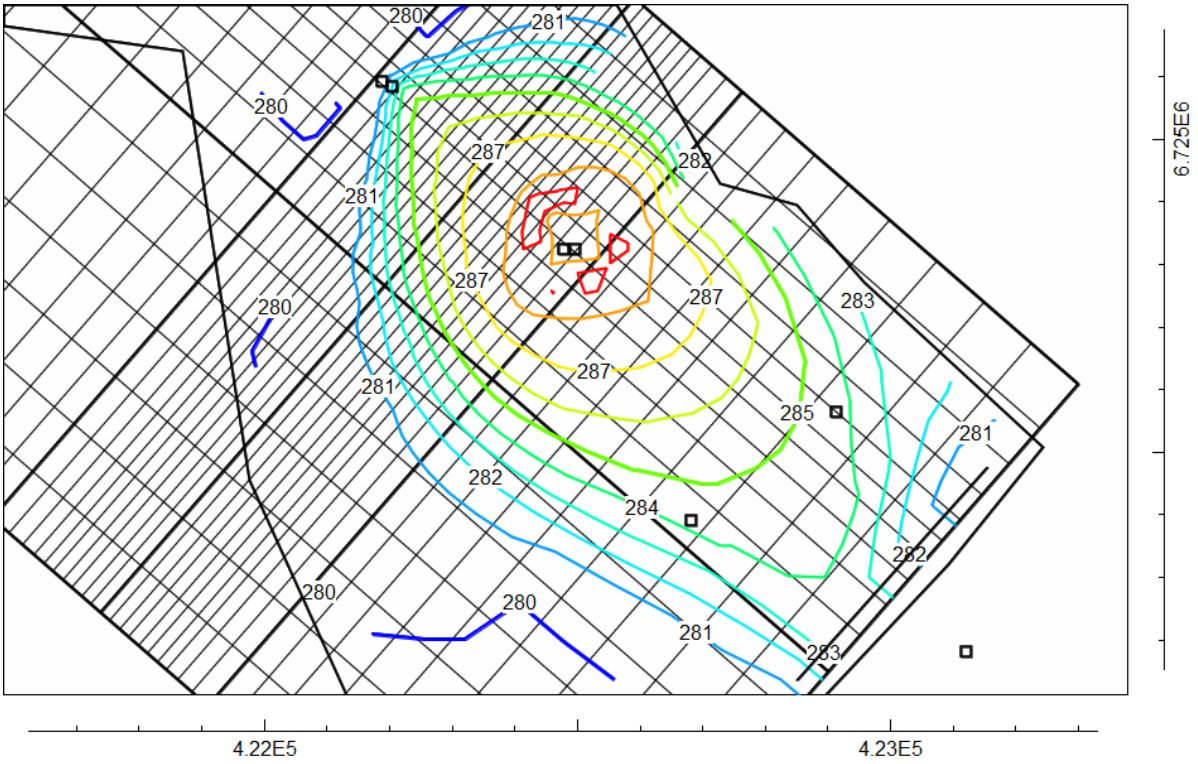

Figure 7-8: Scenario 2a - aquifer temperature after 25 years of operation

Aquifer temperature distribution after 25 years of operation (isosurfaces in Kelvin)

As noted previously, flow (and heat front) displacement is mostly in south-east direction (Porvoonjoki river). After 25 years of operation, abstraction well temperature is only 1.1ºC higher than the average aquifer temperature (7ºC). Porvoonjoki acts as an important heat sink boundary (however the absorbed groundwater flows is max. 3ºC warmer than the average aquifer temperature). The estimated distance between wells in order to avoid the risk of thermal feedback is analytically calculated as 1019m (equation 3-I).

7.2.2. Full heating power design of heat pump (scenario 2b)

In this scenario, a heat pump of 1MW is considered as a complete substitute of the existing chips boiler. The operational principles are similar as in the previous scenario, i.e. 1.2MW constant cooling power from data center is dissipated in the first place increasing water temperature from 7ºC (abstraction well) to 25ºC (after exchanger 1) in order to improve considerably heat pump COP_H.

After that GWHP is operated satisfying totally Pukkila district heating demand and finally excess heat is injected and stored in the aquifer. It should be noted that heat pump production temperature coincide with DH network temperature (no additional peak boiler), therefore heat pump COP_H is lower compared to Scenario 2a. Furthermore, compared to the previous scenario, pumping rate is doubled, which in principle means the necessity of two injection and two abstractions wells (additional pumping tests are needed to establish the maximum yield per well).

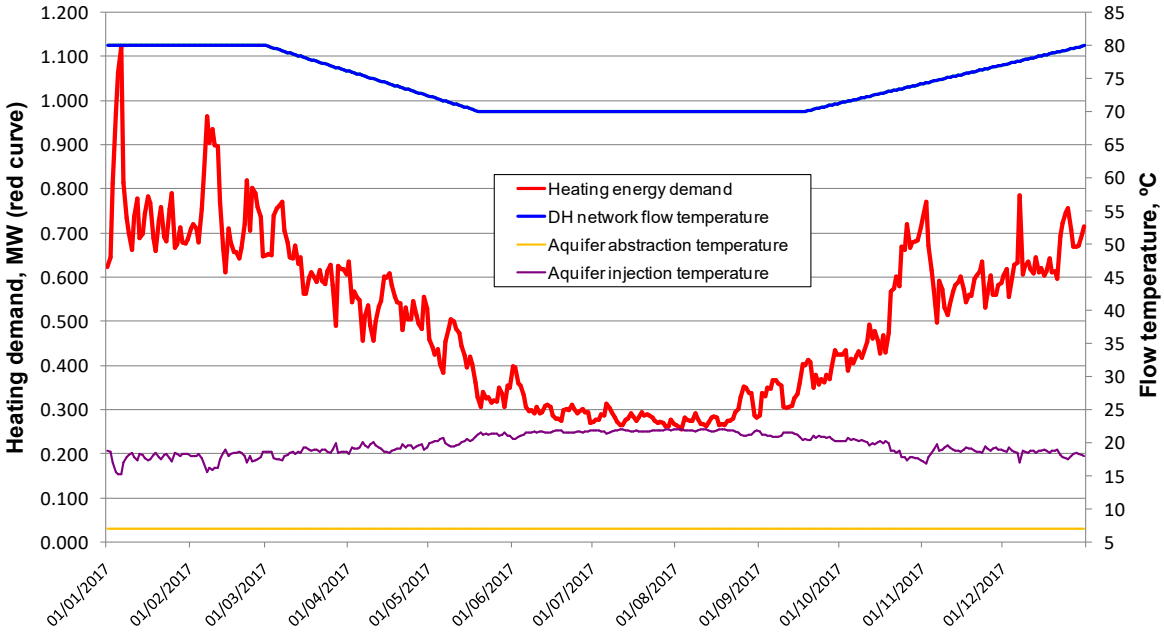

Figure 7-9: Scenario 2b (data center 1.2MW / heat pump 1MW)

Annual heating demand (red curve, left axis), district heating network flow temperature (blue) equal to heat pump production temperature. Heat pump COP varies from 2.8 to 3.7 (annual weighted average 3.2). One way operation with aquifer abstraction temperature 7ºC and injection temperature between 15.3º and 22.2ºC(average 19.8ºC), constant pumping rate 0.016m^3/s

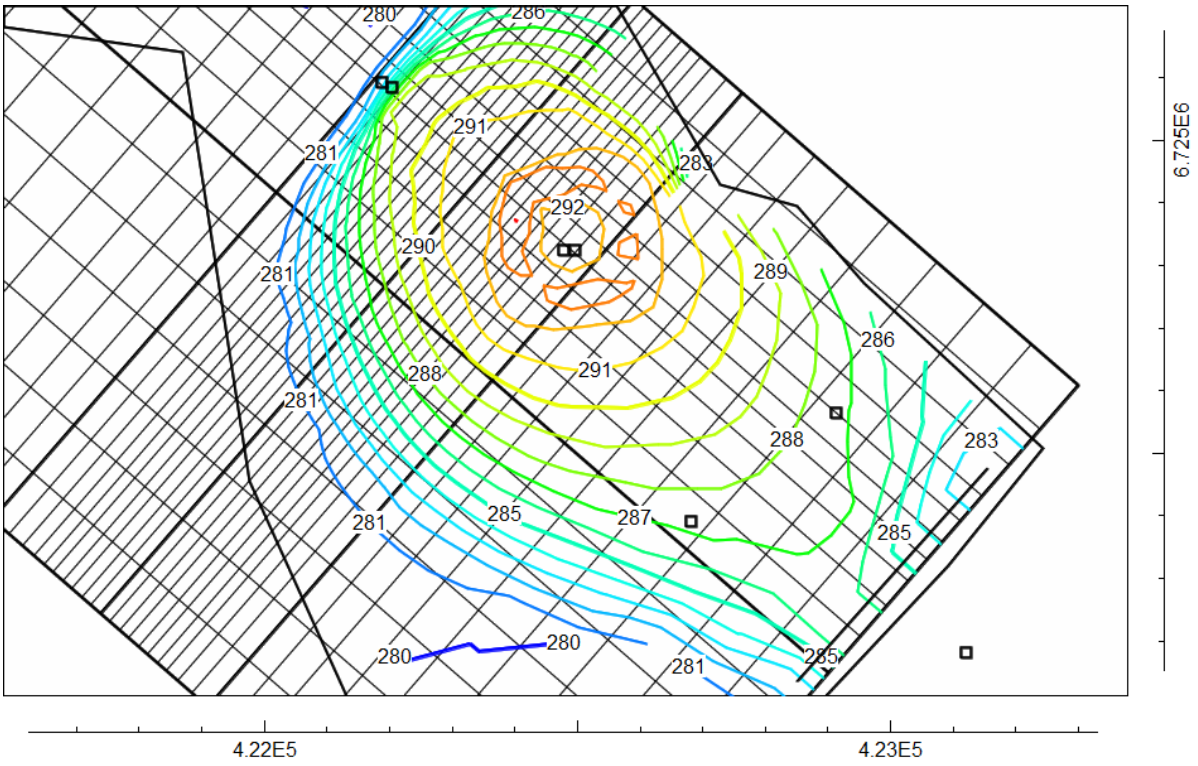

Figure 7-10: Scenario 2b - aquifer temperature after 25 years of operation

Aquifer temperature distribution after 25 years of operation (isosurfaces in Kelvin)

As mentioned previously, flow (and heat front) displacement is mostly in south-east direction (Porvoonjoki river). In this scenario, after 25 years of operation, abstraction well temperature is 3.5ºC higher than the average aquifer temperature (7ºC), and if operation is continued for long time period could potentially compromise the cooling capacity of the abstraction well. Porvoonjoki acts as an important heat sink boundary (in this case the absorbed groundwater flow is max. 6ºC warmer than the average aquifer temperature). The estimated distance between wells in order to avoid the risk of thermal feedback is analytically calculated as 2037m (equation 3-I).

7.3. Summary of the one-way ATES operation

In Chapter 3 the concepts of hydraulic and thermal feedback in one-way ATES operation were discussed in order to analytically estimate the hydraulic and thermal breakthrough times, abstraction drawdown and temperature after long-term operation, as well as the minimum distance between wells. Based on different assumptions (natural hydraulic gradient i=0 or estimated from steady state head simulation), relevant parameters are presented in Table 7-I.

Table 7-I: ATES one-way operation (scenarios 1, 2a, and 2b)

Summary of relevant calculated / simulated parameters for abstraction well drawdown and hydraulic / thermal feedback

Equation	Relevant calculated / simulated parameter	Scenario 1	Scenario 2a	Scenario 2b
-	Average injection flow rate Q [m^3/s]	0.0105	0.008	0.016
-	Distance between wells L [m]	395	395	395
3-C	Calculated drawdown of abstraction well (for grid cell 100x100m) $s_{100x100,cal}$ [m]	2.41	1.84	3.68
6-D	Calculated drawdown of abstraction well (for well radius 0.4m) $s_{well,cal}$ [m]	5.76	4.39	8.78
-	Simulated drawdown of abstraction well after 1 year (for grid cell 100x100m) $s_{100x100,sim}$ [m]	2.08	1.59	3.20
3-D	Hydraulic breakthrough time $t_{hyd,i=0}$ (for i=0) [years]	2.5	3.2	1.6
3-J	Retardation factor R (for i=0)	2.64	2.64	2.64
3-F	Thermal breakthrough time $t_{the,i=0}$ (for i=0) [years]	6.5	8.6	4.3
3-G	Thermal breakthrough time t_{the} (for i=-0.002) [years]	8.1	11.5	4.9
-	Time from start pumping [years]	25.0	25.0	25.0
-	Aquifer initial temperature T_0 [ºC]	7	7	7
-	Average injection temperature T_{inj} [ºC]	2	15.7	19.8
3-H	Ratio $(T_{25y}-T_{inj})/(T_0-T_{inj})$ calculated with t_{the}	0.60	0.68	0.53
3-H	Calculated abstraction temperature after 25 years $T_{25y,cal}$ [ºC]	5.0	9.8	13.0
-	Simulated abstraction temperature after 25 years $T_{25y,sim}$ [ºC]	6.0	8.1	10.5
3-F	Minimum distance between wells for thermal breakthrough of 25 years [m]	773	675	955
3-I	Minimum distance between wells without risk of thermal feedback [m]	1337	1019	2037

A good correlation between the analytically calculated and simulated values can be acknowledged - for drawdown, difference of only 15% (taking into account that the analytical solution assumes infinite domain, neglecting system boundaries). It should be noted also the important drawdown calculated inside the abstraction well in scenario 2b (almost 9m), which is an additional constraint and should be considered.

The calculated long-term abstraction temperature, using the analytical solution for thermal breakthrough time, is more conservative (abstraction well is more affected by a thermal front) compared to the simulated value (due to system's simplifications, ignoring its physical boundaries).

7.4. ATES system for combined heating and cooling scenario

Detailed hourly simulation results for the annual heating and cooling demand of office building is used in order to introduce a dynamic variable cooling load (Tuominen et al. 2014). The data used is for standard office building of 2695 m^2 net area and type D1 (according to Finnish building code, part C3-2010). The data was converted into an average daily based heating and cooling loads and scaled appropriately (factor of 27) in order to optimally match the existing Pukkila district heating network profile demand.

In the present, third scenario, different and reversible operation during summer and winter periods is assumed, creating an ATES well doublet - warm well (north-west #605) and cold well (south-east #705). In the summer operation a primary cooling circuit starts from the cold abstraction well to max.14ºC after the exchanger, providing district cooling (exchanger secondary circuit) to the office buildings during the summer period. After the heat from the district cooling network is absorbed, water at up to 14º is used with GWHP for district heating network operation, and finally injected into the warm well.

During the winter period the process is reversed, water is taken from the warm well, conducted if needed through the district cooling network exchanger, used with GWHP for district heating network operation, and finally injected into the cold well.

7.4.1. Initial ATES model settings

Initially, abstraction temperatures from warm and cold wells are assumed as 7.5ºC and 6ºC respectively. The whole year of ATES operation is simulated, calculating all relevant parameters on a daily-basis.

The average pumping flow rate for each day is calculated as a maximum value between the flow needed for heating and the flow needed for cooling, using equations (7-A) and (7-C). The injection temperature (after GWHP) is calculated according to equation (7-A) and solving for temperature drop ΔT. The electric energy demand for pumping is estimated from equation (7-B). The annual variation of all relevant parameters is presented in Figure 7-11.

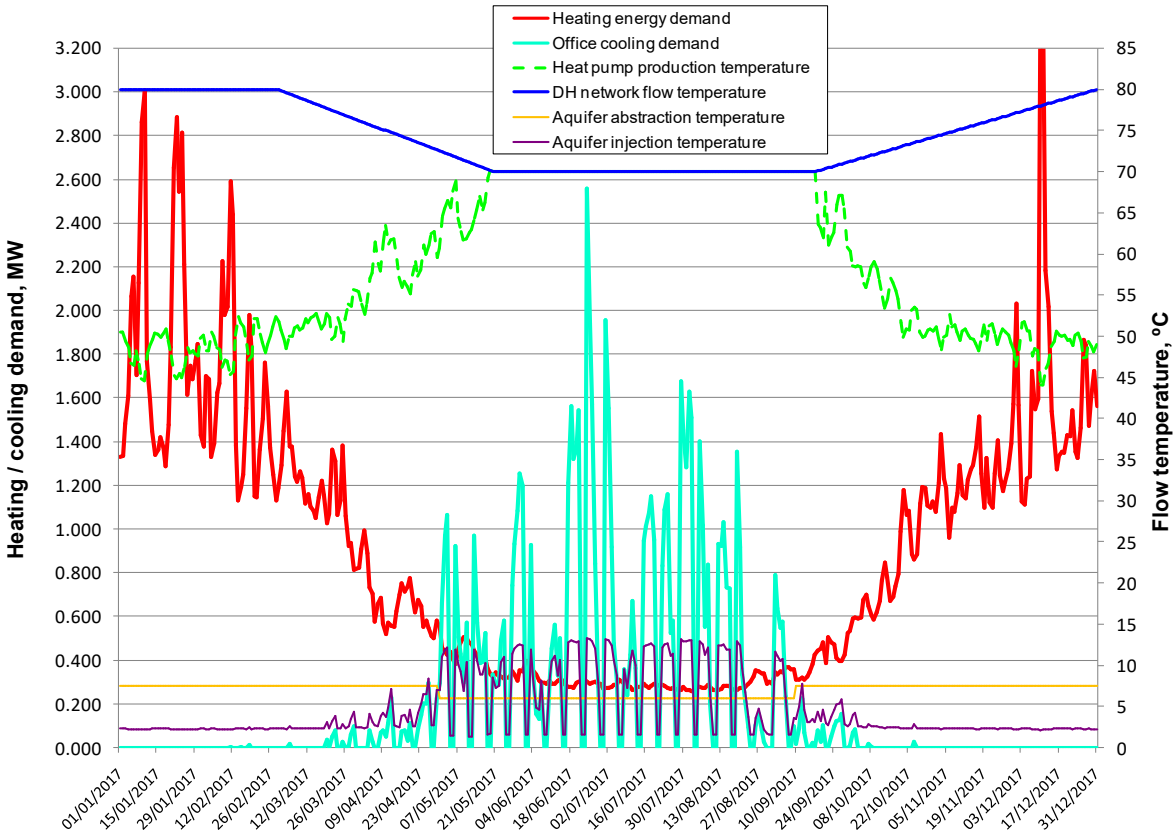

Figure 7-11: Scenario 3 (DC with office profile / base load GWHP 0.35MW)

Annual combined heating demand(red curve, left axis),office cooling demand (cyan curve, left axis). Heat pump COP varies from 2.6 to 4.2 (annual weighted average 3.4). Two way seasonal operation with aquifer abstraction temperature 7.5/6ºC (warm/cold well) and average injection temperature 2.8º/7.9º (cold/warm well), average pumping rate 0.0149m^3/s

In order to study the annual effect of ATES system, both winter and summer periods are simulated in MODFLOW, introducing weekly-based stress periods (injection and abstraction flows, as well as injection temperatures of warm and cold wells are weekly averaged). Whole year reversible operation was studied simulating the process in MODFLOW and making local grid refinement (LGR) near the wells (gradual refinement from 100m to 20m) in order to improve model accuracy.

Summer period lasts from week 18 until week 36 (both inclusive), abstracting from cold well (#705) and injecting into the warm well (#607) respectively. Inversely, winter period comprises weeks 37-52 and 1-17, and the system operates abstracting from warm well and injecting into cold well respectively. Thermal groundwater field evolution (every four weeks, starting from the beginning of the year) is presented in the following images (see Figure 7-12, Figure 7-13, and Figure 7-14):

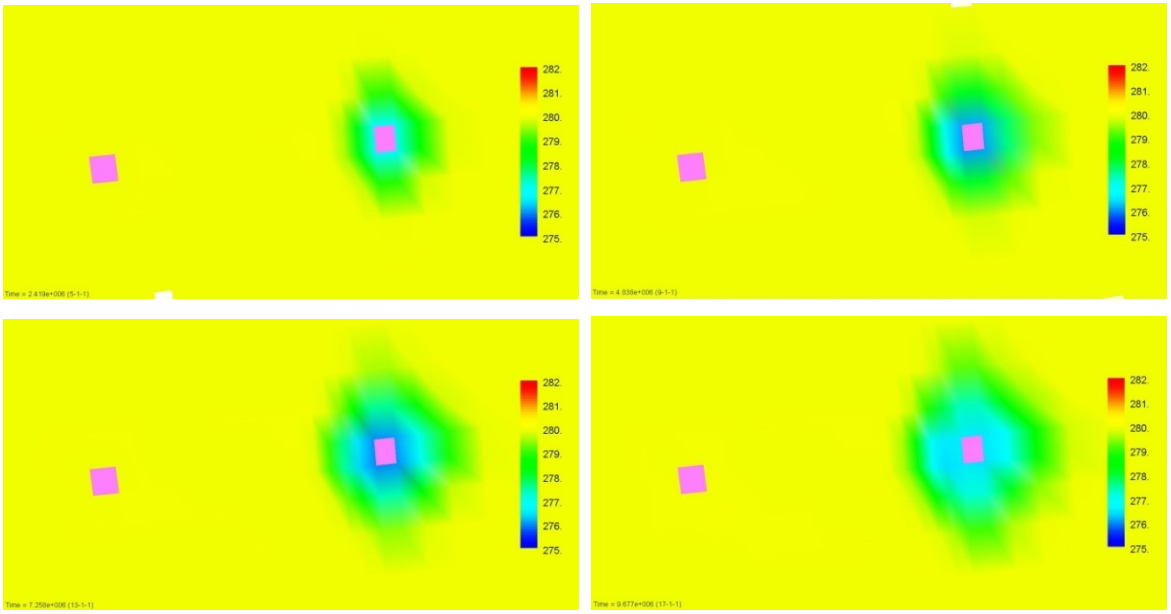

Figure 7-12: Thermal field evolution during winter period (beginning of the year)

First row - aquifer thermal field (week 1 starts on 1 January) after 4 weeks (left) and after 8 weeks (right), second row - after 12 weeks (left)) and after 16 weeks (right). System operation - abstraction from warm well (left) and injection into cold well (right)

As seen from the previous images (Figure 7-12), at the beginning of the first year of operation since water is abstracted from the warm well (left) and injected into the cold one at lower temperature, cold plume develops around the cold well (right). Its maximum expansion is according to the analytically calculated thermal radius of roughly 80m (see Table 7-II).

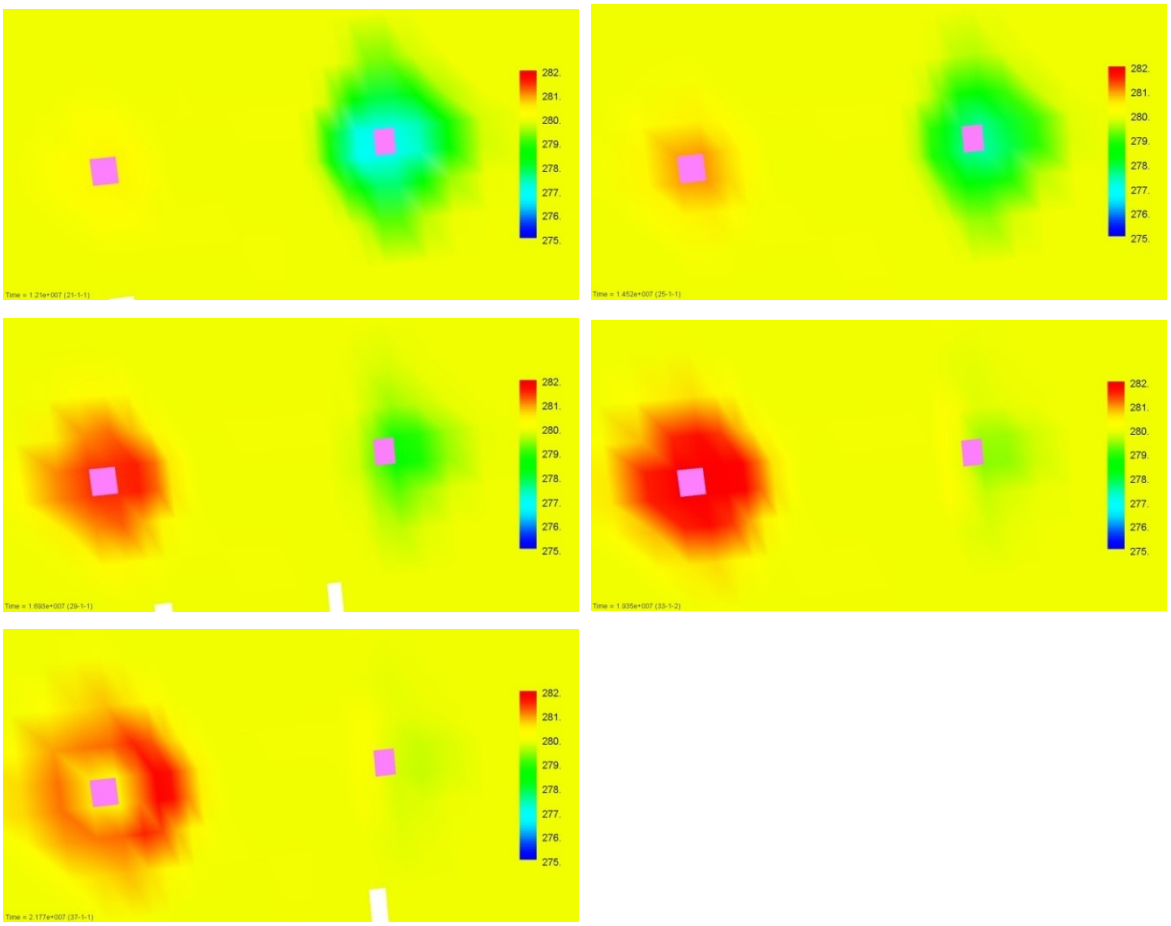

Figure 7-13: Thermal field evolution during summer period

First row - aquifer thermal field after 20 weeks (left) and 24 weeks (right), second row - after 28 weeks (left)) and 32 weeks (right), third row - after 36 weeks. System operation is reversed (week 18) - abstraction from cold well (right) and injection into warm well (left)

During the summer period, ATES operation is reversed in week 18 and water is abstracted from the cold well (right) and injected into the warm one (left). Warm plume expands around the warm well with its maximum expression after roughly 32 weeks and according to the analytically calculated thermal radius of roughly 75m (see Table 7-II). Cold plume almost vanishes at the end of the summer period.

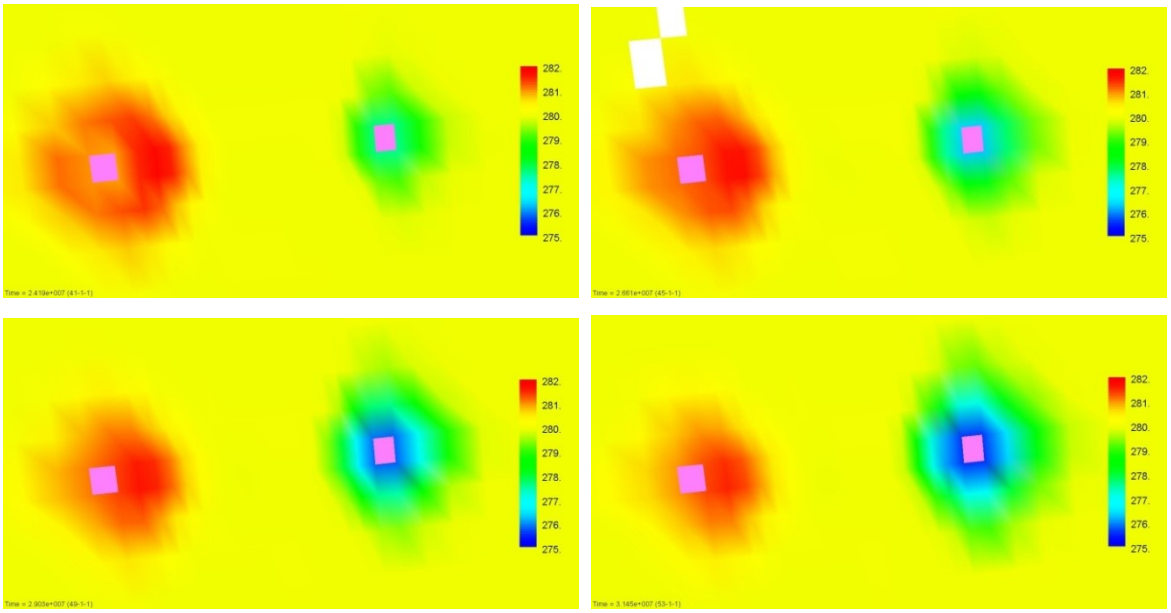

Figure 7-14: Thermal field evolution during winter period (end of the year)

First row - aquifer thermal field after 40 weeks (left) and 44 weeks (right), second row - after 48 weeks (left)) and 52 weeks (right). System operation is reversed again (week 37) - abstraction from warm well (left) and injection into cold well (right)

In week 37 ATES operation is reversed again to winter mode. Water flow is pumped from the warm well and injected into the cold one. Cold thermal plume starts to develop again around the cold well. By the end of the first year of ATES operation, warm and cold temperatures of the nearby well areas are different from the undisturbed aquifer temperature assumed in MODFLOW/MT3DMS model at the beginning of the year (280K). They are also different from the 7.5º/6º abstraction temperatures assumed in the initial setup calculations in Excel. That's why a different method has been developed in the following subchapter in order to estimate these temperatures iteratively, and therefore effectively be able to couple Excel (heating/cooling loads) and MODFLOW/MT3DMS (flow/thermal fronts) models.

7.4.2. Iterative method for estimation of warm and cold wells abstraction temperatures

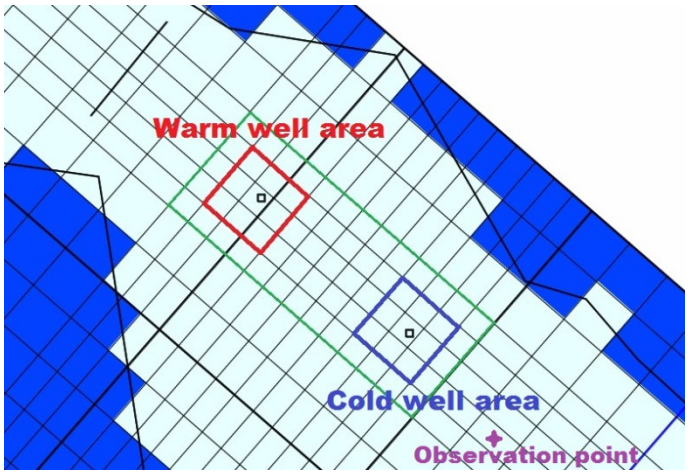

Since abstraction temperatures in the initial setup (for both warm and cold wells) are arbitrarily chosen, a different approach is developed in order to estimate a convergent solution iteratively. Different grid refinement is adopted in MODFLOW model, where nearby areas to warm and cold wells are discretized with 50x50m cell size (green rectangle area, Figure 7-15).

Figure 7-15: Local grid refinement (LGR) in nearby well areas

Green rectangle represents a 50x50m LGR near the wells, red and blue squares represent warm and cold wells areas affected by a calculated thermal radius of roughly 75m. They also are used to estimate the average abstraction temperature (during the abstraction period, summer for the cold well and winter for the warm well). Observation point (pink) is located some 280m downstream the cold well in order to study the cold front effect

The relevant technical parameters for the initial setup are summarized in the following Table 7-II (warm/cold abstraction temperatures 7.5º/6º, simulated with the adopted LGR).

Table 7-II: Initial setup main parameters

GWHP peak heat power, MW	0.350
Average water flow, m^3/day	1284
Average cold well injection temperature, ºC	2.8
Average warm well injection temperature, ºC	7.9
Annual heat demand (incl. office load),MWh	7,749.1
Annual heat demand covered by GWHP, MWh	2,922.6
Annual cooling demand covered (free cooling), MWh	1,839.6
Amount of pumped water (summer period), m^3	230,537
Amount of pumped water (winter period), m^3	238,127
Thermal radius warm well, m	75.9
Thermal radius cold well, m	77.1
Minimum distance between wells, m (defined as 3 times the average thermal radius)	230
Simulated drawdown in warm well (for grid cell 50x50m), m	2.96
Calculated drawdown in warm well (for well radius 0.4m), m	6.04
Simulated drawdown in cold well (for grid cell 50x50m), m	8.41
Calculated drawdown in cold well (for well radius 0.4m), m	13.61

7.4.3. ATES model iterations

Additionally, an 8-year period simulation was performed with the previously developed MODFLOW model in order to study the abstraction temperature variation of the warm and the cold well, as well as to estimate the charged and discharged thermal energy. Warm / cold abstraction temperatures are calculated as an average of warm / cold well area (defined as 3x3 cells square around the well, as seen in Figure 7-15), only during the well's abstraction period (summer for the cold well and winter for the warm well). Since heating demand is dominant, charge and discharge annual cycle calculations are performed for the cold well. The results are summarized in the following Table 7-III. It can be noted that after roughly 3-4 years of operation, abstraction temperatures and heat recovery factor (HRF) converge.

Table 7-III: First iteration of ATES model (8-year period)

Year of operation	1	2	3	4	5	6	7	8
Annually charged energy, MWh	1230	1346	1359	1363	1364	1365	1365	1365
Annual discharged energy, MWh	844	1095	1121	1127	1129	1129	1129	1128
Heat recovery factor (HRF) (calculated for the cold well)	0.69	0.81	0.82	0.83	0.83	0.83	0.83	0.83
Average abstraction cold well temperature, ºC	5.4	4.3	4.1	4.1	4.1	4.1	4.1	4.1
Average abstraction warm well temperature, ºC	7.5	7.8	7.9	7.9	7.9	7.9	7.9	7.9

From the weekly-based calculations it has also been observed that ATES summer operation should be reversed already in week 34 instead of 37. This is implemented in the next model iterations. Finally, after 4 iterations, warm / cold abstraction temperatures converge with good accuracy to 7.2-7.3º / 3.9-4.1º, as shown in Table 7-IV.

Table 7-IV: Consecutive iterations of ATES model

Relevant ATES parameters after 8 years of operation, warm/cold abstraction temperatures are presented in blue/red bold font and tend to converge to 7.2-7.3º/3.9-4.1º

Model iteration	1	2	3	4
Initial warm/cold abstraction temperatures, ºC	7.5/6	7.9/4.1	7.3/4.2	7.3/3.9
Annual charged energy, MWh	1365	1295	1305	1259
Annual discharged energy, MWh	1128	990	1077	973
Heat recovery factor (HRF)	0.83	0.76	0.83	0.77
Average abstraction cold well temperature, ºC	**4.1**	**4.2**	**3.9**	**4.1**
Average abstraction warm well temperature, ºC	**7.9**	**7.3**	**7.3**	**7.2**

7.4.4. Analysis of ATES thermal front

ATES model iteration #4 is adopted in order to study the long-term effect of warm and cold wells´ thermal interaction. The thermal front simulation for the first 8 years of ATES operation is presented in the following Figure 7-16a and Figure 7-17b, for the week when warm and cold plumes achieve their maximum expansion.

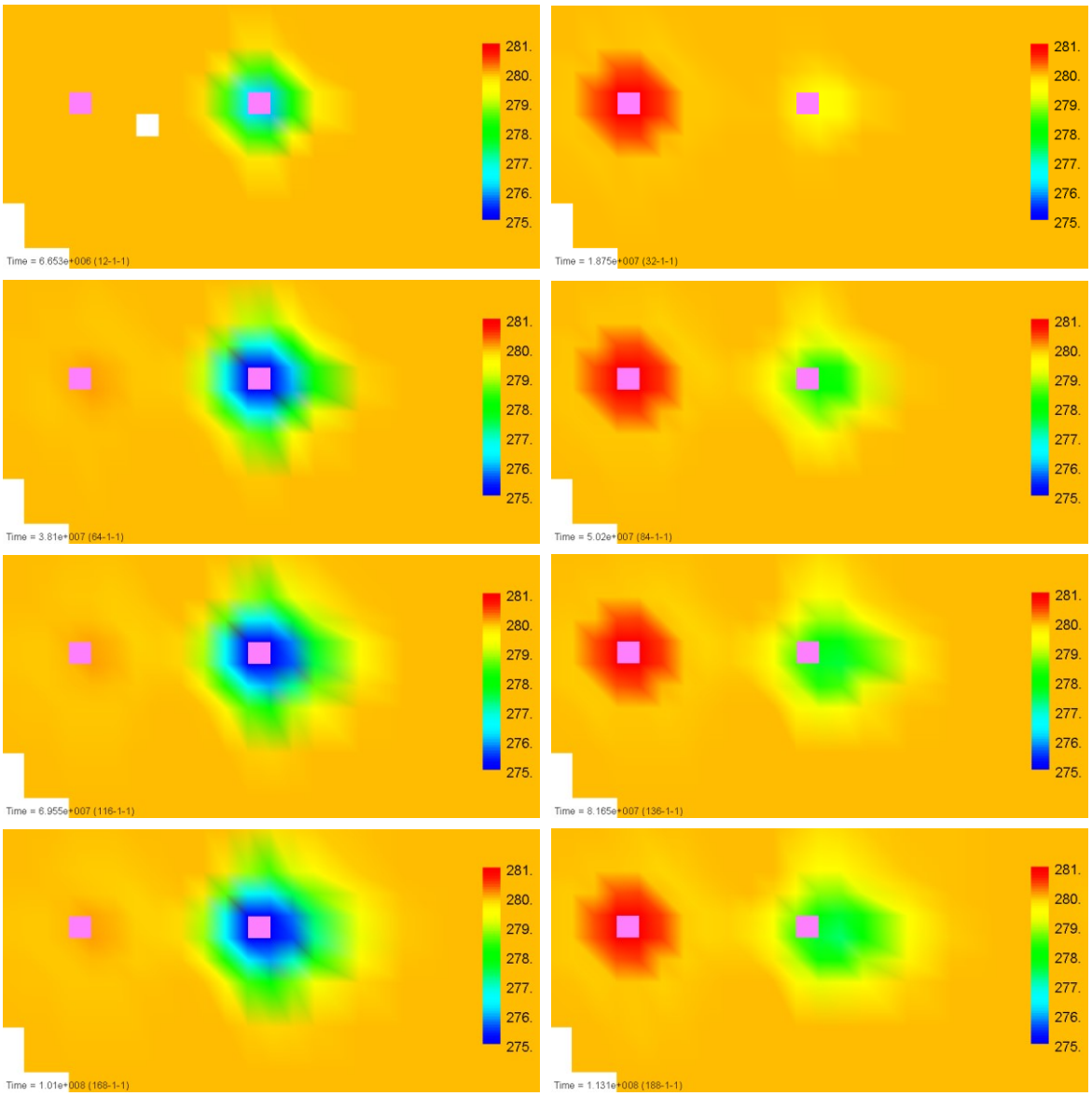

Figure 7-16a: Long-term thermal field evolution of ATES system (years 1-4)

Both wells are represented by a 50x50m pink cell. Left images describe the maximum annual cold well plume expansion (end of winter period, after week 11), right images are the maximum annual warm well plume expansion (end of summer period, after week 31)

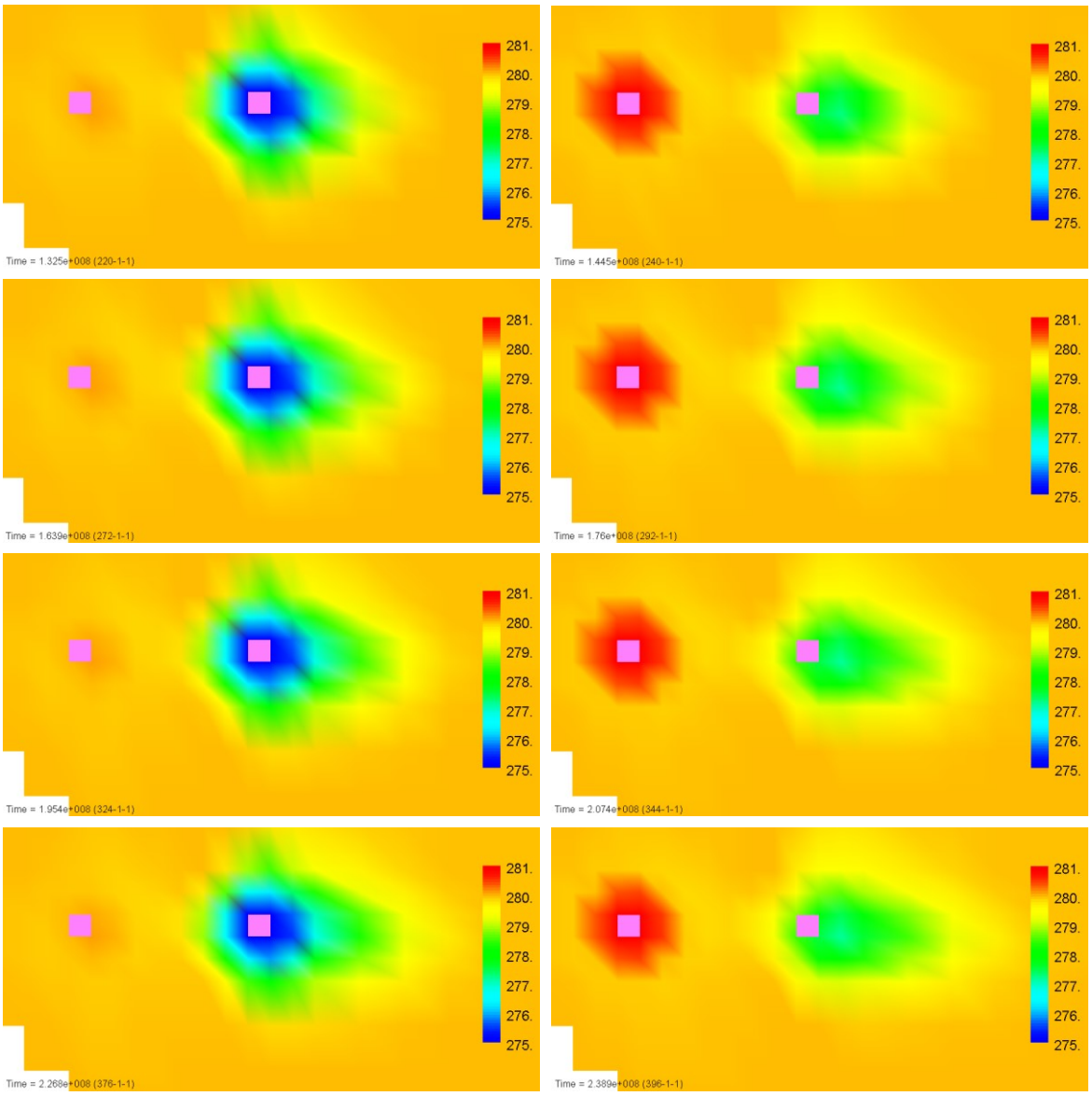

Figure 7-17b: Long-term thermal field evolution of ATES system (years 5-8)

It can be observed that warm well thermal plume maintains more or less within its thermal radius of roughly 75m, since heat injected in the aquifer is less compared to the heat abstracted from it. Moreover, heat plume around the warm well almost vanishes at the end of the summer period (left image), while cold plume around the cold well increases slowly over the years.

After 8 years of ATES operation, cold well thermal plume expands several hundreds of meters to the south-east, following the dominant groundwater flow direction. All in all, it can be concluded that the locations of the wells (cold well located downstream) and the separation between them is favorable for a correct long-term ATES operation.

The temperature evolution of the warm and cold well areas over the 8-year period of ATES operation (including the observation point temperature), as well as the pumping flow rate (negative values in summer period) are presented in the following Figure 7-18. Warm and cold temperatures are calculated as an average temperature of the 3x3 cells´ well area (according to Figure 7-15).

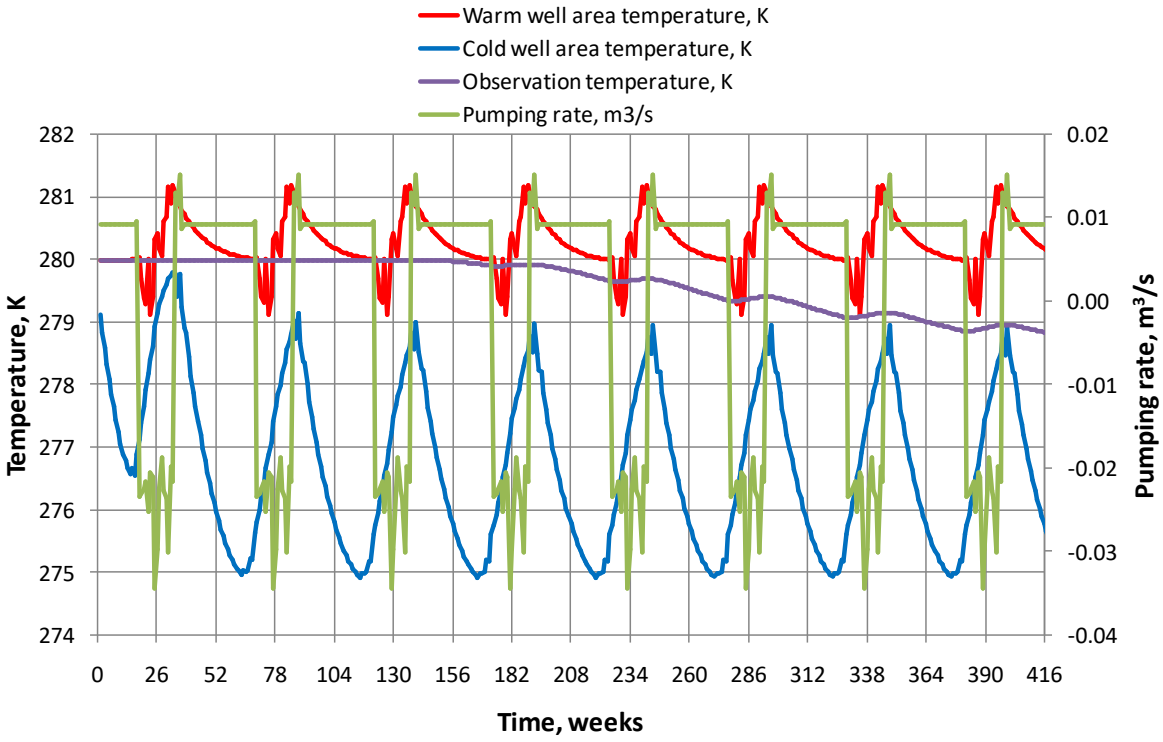

Figure 7-18: 8-year ATES operation (thermal and flow analysis)

Warm / cold well areas and observation point temperature evolution, as well as pumping rate over the 8-year ATES operation (negative pumping rate during the summer period)

From the previous Figure 7-18, it can be observed that after the second year ATES system converges with cyclically varying temperatures: warm well 279-281K, cold well 275-279K. Weekly averaged pumping rates are varying between roughly 0.01 m^3/s (winter period) and -0.025 m^3/s (summer period) with some peaks when heating or cooling loads are exceptionally high. Cold plume reaches the downstream observation point after roughly 3 years of operation and after 8 years its effect is slowly attenuated to roughly -1.2º compared to aquifer's undisturbed temperature.

Aquifer's head and flow fields for the typical weeks of ATES winter and summer operation are shown in Figure 7-19.

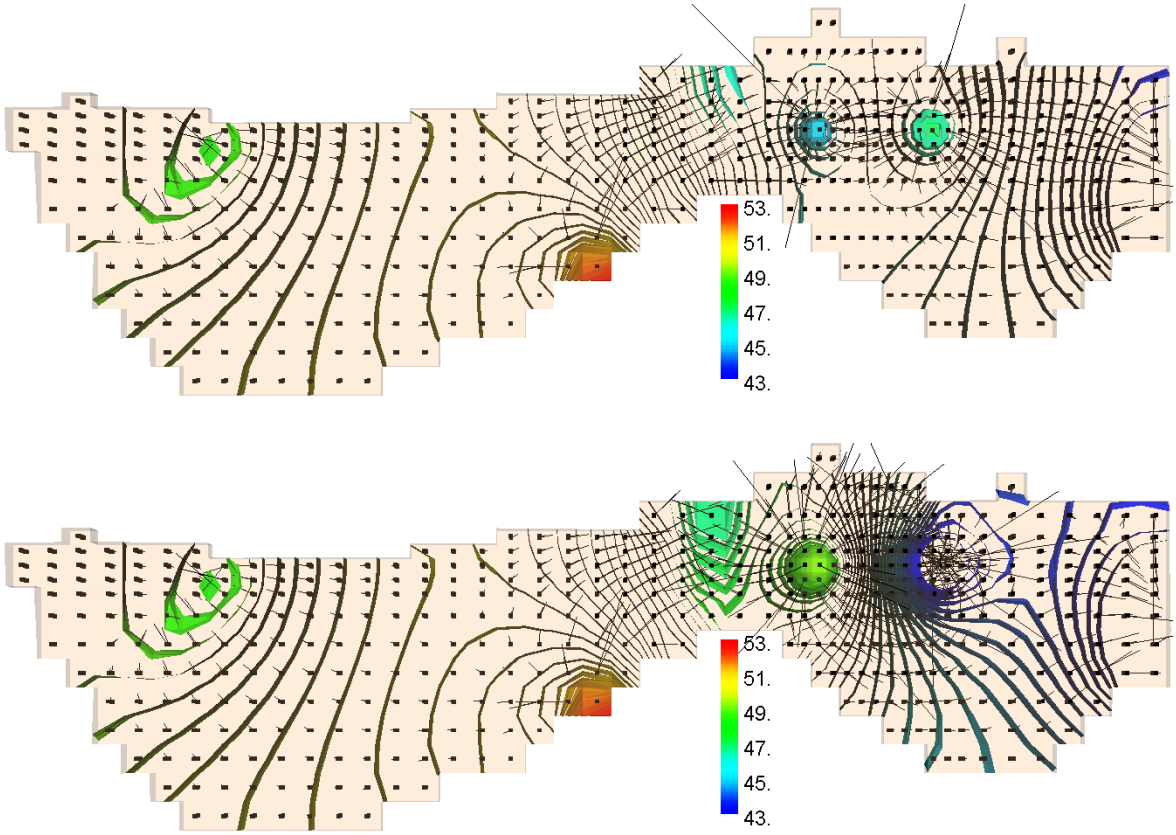

Figure 7-19: ATES system head and flow field

ATES system head isosurfaces and vector flow field. Dots are cells' centers with lines representing velocity direction and magnitude. Color scale is in meters of water head
Upper chart: Head and flow field after 11 weeks, year 8 (winter operation) - abstraction warm well (left, blue) and injection cold well (right, green)
Lower chart: Head and flow field after 31 weeks, year 8 (summer operation) - abstraction cold well (right, blue) and injection warm well (left, green)

During the winter period, abstraction warm well creates a cone of depression (lower head, blue) and injection cold well - cone of ascension (higher head, green). Locally, it provokes groundwater to flow towards the abstraction well and is repelled from the injection well, also reflected in the velocity vector field. During the summer, local flow movements are reversed, from the warm injection well towards the cold abstraction well.

8. Economic analysis of ATES system scenarios

As was mentioned previously, daily-based Excel calculations were performed for all proposed scenarios. Depending on the case, the following parameters were computed:

- DH network flow temperature (assumed 80ºC for days 1-60, 70ºC for days 140-260 and linearly interpolated between 70º and 80º for the rest of the year)
- Heating load covered with GWHP (the maximum load the heat pump could supply limited by Pukkila heating demand)
- Heat pump production temperature T_2 (assumed as a fraction point between DH return temperature of 40ºC and DH flow temperature, depending on the fraction between GWHP heating load covered and demanded, except for 100% HP coverage when it is equal to DH flow temperature)
- Pumping flow rate Q (as maximum flow rate needed either for cooling or heating operation, since no information is available a limit of roughly 700 m^3/day per well would be considered)
- In case of intercalated cooling exchanger - the temperature after the exchanger (assumed maximum value of 25ºC for data center cooling and 14º for primary circuit of DC network)
- Heat pump COP in heating mode (depending on GWHP water source temperature T_1 and HP production temperature T_2). In case of "only heating" scenario T_1 is aquifer abstraction temperature, in case of intercalated cooling exchanger, T_1 is the temperature after the exchanger
- Pump electric energy consumption E (based on the calculated flow rate Q, as well as assumed pressure head and efficiency)
- GWHP electric energy consumption
- Aquifer injection temperature T_3

Based on the previous calculation steps (daily-based), it is possible to obtain the annual values for:

- Annual heating demand supplied with GWHP [MWh]
- Annual cooling demand supplied ATES system [MWh]
- Annual GWHP electricity demand [MWh]
- Annual pumping electricity demand [MWh]
- Average daily pumping flow rate [m^3/day]
- Average aquifer injection temperature [ºC]

8.1. Only heating scenario (1)

In the following Table 8-I the main technical parameters of the system, as well as economic feasibility estimation for annual savings and investment costs are summarized.

Table 8-I: ATES system technical parameters and feasibility (scenario 1)

GWHP peak power, MW	0.350
Average pumping flow, m^3/day	908
Aquifer abstraction / injection temperature, ºC	7º / 2º
Annual heat demand covered by GWHP, MWh	2,919.2

Annual energy costs (-) / savings (+)	**Price**	**Units**	**Total**
Annual electricity demand GWHP	100 €/MWh	-985.5 MWh	-98,550 €
Annual electricity demand - pumping	100 €/MWh	-92.0 MWh	-9,198 €
Annual heat demand fuel savings (chips boiler)	25 €/MWh	3,649.0 MWh	91,224 €
Total energy savings			**-16,524 €**

Investment cost	**Price**	**Units**	**Total**
Preliminary subsurface survey, pumping tests and geological report	30,000 €/u	1	30,000 €
Groundwater source heat pump	500,000 €/MW	0.350	175,000 €
Heat exchangers	35,000 €/MW	0.350	12,250 €
Pumping well (incl. pump and equipment)	170,000 €/u	4	680,000 €
Underground connection pipes PEHD, PN16	150 €/m	550	82,500 €
Total investment cost			**979,750 €**

Although ATES system is used as base load generator it covers roughly 2/3 of annual heating demand. It is to be noted that annual energy costs overcome annual savings, and therefore ATES system is unfeasible, at least since chips are partially substituted by electricity which is four times more expensive, but heat pump average COP (3.0) is lower than the energy ratio (electricity/fuel).

A sensitivity analysis is performed varying GWHP peak power from 0.35 to 0.55MW for two different boiler fuel prices: 25 and 50 €/MWh. The results are presented in Table 8-II (next page).

Table 8-II: ATES system sensitivity analysis (scenario 1)

Upper table: Boiler fuel price (chips) 25€/MWh ; Lower table: Boiler fuel price 50€/MWh
The most profitable case is highlighted in bold

GWHP peak power, MW	0.350	0.450	0.550
Average pumping flow, m^3/day	908	1040	1124
Aquifer abstraction / injection temperature, ºC	7º / 2º	7º / 2º	7º / 2º
Annual heat demand covered by GWHP, MWh	2,919.2	3,470.2	3,918.7
Total energy savings (chips price 25€/MWh), €	-16,524	-26,445	-39,249
Total investment cost, €	979,750	1,033,250	1,086,750

GWHP peak power, MW	0.350	**0.450**	0.550
Average water flow, m^3/day	908	**1040**	1124
Aquifer abstraction / injection temperature, ºC	7º / 2º	**7º / 2º**	7º / 2º
Annual heat demand covered by GWHP, MWh	2,919.2	**3,470.2**	3,918.7
Total energy savings (chips price 50€/MWh), €	74,701	**82,000**	83,210
Total investment cost, €	979,750	**1,033,250**	1,086,750
Payback time, years	13.1	**12.6**	13.1

It is clear that with lower fuel price of 25€/MWh, all options are unfeasible. However, if chips' price increases to 50€/MWh, all options generate positive annual savings and payback time around 13 years. The most profitable case is a 0.45MW GWHP (payback time 12.6 years).

8.2. Constant cooling scenario (2a)

For this scenario, there are summarized the main technical parameters of the system, as well as economic feasibility estimation for annual savings and investment costs (see Table 8-III).

Table 8-III: ATES system technical parameters and feasibility (scenario 2a)

Constant cooling load (data center), MW	0.600
GWHP peak heat power, MW	0.500
Average pumping flow, m^3/day	686
Average aquifer injection temperature, ºC	15.7
Annual heat demand covered by GWHP, MWh	3,706.2

Annual energy cost (-) / savings (+)	**Price**	**Units**	**Total**
Annual electricity demand GWHP	100 €/MWh	-987.5 MWh	-98,748 €
Annual electricity demand - pumping	100 €/MWh	-83.4 MWh	-8,343 €
Annual heat demand fuel savings (chips boiler)	25 €/MWh	4,632.7 MWh	115,817 €
Cooling energy sold (data center)	50 €/MWh	5,256.0 MWh	262,800 €
Total energy savings			**271,527 €**

Investment cost	**Price**	**Units**	**Total**
Preliminary subsurface survey, pumping tests and geological report	30,000 €/u	1	30,000 €
Groundwater source heat pump	500,000 €/MW	0.500	250,000 €
Heat exchangers	35,000 €/MW	1.100	38,500 €
Pumping well (incl. pump and equipment)	170,000 €/u	2	340,000 €
Underground connection pipes PEHD, PN16	150 €/m	550	82,500 €
Total investment cost			**741,000 €**

Dimensioning GWHP for roughly 50% of peak heat load, the annual heat demand supplied by ATES system is 84% of total demand. Compared to the previous case, heat pump average COP is highly improved (3.7) due to the higher HP input temperature, even though the average pumping flow is reduced (-24%).

However, the main difference with the previous case is the possibility to realize important annual revenue selling cooling energy to the data center. This turns the payback time to less than 3 years (2.7) and makes the investment highly profitable.

A sensitivity analysis is performed varying GWHP peak power from 0.4 to 0.6MW and constant cooling between 0.5 and 0.6MW. For this case, some technical constraints are imposed, such as average pumping rate below 700 m^3/day, as well as average injection temperature less than 16ºC.

From the results presented in Table 8-IV, the most profitable case with reasonable injection temperature is selected (as simulated previously, after 25 years of operation increased abstraction temperature is only 1.1ºC).

Table 8-IV: ATES system sensitivity analysis (scenario 2a)

Selected main case highlighted in bold

Constant cooling load (data center), MW	0.600	**0.600**	0.600
GWHP peak heat power, MW	0.600	**0.500**	0.400
Average water flow, m^3/day	686	**686**	686
Average aquifer injection temperature, ºC	15.0	**15.7**	16.7
Annual heat demand covered by GWHP, MWh	4,096.9	**3,706.2**	3,208.8
Cooling energy sold (data center), MWh	5,256.0	**5,256.0**	5,256.0
Total energy savings, €	264,045	**271,527**	275,932
Total investment cost, €	794,500	**741,000**	687,500
Payback time, years	3.0	**2.7**	2.5

Constant cooling load (data center), MW	0.500	0.500	0.500
GWHP peak heat power, MW	0.600	0.500	0.400
Average water flow, m^3/day	571	571	571
Average aquifer injection temperature, ºC	13.0	13.8	15.1
Annual heat demand covered by GWHP, MWh	4,096.9	3,706.2	3,208.8
Cooling energy sold (data center), MWh	4,380.0	4,380.0	4,380.0
Total energy savings, €	221,635	229,117	233,523
Total investment cost, €	791,000	737,500	684,000
Payback time, years	3.6	3.2	2.9

8.3. Constant cooling scenario (2b)

In this scenario chips boiler is completely substituted by the ATES system. In the following Table 8-V are summarized the main technical parameters of the system, as well as economic feasibility estimation for annual savings and investment costs.

Table 8-V: ATES system technical parameters and feasibility (scenario 2b)

Constant cooling load (data center), MW	1.200
GWHP peak heat power, MW	1.000
Average water flow, m^3/day	1371
Average aquifer injection temperature, ºC	19.8
Annual heat demand covered by GWHP, MWh	4,403.4

Annual energy cost (-) / savings (+)	**Price**	**Units**	**Total**
Annual electricity demand GWHP	100 €/MWh	-1,374.1 MWh	-137,409 €
Annual electricity demand - pumping	100 €/MWh	-151.7 MWh	-15,169 €
Annual heat demand fuel savings (chips boiler)	25 €/MWh	5,504.2 MWh	137,606 €
Cooling energy sold (data center)	50 €/MWh	10,512.0 MWh	525,600 €
Total energy savings			**510,628 €**

Investment cost	**Price**	**Units**	**Total**
Preliminary subsurface studies, pumping tests and geological report	30,000 €/u	1	30,000 €
Groundwater source heat pump	500,000 €/MW	1.000	500,000 €
Heat exchangers	35,000 €/MW	2.200	77,000 €
Pumping well (incl. pump and equipment)	170,000 €/u	4	680,000 €
Underground connection pipes PEHD, PN16	200 €/m	550	110,000 €
Total investment cost			**1,397,000 €**

Compared to the previous scenario, heat pump weighted average COP is somehow compromised (3.2), since GWHP needs to produce higher generation temperature equal to DH network flow temperature (no additional peak boiler).

Moreover, in comparison with scenario 2a, the annual revenue from cooling energy is roughly doubled, as well as the investment cost. All in all, the payback time is roughly the same, less than 3 years (2.7) and makes the investment highly profitable. However, the groundwater flow impact is higher (doubled pumping rate), as well as the thermal impact. The average aquifer injection temperature is as high as 19.8º and as seen from the groundwater model simulation, thermal plume expands towards cold well (although main flow direction is towards Porvoonjoki, which acts as a heat sink), and after 25 years of simulation increases the cold well temperature by roughly 3.5ºC.

A sensitivity analysis is performed varying GWHP peak power from 0.8 to 1.2MW and constant cooling between 1 and 1.2MW. For this scenario, the adopted technical constraints are: average pumping rate below 1400 m^3/day, as well as GWHP peak power at least 1MW in order to cover totally the heating demand.

From the results presented in Table 8-VI, the most profitable case with the imposed constraints is selected, apparently average injection temperature is not sensitive to GWHP peak power when HP is the only heat generator (peak boiler totally replaced).

Table 8-VI: ATES system sensitivity analysis (scenario 2b)

Selected main case highlighted in bold

Constant cooling load (data center), MW	1.200	**1.200**	1.200
GWHP peak heat power, MW	1.100	**1.000**	0.900
Average water flow, m^3/day	1371	**1371**	1371
Average aquifer injection temperature, ºC	19.8	**19.8**	19.8
Annual heat demand covered by GWHP, MWh	4,407.3	**4,403.4**	4,394.3
Cooling energy sold (data center), MWh	10,512.0	**10,512.0**	10,512.0
Total energy savings, €	510,612	**510,628**	510,835
Total investment cost, €	1,450,500	**1,397,000**	1,343,500
Payback time, years	2.8	**2.7**	2.6

Constant cooling load (data center), MW	1.000	1.000	1.000
GWHP peak heat power, MW	1.100	1.000	0.900
Average water flow, m^3/day	1143	1143	1143
Average aquifer injection temperature, ºC	18.8	18.8	18.8
Annual heat demand covered by GWHP, MWh	4,407.3	4,403.4	4,394.3
Cooling energy sold (data center), MWh	8,760.0	8,760.0	8,760.0
Total energy savings, €	425,540	425,556	425,763
Total investment cost, €	1,443,500	1,390,000	1,336,500
Payback time, years	3.4	3.3	3.1

It can be concluded, that both scenarios 2a and 2b have similar economic outcomes (payback time). However, scenario 2b has a significantly higher environmental impact on the groundwater area: pumping flow rate is doubled, and after 25 years of operation the thermal feedback to the cold well is much higher, as well as the warm front temperature reaching Porvoonjoki river.

8.4. Combined heating and cooling scenario (3)

The fourth ATES model iteration is used for the analysis (warm/cold abstraction temperatures 7.3º/3.9º). The main technical parameters of the system, as well as the economic feasibility estimation for annual savings and investment costs are summarized in the following Table 8-VII.

Table 8-VII: ATES system technical parameters and feasibility (scenario 3)

GWHP peak heat power, MW	0.350
Average water flow, m^3/day	1283
Average cold well injection temperature, ºC	2.2
Average warm well injection temperature, ºC	7.2
Annual heat demand (incl.office load),MWh	7,749.1
Annual heat demand covered by GWHP, MWh	2,922.6
Annual cooling demand, MWh	1,839.6
Amount of pumped water (summer period), m^3	239,061
Amount of pumped water (winter period), m^3	229,364
Thermal radius warm well, m	77.3
Thermal radius cold well, m	75.7
Minimum distance between wells, m (defined as 3 times the average thermal radius)	229
Simulated drawdown warm well (for grid cell 50x50m), m	2.56
Calculated drawdown warm well (for well radius 0.4m), m	5.06
Simulated drawdown cold well (for grid cell 50x50m), m	7.98
Calculated drawdown cold well (for well radius 0.4m), m	14.13

Annual energy cost (-) / savings (+)	**Price**	**Units**	**Total**
Annual electricity demand GWHP	100 €/MWh	-881.8 MWh	-88,179 €
Annual electricity demand - pumping	100 €/MWh	-141.9 MWh	-14,195 €
Annual heat demand fuel savings (chips boiler)	25 €/MWh	3,653.3 MWh	91,331 €
Cooling energy sold (DC network)	50 €/MWh	1,839.6 MWh	91,978 €
Total energy savings			**80,936 €**

Investment cost	**Price**	**Units**	**Total**
Preliminary subsurface studies, pumping tests and geological report	30,000 €/u	1	30,000 €
Groundwater source heat pump	500,000 €/MW	0.350	175,000 €
Heat exchangers	35,000 €/MW	1.750	61,250 €
Pumping well (incl. pump and equipment)	170,000 €/u	4	680,000 €
Underground connection pipes PEHD, PN16	200 €/m	550	110,000 €
Total investment cost			**1,056,250 €**

GWHP coverage ratio is roughly 38% of the annual heating demand. Investment costs do not include the necessary DC network implementation. Nevertheless, the payback time is still quite long (roughly 13 years). However, according to the previously presented simulation, ATES system is much more balanced, since operation is alternatively reversed creating the classic warm-cold storage areas, with no thermal feedback between wells. On the other hand, it should be noted the excessive drawdown of the cold well. Although, it is within the aquifer's thickness at this point, it should be additionally studied through slug and pumping tests.

A sensitivity analysis is performed varying GWHP peak power from 0.35 to 1MW and the results are presented in Table 8-VIII.

Table 8-VIII: ATES system sensitivity analysis (scenario 3)

Selected main case highlighted in bold

GWHP peak heat power, MW	**0.350**	0.600	1.000
Average water flow, m3/day	**1283**	1688	2161
Average cold well injection temperature, ºC	**2.2**	2.4	2.7
Average warm well injection temperature, ºC	**7.2**	7.1	7.1
Annual heat demand (incl.office load),MWh	**7,749.1**	7,749.1	7,749.1
Annual heat demand covered by GWHP, MWh	**2,922.6**	4,257.1	5,894.7
Annual cooling demand, MWh	**1,839.6**	1,839.6	1,839.6
Amount of pumped water (summer period), m^3	**239,061**	250,716	250,716
Amount of pumped water (winter period), m^3	**229,364**	365,364	538,220
Thermal radius warm well, m	**77.3**	79.1	79.1
Thermal radius cold well, m	**75.7**	95.5	116.0
Minimum distance between wells, m (defined as 3 times the average thermal radius)	**229**	262	293
Total energy savings, €	**80,936**	67,448	36,355
Total investment cost, €	**1,056,250**	1,530,000	2,084,000
Payback time, years	**13.1**	22.7	57.3

As can be seen from Table 8-VIII, the most profitable case is apparently the one when GWHP is only base load generator (0.35MW). This is also the most balanced case, where the amounts of pumped water during the summer and winter periods are more or less equal, and this fact is also reflected in the estimated minimum distance needed between abstraction and injection wells. The higher average pumping flow also makes the 0.6W and 1MW options unviable.

9. Discussion

In the present Thesis, groundwater models were calibrated for steady state condition, using statistical data for static observation well levels (piezometric head), and the estimated main aquifer parameters were used later in order to conduct different transient flow and thermal simulations. For more accurate aquifer parameters estimation, additional geological survey and tests for non-equilibrium (transient) flow conditions should be conducted, as next steps for model calibration and verification. Complementary approaches and methods will be presented and discussed in this chapter.

9.1. Geological survey

In order to study subsurface stratigraphy layers, a geological survey of sediments could be conducted to estimate some relevant parameters of the geologic sediments, such as hydraulic conductivity, porosity or specific yield.

It is observed that hydraulic conductivity is related to sediment grain-size and is proportional to some specific power of characteristic dimension of sediments. Particularly, the Hazen method applicable to sand with grain-size between 0.1 and 3mm relates hydraulic conductivity with a square of sediment characteristic dimension (Fetter, 2001). During well perforation, it is important to keep a detailed log-record for e.g. roughly every meter of penetration, describing sediment type, size and properties, as well as attaching samples for sediment analysis.

9.2. Pumping tests

Pumping tests are needed in order to estimate aquifer transmissivity (**T**) and storativity (**S**). Both parameters can be determined if pumping test is conducted recording drawdown variation in time of the pumping well and one or several observation wells. Observation wells should be located preferably in radial direction from the pumping well with geometrically increasing distances by a factor of 10 (Fetter, 2001). Pumping test could be conducted only with one well, but in this case it is possible to determine only aquifer transmissivity (T). The most important methods for pumping test analysis, assuming more or less constant pumping rate over the studied period, are listed below:

- Theis method - using Theis equation (see Chapter 3, equation 3-A) it is possible to plot a Theis function **W(u)** against **1/u** in a logarithmic chart, also known as Theis type curve (defined by equation 3-A1). By matching the observation well transient drawdown **s** field data with Theis type curve, it is possible to establish a correlation between time **t** and **1/u** as well as between **W(u)** and **s**. Finally, using equation 3-A, both parameters **T** and **S** can be estimated (see Figure 9-1).

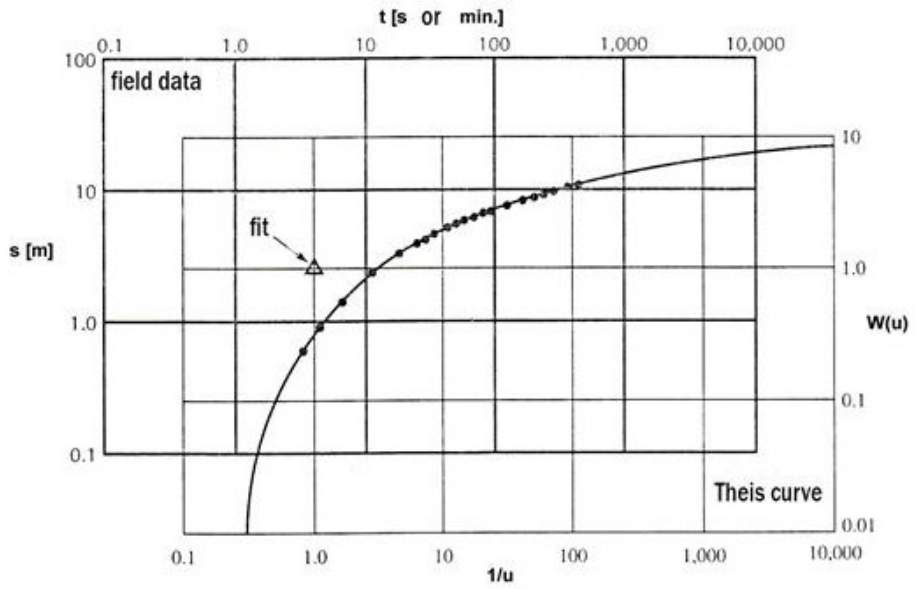

Figure 9-1: Theis type curve method

- Cooper-Jacobs straight line drawdown method - for small values of u-term (when distance from pumping well is short or after certain time from start pumping), all polynomial terms of Theis function (defined in equation 3-A1) could be neglected (drawdown is logarithmically dependent on u-term, simplified equation 3-A2), and therefore observation test results could be plotted as a straight line in a semi-logarithmic chart. By estimating drawdown change per log-cycle (e.g. between 100 and 1000 minutes of pumping), it is possible to calculate **T** and **S** parameters

- Specific capacity data analysis - pumping well specific capacity is defined as a ratio between pumped flow (**Q**) and the drawdown (**s**), when drawdown has been stabilized (doesn't vary over time). One approach is, by using the simplified logarithmic Theis equation (3-A2), iteratively solving for aquifer transsmissivity (**T**), although initial estimation of storativity (**S**) is needed. Different practical formulas have been developed, mostly related to concrete aquifer studies, and directly relating **T** and **Q/s** (e.g. Razack and Huntley, 1991 for alluvial groundwater basin in Morocco or Mace, 1997 for karstic Edwards aquifer in Texas / source Fetter, 2001).

9.3. Slug tests

Before starting with pumping tests, which are expensive and time consuming, alternative initial slug (or bail down tests) should be performed in the first place, since they could be conducted even in small diameter observation wells. A known volume of water is suddenly introduced or removed and well head variation over time is recorded (Fetter, 2001).

Depending on well's hydraulic response, there are several possibilities and methods for slug tests data analysis such as:

- Overdamped response - water levels recovers smoothly to the initial steady state level, following roughly exponential curve. Different techniques are available for analysis, such as Cooper-Brederhoeft-Papadopulos or Hvorslev slug test methods

- Underdamped response - water level oscillates over the initial steady state level with decreasing amplitude in time. Van der Kamp method is normally used for iterative estimation of transmissivity (**T**)

10. Conclusions

This Thesis introduced and developed different methods and calculation techniques in order to model and simulate Aquifer Thermal Energy Storage (ATES) systems for district heating and cooling application. ATES systems were presented and addressed from different perspectives, such as their technical rationale, economic feasibility and environmental impact.

Groundwater flow and thermal models were developed and calibrated, using a variety of available data sources (National Land Survey of Finland, Finnish Environment Institute) and tools (EXCEL, QGIS, MODFLOW, MT3DMS). Heat pump COP estimation analytical model was also implemented and coupled with the groundwater models. The purpose was to study different energy scenarios for ATES integration within the existing Pukkila's district heating network (Nivos Energia), as well as the long-term environmental flow and thermal impact generated to aquifer groundwater areas.

Among the different researched scenarios, the most feasible strategy is to introduce a roughly constant cooling demand (proceeding from e.g. data center or industrial waste heat) in combination with the existing local district heating demand. The introduction of variable cooling demand using standard office simulated data was also modeled, having shown promising results. On the other hand, the "only heating" integration scenario had poor economic results, at least for the assumed present level of boiler's fuel price, and was reasonably feasible only in the case when prices increase.

Nowadays heat pumps are very common and often used for diverse HVAC applications. Their technical maturity and adequacy are widely proved in many applications. Similarly, efficient drilling technology for groundwater usage has been developed and significantly improved during the last decades. Therefore, an integrated ATES system composed by a GWHP coupled with one or several abstraction/injection well doublets is a reasonable technical option and a rational design choice to be considered.

The studied energy scenarios for ATES integration within DH/DC networks were economically feasible and had limited environmental impact even within a 25-year horizon of ATES operation. Combined heating and cooling scenario, with seasonally reversible ATES operation and roughly balanced pumping volumes during summer and winter periods, had lower impact on the aquifer area and seemed to be the most environmentally equilibrated.

All analyses presented in this Thesis were carried out using quite limited and uncertain information regarding the hydrogeology of the studied case area. The fundamental assumptions - normally simplified during the prefeasibility phase - were that the aquifer layer is uniform, confined and isotropic in the considered area (simulation approach), as well as neglecting real physical boundaries (analytical approach).

In the future, the research of this Thesis could be continued and the result accuracy could be improved for example by the following steps:

- additional geological survey and slug & pumping tests in order to improve groundwater model quality
- detailed ATES project planning choosing the concrete well locations and their number, based on the pumping tests
- additional methods and tools for efficient input data gathering and automated data exchange between applications
- study of some additional energy sources integration, such as thermo-solar and industrial waste heat
- more detailed study on how ATES system is affected by energy prices
- more efficient ATES optimization and control strategies

All in all, ATES systems are an efficient and a sustainable alternative for traditional fossil fuel boilers, due to their capacity to annually store and recover cooling & heating energy from the subsurface. Significant technical and economical improvement could be achieved when simultaneous or seasonable cooling and heating loads are dispatched, within integrated district energy (heating & cooling) networks.

References

Anderson, M. P.; Woessner, W. W.; Hunt, R. J. (2015) Applied Groundwater Modeling

Arola, T.; Korkka-Niemi, K. (2014) The effect of urban heat islands on geothermal potential - examples from Quaternary aquifers in Finland

Arola, T.; Okkonen, J.; Jokisalo, J. (2016) Groundwater Utilisation for Energy Production in the Nordic Environment - An Energy Simulation and Hydrogeological Modelling Approach

Bakr, M.; Van Oostrom, N.; Sommer, W. (2013) Efficiency of and interference among multiple Aquifer Thermal Energy Storage systems; A Dutch case study

Banks, D. (2008) An Introduction to Thermogeology

Banks, D. (2009) Thermogeological assessment of open-loop well-doublet schemes - a review and synthesis of analytical approaches

Bedekar, V.; Morway, E. D.; Langevin, C. D.; Tonkin, M. (2016) MT3D-USGS Version 1 - A U.S. Geological Survey Release of MT3DMS Updated with New and Expanded Transport Capabilities for Use with MODFLOW

Bloemendal, M.; Hartog, N. (2018) Analysis of the impact of storage conditions on the thermal recovery efficiency of low-temperature ATES systems

Bloemendal, M.; Jaxa-Rozen, M.; Olsthoorn, T. (2018) Methods for planning of ATES systems

Bloemendal, M.; Olsthoorn, T. (2018) ATES systems in aquifers with high ambient groundwater flow velocity

Bloemendal, M.; Olsthoorn, T.; Boons, F. (2013) How to achieve optimal and sustainable use of the subsurface for Aquifer Thermal Energy Storage

Bloemendal, M.; Olsthoorn, T.; Van de Ven, F. (2015) Combining climatic and geo-hydrological preconditions as a method to determine world potential for ATES

Bozkaya, B.; Li, R.; Labeodan, T.; Kramer, R. P.; Zeiler, W. (2017) Development and evaluation of a building integrated aquifer thermal storage

Bozkaya, B.; Zeiler, W. (2014) Thermal Storage Capacity Control of Aquifer Systems
Caljé, R.J. (2010) Future use of Aquifer Thermal Energy Storage below the historic centre of Amsterdam

Casasso, A.; Sethi, R. (2015) Modelling thermal recycling occurring in groundwater heat pumps (GWHPs)

Clyde, C.G.; Madabhushi, G.V. (1983) Spacing of Wells for Heat Pumps

Drijver, B.; Willemsen, (2001) A. Groundwater as a heat source for geothermal heat pumps

Driscoll, F. G. (1986) Groundwater and wells

Essink, G.O. (2000) Groundwater Modelling

Fetter, C. W. (2001) Applied hydrogeology

Finnish Energy (2013) District heating of buildings. Regulations and guidelines. Publication K12013

Finnish Energy (2016) Large heat pumps in district heating systems

Gao, L.; Zhao, J.; An, Q.; Wang, J.; Liu, X. (2017) A review on system performance studies of aquifer thermal energy storage

Haehnlein, S.; Bayer, P.; Blum, P. (2010) International legal status of the use of shallow geothermal energy

Halford, K. J.; Kuniansky, E. L. USGS (2002) Documentation of Spreadsheets for the Analysis of Aquifer-Test and Slug-Test Data

Harbaugh, A.W. (2005) MODFLOW-2005, The U.S. Geological Survey Modular Ground-Water Model-the Ground-Water Flow Process

Heath, R.C. USGS (1983) Basic Ground-Water Hydrology

Hecht-Mendez, J.; Molina-Giraldo, N.; Blum, P.; Bayer, P. (2010) Evaluating MT3DMS for Heat Transport Simulation of Closed Geothermal Systems

Hecht-Mendez, J.; Molina-Giraldo, N.; Blum, P.; Bayer, P. (2010) Use of MT3DMS for Heat Transport Simulation of Shallow Geothermal Systems

Hynynen, H. (2018) Flow temperature reduction in the development of a district heating network

Kim, J.; Lee, Y.; Yoon, W. S.; Jeon, J. S.; Koo, M.; Keehm, Y. (2010) Numerical modeling of aquifer thermal energy storage system

Kranz, S.; Bartels, J. (2010) Simulation and Data Based Optimisation of an Operating Seasonal Aquifer Thermal Energy Storage

Luoma, S. (2012) Steady-state groundwater flow model of shallow aquifer in Hanko, south Finland

Matthews, D.; Wincott, N.; Billings, J. (2018) Open-loop groundwater source heat pumps - Code of Practice for the UK. Harnessing energy from water in the ground for heating and cooling

Milnes, E.; Perrochet, P. (2013) Assessing the impact of thermal feedback and recycling in open-loop groundwater heat pump (GWHP) systems - a complementary design tool

Neville C. J.; Papadopulos S. S. (2005) Simulating heat transport with a standard solute transport code

Pero, J. (2016) District heating business development in Mäntsälän Sähkö limited company

Piga, B.; Casasso, A.; Pace, F.; Godio, A.; Sethi, R. (2017) Thermal Impact Assessment of Groundwater Heat Pumps (GWHPs) - Rigorous vs. Simplified Models

Positano, P.; Nannucci, M. (2017) The H2O20 FREEWAT participated approach for the Follonica-Scarlino aquifer case study. A common space to generate shared knowledge on the value of water

Possemiers, M (2014) Aquifer Thermal Energy Storage under different hydrochemical and hydrogeological conditions

Rau, G.C.; Andersen, M.S.; Acworth, R.I. (2012) Experimental Investigation of the Thermal Dispersivity Term and Its Significance in the Heat Transport Equation for Flow in Sediments

Reilly, T. E. ; Harbaugh, A. W. USGS (2004) Guidelines for Evaluating Ground-Water Flow Models

Reilly, T. E. USGS (2001) System and Boundary Conceptualization in Ground-Water Flow Simulation. Techniques of Water-Resources Investigations of the U.S. Geological Survey. Book 3, Applications of Hydraulics

Rossetto, R.; De Filippis et al. (2018) Integrating free and open source tools and distributed modelling codes in GIS environment for data-based groundwater management

Rostampour, V ; Jaxa-Rozen, M.; Bloemendal, M; Keviczky, T. (2016) Building Climate Energy Management in Smart Thermal Grids via Aquifer Thermal Energy Storage Systems

Sommer, W. (2015) Modelling and monitoring of Aquifer Thermal Energy Storage

Sommer, W.; Doornenbal, P.; Drijver, B.; van Gaans, P.; Leusbrock, I.; Grotenhuis, J.; Rijnaarts, H. (2014) Thermal performance and heat transport in aquifer thermal energy storage

Sommer, W.; Valstar, J.; Leusbrock, I.; Grotenhuis, T.; Rijnaarts, H. (2015) Optimization and spatial pattern of large-scale aquifer thermal energy storage

Stradiotto, G.M. (2016) Ground Source Heat Pump in District Heating and Cooling System in Elverum

Tuominen, P.; Holopainen, R.; Eskola, L.; Jokisalo, J.; Airaksinen, M. (2014) Calculation method and tool for assessing energy consumption in the building stock

UK Department of Energy and Climate Change (2016) Heat Pumps in District Heating - Case studies

Visser, P. W.; Kooi, H.; Stuyfzand, P. J. (2015) The thermal impact of aquifer thermal energy storage (ATES) systems - a case study in the Netherlands, combining monitoring and modeling

Wahlroos, M.; Pärssinen, M.; Rinne, S.; Syri, S.; Manner, J. (2018) Future views on waste heat utilization - case of data centers in Northern Europe

Zheng, C.; Bennet, G. D. (2002) Applied contaminant transport modeling - theory and practice

Zheng, C.; Wang, P. (1999) MT3DMS - A Modular Three-Dimensional Multispecies Transport Model for Simulation of Advection, Dispersion, and Chemical Reactions of Contaminants in Groundwater Systems; Documentation and User's Guide